Quantum information in quantum cognition

Nicole Yunger Halpern[1, 2] and Elizabeth Crosson[1]
[1] *Institute for Quantum Information and Matter, Caltech, Pasadena, CA 91125, USA*
[2] *Kavli Institute for Theoretical Physics, University of California, Santa Barbara, CA 93106, USA*
(Dated: November 15, 2017)

Matthew Fisher recently postulated a mechanism by which quantum phenomena could influence cognition: Phosphorus nuclear spins may resist decoherence for long times. The spins would serve as biological qubits. The qubits may resist decoherence longer when in Posner molecules. We imagine that Fisher postulates correctly. How adroitly could biological systems process quantum information (QI)? We establish a framework for answering. Additionally, we apply biological qubits in quantum error correction, quantum communication, and quantum computation. First, we posit how the QI encoded by the spins transforms as Posner molecules form. The transformation points to a natural computational basis for qubits in Posner molecules. From the basis, we construct a quantum code that detects arbitrary single-qubit errors. Each molecule encodes one qutrit. Shifting from information storage to computation, we define the model of Posner quantum computation. To illustrate the model's quantum-communication ability, we show how it can teleport information incoherently: A state's weights are teleported; the coherences are not. The dephasing results from the entangling operation's simulation of a coarse-grained Bell measurement. Whether Posner quantum computation is universal remains an open question. However, the model's operations can efficiently prepare a Posner state usable as a resource in universal measurement-based quantum computation. The state results from deforming the Affleck-Lieb-Kennedy-Tasaki (AKLT) state and is a projected entangled-pair state (PEPS). Finally, we show that entanglement can affect molecular-binding rates (by 0.6% in an example). This work opens the door for the QI-theoretic analysis of biological qubits and Posner molecules.

arXiv:1711.04801v1 [quant-ph] 13 Nov 2017

Fisher recently proposed a mechanism by which quantum phenomena might affect cognition [1]. Phosphorus atoms populate biochemistry. A phosphorus nucleus's spin, he argued, can store quantum information (QI) for long times. The nucleus has a spin quantum number $s = \frac{1}{2}$. Hence the nucleus forms a *qubit*, a quantum two-level system. The qubit is the standard unit of QI.

Fisher postulated physical processes that might entangle phosphorus nuclei. Six phosphorus atoms might, with other ions, form *Posner molecules* $\mathrm{Ca_9(PO_4)_6}$ [2–4].[1] The molecules might protect the spins' states for long times. Fisher also described how the QI stored in the spins might be read out. This QI, he conjectured, could impact neuron firing. The neurons could participate in *quantum cognition*.

These conjectures require empirical testing. Fisher has proposed experiments [1], including with Radzihovsky [5]. Some experiments have begun [6].

Suppose that Fisher conjectures correctly. How effectively could the spins process QI? We provide a framework for answering this question, and we begin answering. We translate Fisher's physics and chemistry into information theory. The language of molecular tumbling, heat, etc. is replaced with the formalism of Bloch-sphere rotations, positive operator-valued measures (POVMs), computational bases, etc. Additionally, we identify and quantify QI-storage, -communication, and -computation capacities of the phosphorus nuclear spins and Posners.

This paper is intended for QI scientists, for chemists, and for biophysicists. Some readers may require background about the QI theory behind the results. We refer these readers to App. A and to [7, 8]. Next, we overview this paper's contributions.

Computational bases before and after molecule formation: Phosphorus nuclear spins originate outside Posners, in Fisher's narrative. The spins occupy ions that join together, forming Posners. Molecular formation changes how QI is encoded physically.

Outside of molecules, phosphorus nuclear spins couple little to orbital degrees of freedom (DOFs). Spin states form an obvious choice of computational basis.[2] In a Posner molecule, the spins are indistinguishable. They occupy an antisymmetric state [1, 5]: The spins entangle with orbital DOFs. Which physical states form a useful computational basis is not obvious.

We identify such a basis. Molecule formation, we posit, maps premolecule spin states to antisymmetric molecule states deterministically. The premolecule orbital state determines the map. We formalize the map with a projector-valued measure (PVM). The mapped-to antisymmetric states form the computational basis, in terms of which Posners' QI processing should be expressed.

Quantum error-correcting and -detecting codes: The basis elements may decohere quickly: Posners' geometry protects only spins. The basis elements

---

[1] $\mathrm{Ca_9(PO_4)_6}$ has been called the *Posner cluster* and *Posner molecule*. We call it the *Posner*, for short.

[2] In QI, computations are expressed in terms of a *computational basis* for the system's Hilbert space [7]. Basis elements are often represented by bit strings, as in $\{|00\ldots0\rangle, |00\ldots01\rangle, \ldots |11\ldots1\rangle\}$.

are spin-and-position entangled states. Do the dynamics protect any states against errors?

Hamiltonians' ground spaces may form quantum error-correcting and -detecting codes (QECD codes) [8]. One might hope to relate the Posner Hamiltonian H_{Pos} to a QECD code. Alas, H_{Pos} has not been characterized.[3]

Yet H_{Pos} likely preserves two observables. One, $\mathcal{G}_C$, generates cyclic permutations of the spins. One such permutation shuffles the spins counterclockwise about the molecule's symmetry axis, through an angle $2\pi/3$. This permutation preserves the Posner's geometry [1–4]. The other charge, $S^{z_{\mathrm{in}}}_{12\ldots6}$, is the spins' total z_{in}-component. (The internal-frame axis $\hat{z}_{\mathrm{in}}$ remains fixed relative to the atoms' positions.)

The dynamics likely preserve eigenstates shared by $\mathcal{G}_C$ and $S^{z_{\mathrm{in}}}_{1\ldots6}$. Yet $\mathcal{G}_C$ shares many eigenbases with $S^{z_{\mathrm{in}}}_{1\ldots6}$: The charges fail to form a complete set of commuting observables (CSCO). We identify a useful operator that breaks the degeneracy: $\mathbf{S}^2_{123} \otimes \mathbf{S}^2_{456}$ equals a product of the spin-squared operators $\mathbf{S}^2$ of trios of a Posner's spins. This operator (i) respects the Posner's geometry and (ii) facilitates the construction of Posner states that can fuel universal quantum computation (discussed below).

From the eigenbasis shared by $\mathcal{G}_C$, $S^{z_{\mathrm{in}}}_{1\ldots6}$, and $\mathbf{S}^2_{123} \otimes \mathbf{S}^2_{456}$, we form QECD codes. A state $|\psi\rangle$ in one charge sector of $\mathcal{G}_C$ and one sector of $S^{z_{\mathrm{in}}}_{1\ldots6}$ likely cannot transform, under the dynamics, into a state $|\phi\rangle$ in a second sector of $\mathcal{G}_C$ and a second sector of $S^{z_{\mathrm{in}}}_{1\ldots6}$. Hence $|\psi\rangle$ and $|\phi\rangle$ suggest themselves as codewords. Charge preservation would prevent one codeword from evolving into another.

We construct two quantum codes, each partially protected by charge preservation. Via one code, each Posner encodes one qutrit. The codewords correspond to distinct eigenvalues of $\mathcal{G}_C$. This code detects arbitrary single-physical-qubit errors. Via the second code, each Posner encodes one qubit. This repetition code corrects two bit flips. The codewords correspond to distinct eigenvalues of $S^{z_{\mathrm{in}}}_{1\ldots6}$.

Model of Posner quantum computation: Fisher posits chemical processes, such as binding, that Posners may undergo [1]. We abstract away the chemistry, formalizing the computations effected by the processes. These effected *Posner operations* form the model of *Posner quantum computation*.

The model includes the preparation of singlets $\frac{1}{\sqrt{2}}(|01\rangle - |10\rangle)$. Qubits can rotate arbitrarily when the phosphorus atoms are outside molecules. The qubits evolve trivially, under the identity $\mathbb{1}$, when Posners form. But Posner creation associates a hextuple of qubits with a geometry and with an observable $\mathcal{G}_C$.

A Posner's six qubits can undergo identical arbitrary rotations. Also, measurements can be performed: $\mathcal{G}_C$ has eigenvalues $\tau = 0, \pm 1$. Whether Posners A and B satisfy $\tau_A + \tau_B = 0$ can be measured projectively. If the equation is satisfied, the twelve qubits can undergo coordinated rotations.

Finally, hextuples can cease to correspond to geometries or to $\mathcal{G}_C$'s (as Posners break down into their constituent ions). Thereafter, qubits can rotate independently again, group together into new hextuples, etc.

This model enables us to recast Fisher's narrative [1] as a quantum circuit. We also identify a criterion necessary for constructing, from Posner operations, quantum circuits of nonconstant depth: Molecules must break down and form anew. Only outside molecules can qubits undergo arbitrary rotations. Only in molecules can qubits undergo entangling operations late in a computation. To alternate between rotating and entangling, qubits must leave and enter Posners.

Entanglement generated by, and quantum-communication application of, molecular binding: Two Posners, Fisher conjectures, can bind together [1]. Quantum-chemistry calculations support the conjecture [9]. The binding is expected to entangle the Posners [1]. How much entanglement does binding generate, and entanglement of what sort?

We characterize the entanglement in two ways. First, we compare Posner binding to a Bell measurement [7]. A Bell measurement yields one of four possible outcomes—two bits of information. Posner binding transforms a subspace as a coarse-grained Bell measurement. A Bell measurement is performed, and one bit is discarded, effectively.

Second, we present a quantum-communication protocol reliant on Posner binding. We define a qutrit (three-level) subspace of the Posner Hilbert space. A Posner P may occupy a state $|\psi\rangle = \sum_{j=0}^{2} c_j |j\rangle$ in the subspace. The coefficients $|c_j|^2$ form a probability distribution Q. This distribution has a probability p of being teleported to another Posner, P'. Another distribution, $\tilde{Q}$, consists of combinations of the $|c_j|^2$'s. $\tilde{Q}$ has a probability $1-p$ of being teleported. Measuring P' in the right basis would yield an outcome distributed according to Q or according to $\tilde{Q}$.

The weights of $|\psi\rangle$ (or combinations of the weights) are teleported [10]. The coherences are not. We therefore dub the protocol *incoherent teleportation*. The dephasing comes from the binding's simulation of a coarse-grained Bell measurement. Bell measurements teleport QI coherently.

Incoherent teleportation effects a variant of superdense coding [11]. A trit (a classical three-level system) is communicated effectively, while a bit is communicated directly. The trit is encoded superdensely in the bit, with help from Posner binding.

Posner-molecule state that can serve as a universal resource for measurement-based quantum computation: Measurement-based quantum computation (MBQC) [12–14] is a quantum-computation model alternative to the circuit model [15]. MBQC begins with a many-body entangled state $|\psi\rangle$. Single qubits are mea-

[3] A characterization may be expected in [9].

sured adaptively.

MBQC can efficiently simulate universal quantum computation if begun with the right $|\psi\rangle$. Most quantum states cannot serve as universal resources [16]. Cluster states [12, 17, 18] on 2D square lattices can [12, 13, 19, 20]. So can the Affleck-Kennedy-Lieb-Tasaki (AKLT) state [21–23] on a honeycomb lattice, $|\text{AKLT}_{\text{hon}}\rangle$. Local measurements can transform $|\text{AKLT}_{\text{hon}}\rangle$ into the universal cluster state. Hence $|\text{AKLT}_{\text{hon}}\rangle$ can fuel universal MBQC [20, 24].

We define a variation $|\text{AKLT}'_{\text{hon}}\rangle$ on $|\text{AKLT}_{\text{hon}}\rangle$. $|\text{AKLT}'_{\text{hon}}\rangle$ can be prepared efficiently with Posner operations. Preparing $|\text{AKLT}_{\text{hon}}\rangle$, one projects onto a spin-$\frac{3}{2}$ subspace. Preparing $|\text{AKLT}'_{\text{hon}}\rangle$, one projects onto a slightly larger subspace. Local measurements (supplemented by Posner hydrolyzation, singlet formation, and Posner creation) can transform $|\text{AKLT}'_{\text{hon}}\rangle$ into the universal cluster state. Hence $|\text{AKLT}'_{\text{hon}}\rangle$ can fuel universal MBQC as $|\text{AKLT}_{\text{hon}}\rangle$ can.

Whether Posner operations can implement the extra local measurements, or the adaptive measurements in MBQC, remains an open question. Yet the universality of a Posner state, efficiently preparable by a (conjectured) biological system, is remarkable. Most states cannot fuel universal MBQC [16]. The universality of $|\text{AKLT}'_{\text{hon}}\rangle$ follows from (i) Posners' geometry and (ii) their ability to share singlets.

Like $|\text{AKLT}_{\text{hon}}\rangle$, $|\text{AKLT}'_{\text{hon}}\rangle$ is a projected entangled-pair state (PEPS) [25]. The state is formed from two basic tensors. Each tensor has three physical qubits and three virtual legs. One virtual leg has bond dimension six. Each other virtual leg has bond dimension two. $|\text{AKLT}'_{\text{hon}}\rangle$ is the unique ground state of some frustration-free Hamiltonian $H_{\text{AKLT}'}$ [26, 27]. The relationship between $H_{\text{AKLT}'}$ and H_{Pos} remains an open question. So does whether $H_{\text{AKLT}'}$ has a constant-size gap.

Entanglement's influence on binding probabilities: Entanglement, Fisher conjectures, can affect Posners' probability of binding together [1]. He imagined a Posner A entangled with a Posner A' and a B entangled with a B'. Suppose that A has bound to B. A' more likely binds to B', Fisher argues, than in the absence of entanglement.

We test the principle behind Fisher's conjecture, in a two-Posner example. Let A and B denote the Posners. First, we suppose that (i) neither Posner contains entangled spins and (ii) A shares no entanglement with B. Next, we suppose that (i) each Posner contains one singlet and (ii) A shares one singlet with B. The entanglement boosts the binding probability by $\approx 0.6\%$. Though small, the boost supports Fisher's conjecture. Computing power limited our test's size. Yet our technique can be scaled up to Fisher's four-Posner example.

Comparison with DiVincenzo's criteria: DiVincenzo codified the criteria required for realizing quantum computation and communication [28]. We compare the criteria with Fisher's narrative. At least most criteria are satisfied, if sufficient control is available. Whether the gate set is universal remains an open question.

Organization of this paper: Section I reviews Fisher's proposal. Section II details the physical set-up and models Posner creation. How Posner creation changes the physical encoding of QI appears in Sec. III. QECD codes are presented in Sec. IV.

The model of Posner quantum computation is defined in Sec. V. Posner binding is analyzed, and applied to incoherent teleportation, in Sec. VI. Section VII showcases the universal resource state $|\text{AKLT}'_{\text{hon}}\rangle$.

Section VIII quantifies entanglement's effect on molecular-binding probabilities. Quantum cognition is compared with DiVincenzo's criteria in Sec. IX. Opportunities for further study are detailed in Sec. X.

I. REVIEW: FISHER'S QUANTUM-COGNITION PROPOSAL

Biological systems are warm, wet, and large. Such environments quickly diminish quantum coherences. Fisher catalogued the influences that could decohere nuclear spins in biofluids. Examples include electric and magnetic fields generated by other nuclear spins and by electrons.

These sources, Fisher estimated, decohere the phosphorus-31 (^{31}P) nuclear spin slowly. Coherence times might reach ~ 1 s or $10^5 - 10^6$ s, depending on the ion or molecule occupied by the phosphorus. No other biologically prevalent atom, Fisher conjectures, has such a long-lived nuclear spin.

Phosphorus atoms inhabit many biological ions and molecules. Examples include the phosphate ion, PO_4^{3-}. Three phosphates feature in the molecule *adenosine triphosphate* (ATP). ATP stores energy that powers chemical reactions. Two phosphates can detach from an ATP molecule, forming a *diphosphate* ion. A diphosphate can break into two phosphates, with help from the enzyme *pyrophosphatase*. The two phosphates' phosphorus nuclear spins form a *singlet*, Fisher and Radzihovsky (F&R) conjecture [1, 5]. A singlet is a maximally entangled state. Entanglement is a correlation, shareable by quantum systems, stronger than any achievable by classical systems [7].

Many biomolecules contain phosphate ions. Occupying a small molecule, Fisher argues, could shelter the phosphorus nuclear spin: Small molecules tumble in fluids. The average of an external field $\mathbf{B}$, over uniform tumbling, vanishes. A $\mathbf{B}$ whose average magnitude vanishes cannot decohere spins quickly.

Which small biomolecules could a phosphorus inhabit? An important candidate is $Ca_9(PO_4)_6$. A Posner consists of six phosphate ions (PO_4^{3-}) and nine calcium ions (Ca^{2+}) [2–4]. Posners form in some simulated biofluids and possibly in vivo [29–31]. A Posner could conceivably contain a phosphate that forms a singlet with a phosphate in another Posner. The Posners would share entanglement.

Two Posners can bind together, according to quantum-chemistry calculations [1, 9]. The binding projects the Posners onto a possibly entangled state. Moreover, pre-existing entanglement could affect the probability that Posners bind.

Bindings, influenced by entanglement, could influence neuron firing. Suppose that a Posner A shares entanglement with a Posner A' and that a B shares entanglement with a B'. Posners A and B could enter one neuron, while A' and B' enter another. Suppose that A binds with B. The binding, with entanglement, could raise the probability that A' binds to B'.

Bound-together Posners move slowly, Fisher argues. Compound molecules must displace many water molecules, which slow down the pair. Relatedly, the Posner pair has a large moment of inertia. Hence the pair rotates more slowly than separated Posners by the conservation of angular momentum.

Hydrogen ions H^+ can attach easily to slow molecules, Fisher expects. H^+ *hydrolyzes* Posners, breaking the molecules into their constituent ions. Hence entanglement might correlate hydrolyzation of A and B with hydrolyzation of A' and B'. Hydrolyzation would release calcium ions Ca^{2+} into the neurons. Suppose that many entangled Posners hydrolyzed in these two neurons. The neurons' Ca^{2+} concentrations could rise. The neurons could fire synchronously due to entanglement.

II. PHYSICAL SET-UP AND POSNER-MOLECULE CREATION

This section concerns (i) the physical set-up and (ii) the joining together of phosphates (and calcium ions) in Posner molecules. Part of the material appears in [1, 5] and is reviewed. Part of the material has not, according to our knowledge, appeared elsewhere.

The phosphorus nuclei are associated with spin and spatial Hilbert spaces in Sec. II A. Section II B reviews, and introduces notation for, the Posner's geometry. Section II C models the creation of a Posner from close-together ions. The ions can have distinguishable DOFs before, but not after, forming a Posner.

II A. Spin and spatial Hilbert spaces

Each phosphorus nucleus has two relevant DOFs: a spin and a position. We will sometimes call the position the *orbital* or *spatial* DOF. Let $\mathcal{H}_{\text{nuc}}^{\text{spin}}$ and $\mathcal{H}_{\text{nuc}}^{\text{orb}}$ denote the associated Hilbert spaces. The nucleus has a spin quantum number of $s = \frac{1}{2}$. Hence $\mathcal{H}_{\text{nuc}}^{\text{spin}} = \mathbb{C}^2$. The orbital Hilbert space is infinite-dimensional: $\dim(\mathcal{H}_{\text{nuc}}^{\text{orb}}) = \infty$. Each phosphorus nucleus's Hilbert space decomposes as $\mathcal{H}_{\text{nuc}} = \mathcal{H}_{\text{nuc}}^{\text{spin}} \otimes \mathcal{H}_{\text{nuc}}^{\text{orb}}$.

The electrons' states transform trivially under all relevant operations, Fisher and Radzihovsky (F&R) conjecture [5]. We therefore ignore the electronic DOFs. We ignore calcium ions similarly. We focus on the DOFs that might store QI for long times.

II B. Posner-molecule geometry and notation

Quantum-chemistry calculations have shed light on the shapes available to Posners [2–4, 9]. A Posner's shape depends on the environment. Posners in biofluids have begun to be studied [4]. We follow [1, 5], supposing that more-detailed studies will support [4].

The Posner forms a cube (Fig. 1). At each face's center sits a phosphate. The molecule has one symmetry axis. The axis coincides with a diagonal of the cube. The Posner remains invariant under $2\pi/3$ rotations about this diagonal: The molecule has C_3 symmetry.

This cube diagonal serves as the z-axis $\hat{z}_{\text{in}}$ of a reference frame fixed in the molecule. The atoms' positions remain constant relative to this *internal frame*. The internal frame can move relative to the lab frame, denoted by the subscript "lab." The spins' Bloch vectors are defined with respect to the lab frame.

Imagine gazing down the diagonal, as in Fig 1a. You would see three phosphates that form a triangle. We label the triangle's z_{in}-coordinate by h_+. One hidden phosphate sits directly behind each visible phosphate. We label by h_- the hidden triangle's z_{in}-coordinate. $\hat{z}_{\text{in}}$ points oppositely the direction in which we imagined gazing. Hence $h_+ > h_-$.

ϕ labels the triangles' shared orientation, as shown in Fig. 1b. We denote by φ_j the angular orientation of cube face j (the site of a phosphate): Imagine rotating the x_{in}-axis counterclockwise until it intersects the cube face's center (a phosphate). The angle swept out is φ_j. One visible and one invisible phosphate sit at the angle ϕ; another pair, at $\phi + 2\pi/3$; and another pair, at $\phi + 4\pi/3$. We label the center of cube face j (the site of phosphate j) with an angle and a height: (φ_j, h_j).

II C. Qualitative model for the creation of a Posner molecule

Posners form from phosphate and calcium ions. We model the formation process qualitatively in this section. We first review how, according to Fisher, phosphorus nuclear spins might come to form singlets. We then envision phosphates falling into a Lennard-Jones potential as a Posner forms. F&R have discussed the indistinguishability of phosphorus nuclei in a Posner [1, 5]. We expand upon this discussion, considering how distinguishable ions become indistinguishable.

Several molecules contain phosphate ions PO_4^{3-}. Examples include ATP (Sec. I). Each ATP molecule contains three phosphates (hence the "triphosphate"). Two of the phosphates can break off, forming a diphosphate ion. The enzyme pyrophosphatase can hydrolyze a

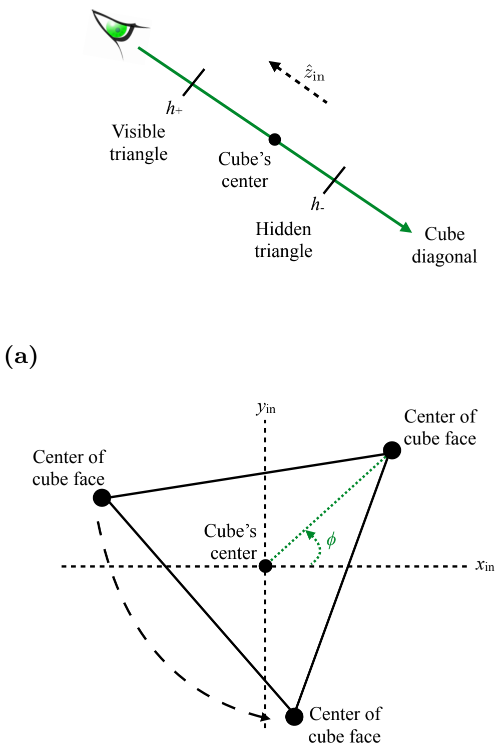

FIG. 1: Posner-molecule geometry and coordinates: Quantum-chemistry calculations have shed light on the Posner molecule's geometry [2–4, 9]. The molecule forms a cube. At each cube face's center sits one phosphate ion (PO_4^{3-}). The molecule appears to have one symmetry axis when in biofluids [1, 4]. The axis coincides with a cube diagonal. Imagine gazing down the diagonal, as in Fig. 1a. In the opposite direction points the internal z-axis, $\hat{z}_{\rm in}$. (The internal reference frame remains fixed relative to the atoms' positions.) Gazing down the diagonal, you see three phosphate ions (the large, black dots in Fig. 1b). The phosphates form a triangle. ϕ denotes the least angle swept out counterclockwise from the $+x_{\rm in}$-axis to a phosphate. The triangle remains invariant under rotations, about the symmetry axis, through an angle $2\pi/3$. The long-dash line in Fig. 1b illustrates such a rotation. The invariance endows the Posner with C_3 symmetry. Directly behind the visible phosphates sit the other three phosphates (Fig. 1a). We denote the triangles' $z_{\rm in}$-coordinates by $h_\pm$.

diphosphate, cleaving the ion into separated phosphates. The separated phosphates contain phosphorus nuclear spins that, Fisher conjectures [1], form a singlet.

Let 1 and 2 label the phosphorus nuclear spins. Let $\hat{z}_{\rm enz}$ denote the z-axis of a reference frame fixed in the enzyme. Let $\hat{S}_{z_{\rm enz}}$ denote the $z_{\rm enz}$-component of a phosphorus nucleus's spin operator. Let $|\uparrow\rangle$ and $|\downarrow\rangle$ denote the $\hat{S}_{z_{\rm enz}}$ eigenstates: $\hat{S}_{z_{\rm enz}}|\uparrow\rangle = \frac{\hbar}{2}|\uparrow\rangle$, and $\hat{S}_{z_{\rm enz}}|\uparrow\rangle = -\frac{\hbar}{2}|\uparrow\rangle$.

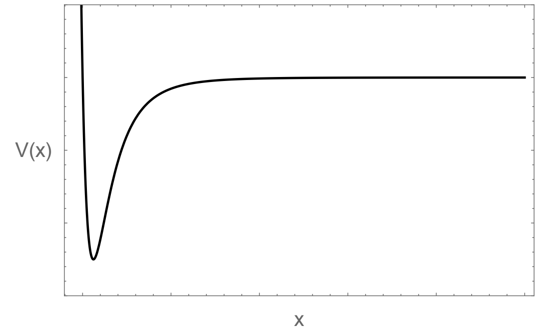

FIG. 2: Lennard-Jones potential: The Lennard-Jones potential, $V_{\rm LJ}(x) = \frac{a}{x^{12}} - \frac{b}{x^6}$, models van der Waals forces between particles. The real parameters $a, b > 0$. We grossly approximate, with $V_{\rm LJ}(x)$, the potential experienced by phosphate ions coalescing into a Posner molecule. x denotes the distance from a phosphate to the system's center of mass.

The singlet has the form

$$|\Psi^-\rangle := \frac{1}{\sqrt{2}}(|\uparrow\rangle|\downarrow\rangle - |\downarrow\rangle|\uparrow\rangle)\,. \tag{1}$$

The singlet is one of the four *Bell pairs*. The Bell pairs are mutually orthogonal, maximally entangled states of pairs of qubits [7]. Bell pairs serve as units of entanglement in QI.

Phosphorus nuclei are identical fermions, as F&R emphasize [1, 5]. But some of the nuclei's DOFs might be distinguishable before Posners form. Consider, for example, two ATP molecules on opposite sides of a petri dish. Call the molecules A and B. A diphosphate could break off from each ATP molecule. Each diphosphate could hydrolyze into two phosphates, A_1 and A_2 or B_1 and B_2. Consider the phosphorus nuclear spins of one phosphate pair—say, of A_1 and A_2. These spins would be indistinguishable: Neither nucleus could be associated with an upward-pointing spin or with a downward-pointing spin.

But the spatial DOF of A_1 and A_2 could be distinguished from the spatial DOF of B_1 and B_2: We can imagine painting phosphate pair A red and phosphate pair B blue. The phosphate pairs could diffuse to the dish's center. The red pair and the blue pair could be tracked along their trajectories.

Consider six phosphates (and nine Ca^{2+} ions) approaching each other. We model the ions qualitatively as subject to a Lennard-Jones potential. Such potentials feature in molecular-dynamics simulations [32]. The model encapsulates interatomic forces' key features.

We temporarily approximate each phosphate as having a classical position. Let x denote some phosphate's distance from the ions' center of mass. Figure 2 illustrates the Lennard-Jones potential,

$$V_{\rm LJ}(x) = \frac{a}{x^{12}} - \frac{b}{x^6}\,. \tag{2}$$

The real parameters $a, b > 0$.

The potential has two limiting behaviors. The behaviors split where the derivative vanishes: $\frac{dV_{\rm LJ}(x)}{dx} = 0 \quad \Rightarrow \quad x = \left(\frac{2a}{b} \right)^{1/6} =: x_0$. At large distances $x \gg x_0$, the negative term in Eq. (2) dominates. The derivative is positive, so $V_{\rm LJ}(x)$ attracts. Far-apart ions approach each other. At short distances $x \ll x_0$, the positive term dominates. The derivative is negative, so $V_{\rm LJ}(x)$ repels. The ions cannot coincide at the same position.

Consider an ion approaching $x = 0$ from afar. $V_{\rm LJ}(x)$ drops precipitously when the concavity changes from negative to positive: $\frac{d^2 V_{\rm LJ}(x)}{dx^2} = 0 \quad \Rightarrow \quad x = \left(\frac{26a}{7b} \right)^{1/6}$. This point forms a "lip" of the potential. The ions have more energy, separated, than they would have in a molecule. The ions slide down the potential well, releasing binding energy as heat. The heat disrupts the environment, which effectively measures the ions' state.[4]

At the well's bottom, the ions constitute a Posner molecule. The phosphorus nuclei's quantum states have position representations (wave functions) that overlap significantly. The nuclei are indistinguishable [5]: No nuclear pair can be identified as red-painted or as blue-painted. The six phosphorus nuclei occupy a totally antisymmetric spin-and-spatial state. We will abbreviate "totally antisymmetric" as "antisymmetric."

II D. Formalizing the model for Posner-molecule creation

Let us model, with mathematical tools of QI, the environment's measuring of the ions, the creation of a Posner, and the antisymmetrization process. Let $t_{\rm Pos}$ denote the scale of the time over which the ions slide down the Lennard-Jones well from the lip, emit heat, jostle about, and settle into the Posner geometry.

The environment effectively measures the ions with a frequency $1/t_{\rm Pos}$. We model the measurement with a *projector-valued measure* (PVM) [7]. Consider the Hilbert space $(\mathcal{H}_{\rm nuc})^{\otimes 6}$ of the Posner's six phosphorus nuclei. An antisymmetric subspace $\mathcal{H}^-_{\text{no-coll.}}$ consists of the states available to the indistinguishable nuclei. (The states are detailed in Sec. III C.) The subscript stands for "no-colliding-nuclei": No two nuclei can inhabit the same Posner-cube face.

Let $\Pi^-_{\text{no-coll.}}$ denote the projector onto $\mathcal{H}^-_{\text{no-coll.}}$. The PVM has the form

$$\left\{ \Pi^-_{\text{no-coll.}}, \mathbb{1} - \Pi^-_{\text{no-coll.}} \right\} . \tag{3}$$

Suppose that one length-$(1/t_{\rm Pos})$ time interval has just passed. The environment has measured the ions. Suppose that, during the interval, the ions have emitted considerable heat. The environment has registered the outcome "Yes, a Posner has formed." $\Pi^-_{\text{no-coll.}}$ has projected the ions' joint state.

Suppose, instead, that the ions have not emitted much heat. The environment has registered the outcome "No, no Posner has formed." $\mathbb{1} - \Pi^-_{\text{no-coll.}}$ has projected the ions' joint state.[5,6]

Let $\hat{\mathbf{S}}_{1\ldots6}$ denote the six phosphorus nuclei's total spin operator. We assume that Posner creation can be modeled as a two-stage process. First, the independent phosphates tumble in the fluid. The spins rotate unitarily.

Second, the phosphates combine into a Posner via an evolution that preserves $(\hat{S}^{z_{\rm lab}})^{\otimes 6}$. The assumption follows from Fisher's claims that the spins barely decohere [1]: The spins do not entangle with anything. At worst, therefore, the spins rotate on the Bloch sphere during Posner creation. Most rotations fail to preserve $\hat{S}^{z_{\rm lab}}$. But Posner creation that involves rotations is mathematically equivalent to (i) rotations followed by (ii) $(\hat{S}^{z_{\rm lab}})^{\otimes 6}$-conserving Posner creation. The initial rotations can be absorbed into the pre-Posner rotations. We therefore will say that Posner creation "essentially preserves" $(\hat{S}^{z_{\rm lab}})^{\otimes 6}$.

III. ENCODED STATES AND THEIR CHANGING PHYSICAL REPRESENTATIONS

Phosphorus nuclear spins cleanly encode QI before Posners form. The spins, Fisher conjectures, are decoupled from the nuclei's positions [1]. Posner creation antisymmetrizes the spin-and-orbital state. The spins become entangled with the positions, no longer encoding QI cleanly.

But, we posit, Posner creation maps each pre-Posner spin state to an antisymmetric Posner state deterministically. Posner creation preserves QI but changes how QI is encoded physically. Hence spin configurations can

---

4 That the environment measures the state via heat transfer was proposed in [1].

5 One might try to model the environment as measuring the ions continuously. This model is unfaithful: The environment would continuously project the ions onto states inaccessible to a Posner. No Posner could form, due to the quantum Zeno effect [33]. The Posner-creation time $t_{\rm Pos}$ sets the measurement's time scale.

6 F&R suggest that, upon forming, a molecule is entangled with its environment [5, Eq. (7)]. Our PVM is consistent with F&R's model, by the principle of deferred measurement [7]: Let S denote a general quantum system. A measurement of S consists of two steps: First, S is entangled with a memory M. Second, M is measured. Suppose that (i) the entanglement is maximal and (ii) the M measurement is projective. The M measurement projects the system's state. Suppose that S evolves after the M measurement. This entangling, M measurement, and evolution is equivalent to the entangling, followed by the S evolution, followed by the M measurement. The M measurement can be deferred until after the evolution. Deferral fails to alter the measurement statistics. Let S denote the nuclei, and let M denote the environment. The M measurement is deferred in F&R's model, not in ours. The models are equivalent, by the deferred-measurement principle.

label a computational basis for the Posner Hilbert space, e.g., $\uparrow\uparrow\uparrow\uparrow\uparrow\uparrow \equiv 000000$.

This section is organized as follows. Section III A concerns pre-molecule phosphorus nuclear spins. Section III B introduces notation. A map between (i) physical states of pre-Posner spins and (ii) logical states is formalized. Logical states are mapped to Posner states in Sec. III C.

III A. Physical encoding of quantum information in the phosphorus nuclei that will form a Posner molecule

Consider six phosphates that approach each other, soon to form (with Ca^{2+} ions) a Posner. We index the phosphorus nuclei as $a = 1, 2, \ldots, 6$. Each nucleus has a spin DOF and an orbital DOF. Nucleus a occupies some quantum state $\rho_a \in \mathcal{D}(\mathcal{H}_{\text{nuc}})$. $\mathcal{D}(\mathcal{H})$ denotes the set of density operators (trace-one linear operators) defined on the Hilbert space $\mathcal{H}$. ρ_a may be pure (unentangled with any external DOFs) or mixed (entangled with external DOFs, e.g., another phosphorus nucleus's spin).

Tracing out the orbital DOF yields the reduced spin state: $\rho_a^{\text{spin}} := \text{Tr}_{\text{orb}}(\rho_a) \in \mathcal{D}(\mathbb{C}^2)$. The magnetic spin quantum number $m_a = \pm\frac{1}{2}$ quantifies the spin's z_{lab}-component.

Shifting focus from chemistry to information theory, we adopt QI notation: We usually omit hats from operators, and we often omit factors of $\hbar$ and $\frac{1}{2}$. We often replace the spin operator's α-component with the Pauli α-operator, for $\alpha = x, y, z$: $\hat{S}^\alpha \equiv S^\alpha = \frac{\hbar}{2}\,\sigma^\alpha \equiv \sigma^\alpha$. The σ^z eigenstates are often labeled as $|0\rangle := |\uparrow\rangle$ and $|1\rangle := |\downarrow\rangle$.

Tracing out the spin DOF from ρ_a yields the reduced orbital state: $\rho_a^{\text{orb}} := \text{Tr}_{\text{spin}}(\rho_a) \in \mathcal{D}(\mathcal{H}_{\text{nuc}}^{\text{orb}})$. We parameterize $\mathcal{H}_{\text{nuc}}^{\text{orb}}$ with the eigenstates $|\mathbf{x}\rangle$ of the position operator, $\mathbf{x}$. The coordinates are defined with respect to the lab frame. $\{|\mathbf{x}\rangle\}$ forms a continuous set.

The spin and/or orbital DOFs can store QI. But water and other molecules buffet the phosphates. An independent phosphate's position decoheres quickly. The spin, in contrast, is expected to remain coherent for long times (see Sec. IX and [1]). The spins encode protected QI.

The nuclear spins form six qubits. The qubits correspond to the Hilbert space $(\mathcal{H}_{\text{nuc}}^{\text{spin}})^{\otimes 6} = \mathbb{C}^{12}$, which has dimensionality $2^6 = 64$. A useful basis for $\mathcal{H}_{\text{nuc}}^{\text{spin}}$ consists of tensor products of σ^z eigenstates: $\mathcal{B}_{\text{comp}} := \{|0, 0, \ldots, 0\rangle, |0, 0, \ldots, 0, 1\rangle, \ldots, |1, 1, \ldots, 1\rangle\}$. The notation $|A, B, \ldots, K\rangle \equiv |A\rangle \otimes |B\rangle \otimes \ldots \otimes |K\rangle$. The set $\mathcal{B}_{\text{comp}}$ is called the *computational basis for the physical states*.

Consider N hextuples of phosphates (N sets of six phosphates). The phosphorus nuclei correspond to a spin space $\mathbb{C}^{6N}$. We suppose, without loss of generality, that the $6N$ spins occupy a pure joint state $|\psi\rangle$. Each hextuple could contain three singlets, for example. Or a spin in some hextuple A could form a singlet with a spin in some hextuple B.

III B. Notation and quick review: Encodings

Imagine an agent Alice who wishes to send another agent, Bob, a message. A quantum message is a quantum state $|\psi_{\text{L}}\rangle \in \mathcal{H}_{\text{L}}$. $|\psi_{\text{L}}\rangle$ is called the *logical state*. Let $\mathcal{B}_{\text{comp}}^{\text{L}}$ denote a preferred basis for the Hilbert space $\mathcal{H}_L$. Operations are expressed in terms of this *computational basis for the logical space*.

Alice must encode $|\psi_{\text{L}}\rangle$ in the state of a physical system. The agents would choose a *code*, a dictionary between the computational basis $\mathcal{B}_{\text{comp}}^{\text{L}}$ for the logical space and the computational basis $\mathcal{B}_{\text{comp}}$ for the physical space. Alice would decompose $|\psi_{\text{L}}\rangle$ in terms of $\mathcal{B}_{\text{comp}}^{\text{L}}$ elements $|j_{\text{L}}\rangle$; replace each $|j_{\text{L}}\rangle$ with a $\mathcal{B}_{\text{comp}}$ element $|j\rangle$; and prepare the resultant *physical state*: $|\psi_{\text{L}}\rangle = \sum_j c_j |j_{\text{L}}\rangle = \sum_j c_j |j\rangle = |\psi\rangle$.

$\mathcal{H}_{\text{L}}$ cannot be arbitrarily large, if the encoding is *faithful*. A faithful encoding can be reversed, yielding the exact form of $|\psi_{\text{L}}\rangle$. The six-qubit state $|\psi\rangle$ can faithfully encode a $|\psi_{\text{L}}\rangle$ of ≤ 6 qubits, called *logical qubits*. The phosphorus nuclear spins—the physical DOFs that encode the logical qubits—are called *physical qubits*.

Suppose that $|\psi_{\text{L}}\rangle$ is a state of six logical qubits. We label the logical space's computational basis as $\mathcal{B}_{\text{comp}}^{\text{L}} = \{|00\ldots0\rangle, |00\ldots01\rangle, \ldots, |11\ldots1\rangle\}$. A simple code from $\mathcal{B}_{\text{comp}}$ to $\mathcal{B}_{\text{comp}}^{L}$ has the form

$$|m_1, \ldots, m_6\rangle \equiv |m_1 \ldots m_6\rangle\,, \tag{4}$$

for $m_1, \ldots, m_6 = 0, 1$. For example, all six physical qubits' pointing upward is equivalent to all six logical qubits' pointing upward: $|0, \ldots, 0\rangle = |0 \ldots 0\rangle$.

III C. Transformation of the encoding during Posner-molecule creation

Consider six phosphates that join together, forming a Posner. The phosphorus nuclei might begin with distinguishable DOFs (Sec. II C). The spins entangle with each other and with orbital DOFs [1, 5]. The QI $|\psi_{\text{L}}\rangle$ stored in the spins "spills" into the orbital DOFs.

But, we posit, Posner creation maps each pre-Posner spin state to an antisymmetric Posner state deterministically. The physical qubits change from spins to spin-and-orbital DOFs. The physical state's form changes from $|\psi\rangle \in \mathbb{C}^{12}$ to some $|\psi'\rangle \in \mathcal{H}_{\text{no-coll.}}^{-}$. The Posner state $|\psi'\rangle$ encodes $|\psi_{\text{L}}\rangle$ faithfully.

Reparameterizing position will prove useful. We labeled by $\mathbf{x}$ a pre-Posner phosphorus nucleus's position. A Posner's phosphorus nuclei occupy the centers of cube faces (Fig. 1). Let $\mathbf{r} = (r, \varphi, h)$ label a nucleus's position relative to the cube's center. The cube's size determines each nucleus's distance r from the cube center. Hence we suppress the r: $|\mathbf{r}\rangle \equiv |\varphi, h\rangle$. The angle variable is restricted to $\varphi = \phi, \phi + 2\pi/3, \phi + 4\pi/3$ (Fig. 1b). The height variable is restricted to $h = h_\pm$ (Fig. 1a).

Which states can one phosphorus nucleus occupy when in a Posner? One might reason naïvely as follows. The basis $\{|0\rangle, |1\rangle\}$ spans the nuclear-spin space $\mathcal{H}_{\rm nuc}^{\rm spin}$. The basis $\{|\varphi, h\rangle\}$ spans the nuclear-position space $\mathcal{H}_{\rm nuc}^{\rm orb}$. Hence a product basis spans the nuclear Hilbert space $\mathcal{H}_{\rm nuc} = \mathcal{H}_{\rm nuc}^{\rm spin} \otimes \mathcal{H}_{\rm nuc}^{\rm orb}$:

$$\begin{aligned}&\{|0; \phi, h_+\rangle, |0; \phi, h_-\rangle, |0; \phi + 2\pi/3, h_+\rangle, |0; \phi + 2\pi/3, h_-\rangle,\\ &|0; \phi + 4\pi/3, h_+\rangle, |0; \phi + 4\pi/3, h_-\rangle, |1; \phi, h_+\rangle, |1; \phi, h_-\rangle,\\ &|1; \phi + 2\pi/3, h_+\rangle, |1; \phi + 2\pi/3, h_-\rangle, |1; \phi + 4\pi/3, h_+\rangle,\\ &|1; \phi + 4\pi/3, h_-\rangle\}\,. \end{aligned} \tag{5}$$

We have condensed tensor products $|m\rangle \otimes |\varphi, h\rangle$ into $|m; \varphi, h\rangle$. One might expect the phosphorus nucleus to be able to occupy any state in (5). The hextuple of nuclei would be able to occupy a product state

$$|m_1; \varphi_1, h_1\rangle \otimes \ldots \otimes |m_6; \varphi_6, h_6\rangle\,. \tag{6}$$

The nuclei cannot occupy such a state, due to their indistinguishability. The nuclei are fermions. Hence Posner formation antisymmetrizes the nuclei's joint state. We have assumed, in the spirit of [1], that Posner creation essentially preserves each phosphorus nucleus's $S^{z_{\rm lab}}$ (Sec. II D). Hence the pre-Posner nuclei's set $\{m\}$ of spin quantum numbers equals the in-Posner nuclei's set. But Posner creation prevents any particular m from corresponding, anymore, to any particular nucleus. The nuclei delocalize across the cube-face centers.

Let us mathematize this physics. The one-nucleus states (5) combine into the antisymmetric six-nucleus states

$$\begin{aligned}&\frac{1}{\sqrt{6!}} \sum_{\alpha=1}^{6!} \bigotimes_{j=1}^{6} (-1)^{\pi_\alpha} |m_{\pi_\alpha(j)}, \mathbf{r}_{\pi_\alpha(j)}\rangle \\ &:= |(m_1, \mathbf{r}_1)(m_2, \mathbf{r}_2)(m_3, \mathbf{r}_3); (m_4, \mathbf{r}_4)(m_5, \mathbf{r}_5)(m_6, \mathbf{r}_6)\rangle\,.\end{aligned} \tag{7}$$

Each term contains a tensor product of six one-nucleus kets. Each ket is labeled by one tuple $(m_{\pi_\alpha(j)}, \mathbf{r}_{\pi_\alpha(j)})$. No tuple equals any other tuple in the same term, by Pauli's exclusion principle. Permuting one term's six tuples yields another term, to within a minus sign.

π_α denotes the $\alpha^{\rm th}$ term's permutation. The permutation's sign, $(-1)^{\pi_\alpha} = (-1)^{\text{parity of permutation}}$, equals the term's sign.[7] The semicolon in Eq. (7) separates the h_+ spins from the h_- spins. (7) is equivalent to a Slater determinant [34].

If not for the Posner's geometry, two tuples could contain the same position variables. $\mathbf{r}_1$ could equal $\mathbf{r}_3$, for example, if m_1 did not equal m_3. But each cube face can house only one phosphate. The phosphorus nuclei's state occupies the *no-colliding-nuclei subspace* $\mathcal{H}_{\text{no-coll.}}^-$ of the antisymmetric subspace.

Posner creation, we posit, projects the nuclei's state onto $\mathcal{H}_{\text{no-coll.}}^-$. The projector has the form

$$\Pi_{\text{no-coll.}}^- := {\sum}' \left| \begin{smallmatrix}(m_1,\mathbf{r}_1)(m_2,\mathbf{r}_2)(m_3,\mathbf{r}_3);\\ (m_4,\mathbf{r}_4)(m_5,\mathbf{r}_5)(m_6,\mathbf{r}_6)\end{smallmatrix} \right\rangle \left\langle \begin{smallmatrix}(m_1,\mathbf{r}_1)(m_2,\mathbf{r}_2)(m_3,\mathbf{r}_3);\\ (m_4,\mathbf{r}_4)(m_5,\mathbf{r}_5)(m_6,\mathbf{r}_6)\end{smallmatrix} \right|\,. \tag{8}$$

The sum $\sum'$ runs over values of $(m_1, \ldots, m_6)$. The value of $(\mathbf{r}_1, \ldots \mathbf{r}_6) = \big((h_+, \phi), \ldots, (h_-, \phi + 4\pi/3)\big)$ remains invariant throughout the terms.[8] In every term, the first spin quantum number, m_1, would correspond to the position $\mathbf{r}_1 = (h_+, \phi)$. Different terms correspond to different values $m_1 = 0, 1$.

Projection by $\Pi_{\text{no-coll.}}^-$ applies the map

$$\begin{aligned}&|m_1\rangle \otimes \ldots \otimes |m_6\rangle \mapsto \\ &|(m_1, \mathbf{r}_1)(m_2, \mathbf{r}_2)(m_3, \mathbf{r}_3); (m_4, \mathbf{r}_4)(m_5, \mathbf{r}_5)(m_6, \mathbf{r}_6)\rangle.\end{aligned} \tag{9}$$

The left-hand side (LHS) represents an element of the computational basis $\mathcal{B}_{\rm comp}$ for the space $(\mathcal{H}_{\rm nuc})^{\otimes 6}$ of the pre-Posner physical qubits. The right-hand side (RHS) represents an element of the computational basis $\mathcal{B}_{\rm comp}^{\rm Pos}$ for the space $\mathcal{H}_{\text{no-coll.}}^-$ of the in-Posner physical qubits.

Each pre-Posner state consists of a unique assignment of m-values to nuclei, a unique distribution of six fixed m-values across six kets. Similarly, each Posner state consists of a unique assignment of m-values to positions, a unique distribution of six fixed m-values across six $\mathbf{r}$-values. Sixty-four pre-Posner $\mathcal{B}_{\rm comp}$ states exist. Hence 64 $\mathcal{B}_{\rm comp}^{\rm Pos}$ basis elements must exist. A counting argument in App. C confirms this conclusion.

Let us combine the map (9) with the simple code (4). The result is another simple code. This code maps between (i) elements of the computational basis $\mathcal{B}_{\rm comp}^{\rm Pos}$ for the Posner space and (ii) elements of the computational basis $\mathcal{B}_{\rm comp}^{\rm L}$ for the logical space:

$$\begin{aligned}&|(m_1, \mathbf{r}_1)(m_2, \mathbf{r}_2)(m_3, \mathbf{r}_3); (m_4, \mathbf{r}_4)(m_5, \mathbf{r}_5)(m_6, \mathbf{r}_6)\rangle \\ &= |m_1 m_2 \ldots m_6\rangle\,.\end{aligned} \tag{10}$$

Equation (10) shows how the QI, initially stored in pre-Posner spin states, is encoded faithfully in spin-and-

[7] A permutation's parity is defined as follows. Let π_0 denote the first term's permutation. Consider beginning with π_0 and swapping ket labels pairwise. Some minimal number n_ℓ of swaps yields permutation π_ℓ. The parity of n_ℓ is the parity of π_ℓ.

[8] Each pre-Posner spin variable m pairs with one position $\mathbf{r}$. What determines which spin pairs with $\mathbf{r}_1$? Two factors: (i) the choice of coordinate system and (ii) the phosphates' pre-Posner positions and momenta. See App. B for details.

orbital states. We will often replace the physical state's label (the LHS) with the logical state's label (the RHS), to streamline notation.

IV. CHARGE-PROTECTED ENCODINGS FOR QUANTUM INFORMATION STORED IN POSNER MOLECULES

The computational-basis elements (10) are states of spin-and-orbital DOFs. The Posner's dynamics conserve the spins' states for long times, Fisher hypothesizes [1]. The dynamics might not conserve the orbital DOFs' states. Hence the dynamics may not not conserve the states (10).

But we posit, guided by [1, 5], that the Posner's dynamics conserve certain charges: (i) the generator $\mathcal{G}_C$ of a permutation operator C (Sec. IV A) and (ii) the total spin operator's z_{in}-component, $S^{z_{\text{in}}}_{1\ldots6}$ (Sec. IV B). Eigenstates shared by these charges (Sec. IV C) may be conserved.

The dynamics likely will not map an eigenstate $|\psi\rangle$, associated with different eigenvalues τ_ψ and $m^{(\psi)}_{1\ldots6}$ of the charges, into an eigenstate $|\phi\rangle$ associated with eigenvalues τ_ϕ and $m^{(\phi)}_{1\ldots6}$. These eigenstates may serve as long-lived codewords. Charge preservation help "protect" such codes.

We identify a quantum error-detecting code partially protected by C. A repetition code is partially protected by $S^{z_{\text{in}}}_{1\ldots6}$. Section IV D introduces these codes.

IV A. Charge 1: The generator $\mathcal{G}_C$ of the permutation operator C

Imagine transforming a Posner, geometrically, as follows. The rotation is clockwise, about the symmetry axis $\hat{z}_{\text{in}}$, through an angle $2\pi/3$. Only the molecule's architecture rotates: its atoms, its internal coordinate system, its geometry. Imagine that the spins (represented by the m_a's) could remain untouched. The transformed Posner would look identical to the original Posner [2–4, 9].

This symmetry characterizes the molecule's geometry, revealed by quantum-chemistry calculations [2–4, 9]. Hence our introduction of the symmetry in terms of a rotation of the architecture. But QI is expressed more naturally in terms of spins. We therefore recast the transformation, as a counterclockwise cyclic permutation of the spins (Fig. 1b). This spin transformation may be viewed as active; the earlier geometric transformation, as passive.

Let the operator C represent this spin permutation. C cyclically permutes the h_+ spins [the first three m-values in (10)] separately from the h_- spins (the final three m-values). C transforms the $\mathcal{B}^{\text{Pos}}_{\text{comp}}$ elements (10) as

$$\begin{aligned} C \,:\, & |m_1 m_2 m_3 m_4 m_5 m_6\rangle \\ & \equiv |(m_1,\mathbf{r}_1)(m_2,\mathbf{r}_2)(m_3,\mathbf{r}_3);(m_4,\mathbf{r}_4)(m_5,\mathbf{r}_5)(m_6,\mathbf{r}_6)\rangle \\ & \mapsto |(m_3,\mathbf{r}_1)(m_1,\mathbf{r}_2)(m_2,\mathbf{r}_3);(m_6,\mathbf{r}_4)(m_4,\mathbf{r}_5)(m_5,\mathbf{r}_6)\rangle \\ & \equiv |m_3 m_1 m_2 m_6 m_4 m_5\rangle\,. \end{aligned} \tag{11}$$

The $\mathcal{B}^{\text{Pos}}_{\text{comp}}$ elements (10) are not C eigenstates.

But C eigenstates can be constructed. We adopt F&R's notation for the eigenvalues,

$$\begin{aligned} &\omega^\tau\,, \quad \text{wherein} \quad \omega := e^{i2\pi/3} \text{ and} \\ &\tau = 0,1,2 \quad \text{or, equivalently,} \quad \tau = 0,\pm1\,. \end{aligned} \tag{12}$$

F&R call τ a three-level "pseudospin." We call τ, instead, the eigenvalue of the observable $\mathcal{G}_C$ that generates C.[9] The general form of a C eigenstate appears in [5]. F&R use second quantization.

We translate into QI. We also extend [5] by characterizing the eigenspaces of C and by identifying a useful basis for each eigenspace (Sec. IV C). The $\tau = 0$ eigenspace has degeneracy 24; the $\tau = 1$ eigenspace, degeneracy 20; and the $\tau = -1$ eigenspace, degeneracy 20. The $\tau = 0$ eigenspace will play an important role in Posner resource states for universal quantum computation (Sec. VII). The other charge assumed to be conserved, $S^{z_{\text{in}}}_{1\ldots6}$, shares this eigenbasis.

IV B. Charge 2: The total spin operator $S^{z_{\text{in}}}_{1\ldots6}$

Fisher conjectures that phosphorus nuclear spins in Posners have long coherence times [1]. We interpret this conjecture as meaning that the Posner's dynamics conserves $S^{z_{\text{in}}}_{1\ldots6} = \bigoplus_{a=1}^{6} S^{z_{\text{in}}}_a$ for long times. The total magnetic spin quantum number, $m_{1\ldots6} = \sum_{j=1}^{6} m_j$, remains constant.

This interpretation is supported by two arguments in App. D. Possible interactions between a Posner's phosphorus nuclear spins conserve $S^{z_{\text{in}}}_{1\ldots6}$. So, we argue, do collisions with other molecules.

---

[9] A pseudospin is a physical DOF that transforms according to a certain rule. τ is, rather, the eigenvalue of an observable. Suppose that τ were a three-level quantum pseudospin. τ would occupy a quantum state in some three-dimensional effective Hilbert space $\mathcal{H}_{\text{pseudo}}$. No such space can be associated uniquely with a Posner, to our knowledge. Rather, the Posner Hilbert space $\mathcal{H}^-_{\text{no-coll.}}$ has dimensionality 64. $\mathcal{H}^-_{\text{no-coll.}}$ equals a direct sum of the three $\mathcal{G}_C$ eigenspaces: $\mathcal{H}^-_{\text{no-coll.}} = \mathcal{H}_{\tau=0} \oplus \mathcal{H}_{\tau=1} \oplus \mathcal{H}_{\tau=2}$. Each subspace is degenerate. Hence no subspace can serve as one element in a basis for any $\mathcal{H}_{\text{pseudo}}$. One could conjure up a $\mathcal{H}_{\text{pseudo}}$ by choosing one state $|\tau{=}0\rangle \in \mathcal{H}_{\tau=0}$, one $|\tau{=}1\rangle \in \mathcal{H}_{\tau=1}$, and one $|\tau{=}2\rangle \in \mathcal{H}_{\tau=2}$; then constructing $\mathcal{H}_{\text{pseudo}} = \text{span}\{|\tau{=}0\rangle, |\tau{=}1\rangle, |\tau{=}2\rangle\}$. We do so in Sections IV D 1 and VI. But the choice of $|\tau{=}0\rangle$ is nonunique, as is the choice of $|\tau{=}1\rangle$, as is the choice of $|\tau{=}2\rangle$. Hence no unique three-level Hilbert space corresponds to a Posner, to our knowledge. Hence τ appears not to label a unique quantum pseudospin.

We decompose $\mathcal{H}^{-}_{\text{no-coll.}}$ into composite-spin subspaces in App. E. That appendix also reviews addition of quantum angular momentum.

IV C. Eigenbasis shared by the conserved charges

We introduced the computational basis $\mathcal{B}_{\text{comp}}$ for $\mathcal{H}^{-}_{\text{no-coll.}}$ in Eq. (7). Most $\mathcal{B}_{\text{comp}}$ elements transform nontrivially under C [Eq. (11)]. The Posner dynamics conserve C. So, too, would the dynamics ideally conserve quantum codewords. We therefore seek a useful C eigenbasis from which to construct QEC codes.

The C eigenspaces have degeneracies. Which basis should we choose for each eigenspace? A basis shared with $S^{z_{\text{in}}}_{1\ldots6}$, the other conserved charge.

Yet C and $S^{z_{\text{in}}}_{1\ldots6}$ do not form a complete set of commuting observables (CSCO) [35]. Many eigenbases of C are eigenbases of $S^{z_{\text{in}}}_{1\ldots6}$. Another operator is needed to break the degeneracy, to complete the CSCO. We choose the spin-squared sum

$$\mathbf{S}^2_{123} + \mathbf{S}^2_{456} \equiv (\mathbf{S}_1 + \mathbf{S}_2 + \mathbf{S}_3)^2 + (\mathbf{S}_4 + \mathbf{S}_5 + \mathbf{S}_6)^2 \quad (13)$$

$$\equiv \sum_{a=1}^{3} \mathbb{1}^{\otimes(a-1)} \otimes \mathbf{S}_a \otimes \mathbb{1}^{\otimes(3-a)} + \sum_{a=4}^{6} \mathbb{1}^{\otimes(a-4)} \otimes \mathbf{S}_a \otimes \mathbb{1}^{\otimes(6-a)} \,. \quad (14)$$

Geometry and measurement-based quantum computation (Sec. VII B) motivate the choice of $\mathbf{S}^2_{123} + \mathbf{S}^2_{456}$: A Posner contains two triangles of spins (Fig. 1a). The positions in the h_+ triangle are labeled $\mathbf{r}_1$, $\mathbf{r}_2$, and $\mathbf{r}_3$. Hence the first three tuples in Eq. (10) correspond to the h_+ triangle. Hence the magnetic spin quantum numbers m_1, m_2, and m_3 may be viewed as occupying the h_+ triangle. These spins' joint state is equivalent to a three-qubit logical state, $|m_1 m_2 m_3\rangle$. An analogous argument concerns h_-. Hence the antisymmetric state (10) is equivalent to a product of two three-logical-qubit states:[10]

$$|(m_1, \mathbf{r}_1)(m_2, \mathbf{r}_2)(m_3, \mathbf{r}_3); (m_4, \mathbf{r}_4)(m_5, \mathbf{r}_5)(m_6, \mathbf{r}_6)\rangle \equiv |m_1 m_2 m_3\rangle |m_4 m_5 m_6\rangle \,. \quad (21)$$

[10] In greater detail,

$$\begin{aligned} &|(m_1, \mathbf{r}_1)(m_2, \mathbf{r}_2)(m_3, \mathbf{r}_3); (m_4, \mathbf{r}_4)(m_5, \mathbf{r}_5)(m_6, \mathbf{r}_6)\rangle && (15)\\ &\quad \equiv |m_1 m_2 m_3 m_4 m_5 m_6\rangle && (16)\\ &\quad \equiv |m_1\rangle|m_2\rangle|m_3\rangle|m_4\rangle|m_5\rangle|m_6\rangle && (17)\\ &\quad = (|m_1\rangle|m_2\rangle|m_3\rangle)(|m_4\rangle|m_5\rangle|m_6\rangle) && (18)\\ &\quad \equiv |m_1, m_2, m_3\rangle|m_4, m_5, m_6\rangle && (19)\\ &\quad \equiv |m_1 m_2 m_3\rangle|m_4 m_5 m_6\rangle \,. && (20) \end{aligned}$$

Equation (16) is equivalent to Eq. (10). Equation (17) is equivalent to Eq. (4). Equation (18) follows from the tensor product's associativity. Equation (19) consists of a rewriting with new notation. Equation (20) is analogous to Eq. (4).

The trios function logically as independent units. Such trios can be used to prepare universal quantum-computation resource states (Sec. VII B). Hence the spin-operator trios in Eq. (13).

Each qubit trio corresponds to a Hilbert space $\mathbb{C}^6$. Let us focus on qubits 1-3, for concreteness. C, $S^{z_{\text{in}}}_{123}$, and $\mathbf{S}^2_{123}$ share the basis in Table I. Each basis element is symmetric with respect to cyclic permutations of the three logical qubits.

Tensoring together two one-triangle states yields a state of a Posner's phosphorus nuclear spins: $|000\rangle|000\rangle, |000\rangle|W\rangle, \ldots, |\overline{\omega^2}\rangle|\overline{\omega^2}\rangle$. Sixty-four such states exist. We classify them with quantum numbers in App. F.

We have pinpointed an eigenbasis shared by the conserved charges. The Posner dynamics are expected not to map states in one charge sector to states in another. Hence different-sector states suggest themselves as quantum codewords. We present partially charge-protected QECD codes next.

IV D. Quantum error-detecting and -correcting codes accessible to Posner molecules

We exhibit two codes formed from states accessible to Posners. Each codeword is an eigenstate of a conserved charge, C or $S^{z_{\text{in}}}_{1\ldots6}$. Each code's codewords correspond to distinct eigenvalues of the charge. Hence the Posner dynamics likely do not map any codeword into any other.

Section IV D 1 introduces a quantum error-detecting code. One Posner, we show, can encode one logical qutrit. The code detects one arbitrary physical-qubit error. Section IV D 2 shows how to implement a repetition code with Posner states. The code corrects two bit flips.

More Posner codes, we expect, await discovery. Opportunities are detailed in Sec. X.

We have already discussed an encoding of logical states in physical systems (Sec. III B). Earlier, the logical Hilbert space $\mathcal{H}_{\text{L}}$ shared the physical Hilbert space's dimensionality, 64. Section III B concerned a bijective, injective map between the spaces. QECD encodes a small logical space in a larger physical space. Notation will reflect the distinction between Sec. III B and QECD: Script subscripts $\mathcal{L}$ (as in $\mathcal{H}_{\mathcal{L}}$) will replace the Roman L (as in $\mathcal{H}_{\text{L}}$). QECD is reviewed in App. A 3.

IV D 1. Qutrit error-detecting code formed from Posner-molecule states

One Posner, we show, can encode one logical qutrit. The code detects arbitrary single-physical-qubit errors. The physical qubits are the spin-and-orbital DOFs of Sec. III C.

The code has the form

$$\mathcal{H}^{\text{qutrit}}_{\mathcal{L}} = \text{span}\left\{ |0_{\mathcal{L}}\rangle, |1_{\mathcal{L}}\rangle, |2_{\mathcal{L}}\rangle \right\} \,, \quad (22)$$

State	Decomposition	S_{123}	m_{123}	τ
$\|000\rangle$	$\|000\rangle$	3/2	3/2	0
$\|W\rangle$	$\frac{1}{\sqrt{3}}(\|100\rangle + \|010\rangle + \|001\rangle)$	3/2	1/2	0
$\|\bar{W}\rangle$	$\frac{1}{\sqrt{3}}(\|011\rangle + \|101\rangle + \|110\rangle)$	3/2	−1/2	0
$\|111\rangle$	$\|111\rangle$	3/2	−3/2	0
$\|\omega\rangle$	$\frac{1}{\sqrt{3}}(\|100\rangle + \omega^2\|010\rangle + \omega\|001\rangle)$	1/2	1/2	1
$\|\bar{\omega}\rangle$	$\frac{1}{\sqrt{3}}(\|011\rangle + \omega^2\|101\rangle + \omega\|110\rangle)$	1/2	−1/2	1
$\|\omega^2\rangle$	$\frac{1}{\sqrt{3}}(\|100\rangle + \omega\|010\rangle + \omega^2\|001\rangle)$	1/2	1/2	2
$\|\overline{\omega^2}\rangle$	$\frac{1}{\sqrt{3}}(\|011\rangle + \omega\|101\rangle + \omega^2\|110\rangle)$	1/2	−1/2	2

TABLE I: Symmetric basis for a trio of qubits: A Posner molecule consists of two triangles of spins (Fig. 1). The triangles encode quantum information independently, in accordance with Eq. (21). Each triangle therefore functions as a trio of logical qubits. The three physical qubits correspond to an eight-dimensional Hilbert space, $\mathbb{C}^6$. A useful basis is an eigenbasis shared by the conserved charges, C (a permutation operator) and $S_{123}^{z_{\rm in}}$ (the z-component, relative to the internal $\hat{z}_{\rm in}$-axis, of the total spin). These operators share many basis. The eigenbasis shared also by $\mathbf{S}_{123}^2$ proves useful in the preparation of universal quantum-computation resource states (Sec. VII). τ describes, here, how a triangle transforms under the permutation represented by C.

wherein

$$|0_{\mathcal{L}}\rangle = \frac{1}{\sqrt{2}}(|W\rangle|\bar{W}\rangle - |\bar{W}\rangle|W\rangle)\,, \tag{23}$$

$$|1_{\mathcal{L}}\rangle = \frac{1}{\sqrt{2}}(|\omega^2\rangle|\overline{\omega^2}\rangle - |\overline{\omega^2}\rangle|\omega^2\rangle)\,, \quad \text{and} \tag{24}$$

$$|2_{\mathcal{L}}\rangle = \frac{1}{\sqrt{2}}(|\omega\rangle|\bar{\omega}\rangle - |\bar{\omega}\rangle|\omega\rangle)\,. \tag{25}$$

Each logical state $|j_{\mathcal{L}}\rangle$ occupies the $\tau = j$ subspace.

The codewords satisfy the two quantum error-detection criteria [8, 36–40]. First, the states are locally indistinguishable:

$$\langle j_{\mathcal{L}}|\sigma^x|j_{\mathcal{L}}\rangle = \langle j_{\mathcal{L}}|\sigma^y|j_{\mathcal{L}}\rangle = 0 \quad \text{and} \tag{26}$$

$$\langle j_{\mathcal{L}}|\sigma^z|j_{\mathcal{L}}\rangle = \frac{1}{12} \tag{27}$$

for all j. That is, the codewords satisfy the diagonal criterion. Second, the codewords satisfy the off-diagonal criterion,

$$\langle j_{\mathcal{L}}|\sigma^\alpha|k_{\mathcal{L}}\rangle = 0 \qquad \forall j \neq k\,, \quad \forall \alpha = x, y, z\,, \tag{28}$$

by direct calculation.

IV D 2. Repetition code formed from Posner-molecule states

The repetition code originated in classical error correction [41]. Each logical bit is cloned until n copies exist: $0 \mapsto \underbrace{00\ldots0}_{n}$, and $1 \mapsto \underbrace{11\ldots1}_{n}$. Suppose that errors flip under half the bits. For example, 000000 may transform into 011000. One decodes the bit string by counting the zeroes, counting the ones, and following majority rule. More physical bits end as 0s than as 1s in our example. A logical zero, the receiver infers, was likely sent.

The repetition code can be translated into quantum states. For example, let $\mathcal{H}_{\mathcal{L}}^{\rm rep} = \{|0_{\mathcal{L}}\rangle, |1_{\mathcal{L}}\rangle\}$, wherein $|0_{\mathcal{L}}\rangle = |000000\rangle$ and $|1_{\mathcal{L}}\rangle = |111111\rangle$. This code corrects two σ^x errors. But each codeword is unentangled.[11] Hence $\mathcal{H}_{\mathcal{L}}^{\rm rep}$ fails to satisfy the off-diagonal error-detection criterion,

$$\langle j_{\mathcal{L}}|\sigma^\alpha\sigma^\beta|k_{\mathcal{L}}\rangle = 0 \qquad \forall j \neq k\,, \tag{29}$$

whenever $\alpha \neq x$ and/or $\beta \neq x$.

V. THE MODEL OF POSNER QUANTUM COMPUTATION

Fisher has conjectured that certain chemical processes occur in biofluids [1]. We abstract away the chemistry, identifying the computations that the processes effect. We call the computations *Posner operations*.[12] The operations form a model of quantum computation, *Posner quantum computation*.

The model's operations, we will show, can be used (i) to teleport QI incoherently and (ii) to prepare, efficiently, universal resource states for measurement-based quantum computation (Sections VII-VII). Whether the model's operations can realize universal quantum computation remains an open question (Sec. IX).

---

[11] More precisely, the element $|000000\rangle$ of the computational basis for the logical space (Sec. III C) is unentangled. The spin-and-orbital state represented by $|000000\rangle$ [by Eq. (10)] is entangled.

[12] We occasionally call the processes "Posner operations."

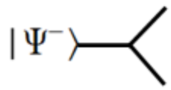

FIG. 3: Circuit-diagram element that represents singlet-state preparation (operation 1).

Posner quantum computation is defined in Sec. V A. The model is analyzed in Sec. V B. We discuss the model's ability to entangle, the requirements for running arbitrary-depth quantum circuits, and the control required to perform QI-processing tasks. Fisher's narrative [1] is also cast as a quantum circuit.

V A. Definition of Posner quantum computation

Terminological notes are in order. When discussing physical processes, we discuss phosphorus nuclear spins, spin-and-orbital DOFs, and Posners. When discussing logical DOFs, we discuss qubits. A circuit-diagram element represents each operation (Figures 3-12):

1. **Singlet-state preparation** (Fig. 3): *Arbitrarily many singlets* $|\Psi^-\rangle$ *can be prepared.* Singlets are prepared when an enzyme hydrolyzes diphosphates into entangled phosphate pairs (Sec. II C).[13]

   These singlets are prepared differently than in conventional quantum circuits. Conventionally, one prepares two qubits in the state $|0\rangle^{\otimes 2}$; performs a Hadamard[14] on the first qubit; and performs a CNOT,[15] controlling on the first qubit: $\text{CNOT}(H \otimes \mathbb{1})|00\rangle = |\Psi^-\rangle$.

   In contrast, Fisher posits that enzymes prepare singlets by projective measurements [1]. We formalize Fisher's statement as follows. A diphosphate's phosphorus nuclear spins occupy some state ρ_{diphos}. The diphosphate enters a pyrophosphatase enzyme. The enzyme measures the PVM $\{|\Psi^-\rangle\langle\Psi^-|, \mathbb{1} - |\Psi^-\rangle\langle\Psi^-|\}$.

   Suppose that the diphosphate separates into two disconnected phosphates. The spins' state has been projected with $|\Psi^-\rangle\langle\Psi^-|$.

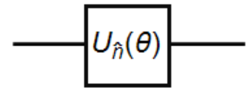

FIG. 4: Circuit-diagram element that represents a rotation of a qubit not in any Posner (operation 2): $\hat{n}$ denotes the axis rotated about. θ denotes the angle rotated through.

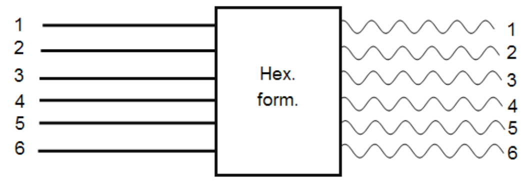

FIG. 5: Circuit-diagram element that represents hextuple formation (operation 3): Straight lines represent qubits not in hextuples. Each wavy line represents a qubit in a hextuple (that is not paired with any other hextuple as a result of operation 5). As the lines' labels show, the circuit element is defined as preserving the qubits' ordering.

   Suppose, instead, that the diphosphate leaves the enzyme uncleaved. The second possible measurement outcome has obtained. The diphosphate cannot form a Posner molecule with other ions. Hence the diphosphate cannot participate in quantum cognition. Hence the diphosphate plays no role in Posner quantum computation. Hence the PVM's $\mathbb{1} - |\Psi^-\rangle\langle\Psi^-|$ outcome plays no role. Any diphosphate that remains uncleaved "is discarded," in QI language. The $|\Psi^-\rangle\langle\Psi^-|$ outcome is classically postselected on. Classical postselection provides no superquantum computational power; see footnote 17.

   In summary, Posner operations include the preparation of $|\Psi^-\rangle$. Quantum-cognition systems prepare $|\Psi^-\rangle$ by measuring a PVM nondestructively, then postselecting classically on the "yes" outcome. "No"-outcome ions do not participate in later chemical events of interest.

2. **Rotations of independent qubits** (Fig. 4): *Any qubit can rotate through any angle* θ *about any axis* $\hat{n}$*, via a unitary* $U_{\hat{n}}(\theta)$. $\hat{n}$ is defined relative to the lab frame. Qubits rotate as phosphates tumble in the fluid.

3. **Hextuple formation** (Fig. 5): *Qubits can group together in hextuples (groups of six). Hextuple formation evolves the logical qubits trivially, under the operator* $\mathbb{1}$. *But hextuple formation associates the qubits with a geometry and with an observable* $\mathcal{G}_C$.

   Logical qubits form hextuples as ions bind together, forming Posners. A logical qubit can occupy, at most,

---

[13] Biofluids might prepare phosphorus nuclear spins in nonsinglet states. For example, one phosphate might detach from ATP, leaving adenosine diphosphate (ADP). Identifying the phosphate's quantum state would require physical modeling outside this paper's scope. Therefore, we suppose that qubits can be prepared only in singlets.

[14] The *Hadamard gate* H transforms one qubit [7]. In terms of Pauli operators, $H = \frac{1}{\sqrt{2}}(\sigma_x + \sigma_z)$. The gate has a geometric interpretation expressed in terms of the Bloch sphere: The state rotates through 180° about the axis $\frac{1}{\sqrt{2}}(\hat{x} + \hat{z})$.

[15] The *CNOT*, or *controlled-not*, gate transforms two qubits [7]. One qubit is called the *control*, and one is called the *target*. If the control occupies the state $|0\rangle$, the CNOT preserves the target's state. If the first qubit occupies $|1\rangle$, the target evolves under σ_x. The CNOT has the form $|0\rangle\langle 0| \otimes \mathbb{1} + |1\rangle\langle 1| \otimes \sigma_x$.

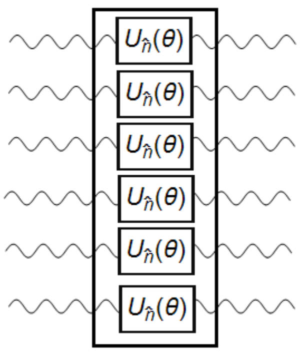

FIG. 6: Circuit-diagram element that represents hextuple-coordinated single-qubit rotations (operation 4). $\hat{n}$ denotes the axis rotated about. θ denotes the angle rotated through.

one hextuple. Section III C explains why hextuple formation fails to change logical qubits' states: The spins' state changes, suggesting that the logical qubits' state changes. But the logical information's physical encoding changes, too.

Hextuple creation impacts the logical system in three ways: (i) Each hextuple has an observable $\mathcal{G}_C$. (ii) Hextuple creation induces a geometry that influences operation 4. (iii) The six logical qubits' Hilbert space transforms from $\mathbb{C}^{12}$ to the isomorphic $\mathcal{H}^-_{\text{no-coll.}}$. Let us detail these three effects.

First, creating a hextuple creates an observable $\mathcal{G}_C$ (Sec. IV A). $\mathcal{G}_C$ has eigenvalues $\tau = 0, 1, 2$ (equivalently, $\tau = 0, \pm 1$). τ impacts operation 5.

Second, hextuple creation induces a geometry. Each logical qubit is assigned to a cube face, in accordance with Sec. III C. The six qubits can be distributed across the six faces in any of 6! ways. Physically, different assignments follow from different pre-Posner orbital states (App. B). The six qubits form two triangles, called *trios* below, in accordance with Fig. 1. This geometry limits the single-qubit unitaries that can evolve the six qubits (operation 4). The geometry also influences our construction of universal quantum-computation resource states (Sec. VII).

Third, hextuple creation changes the system's Hilbert space from $(\mathbb{C}^2)^{\otimes 6}$ to $\mathcal{H}^-_{\text{no-coll.}}$ (Sec. III C). $\mathcal{H}^-_{\text{no-coll.}}$ is isomorphic to $(\mathbb{C}^2)^{\otimes 6}$, as the map (10) is injective and bijective. Hence we will keep referring to the logical space as $(\mathbb{C}^2)^{\otimes 6}$.

4. **Hextuple-coordinated single-qubit rotations** (Fig. 6): *The qubits in a hextuple can undergo identical arbitrary single-qubit rotations simultaneously, via* $[U_{\hat{n}}(\theta)]^{\otimes 6}$. The qubits rotate as the Posner tumbles about an axis $\hat{n}$ relative to the lab frame.

5. **Posner-binding measurement** (Figures 7 and 8): *Let A and B denote two hextuples formed via operation 3. Whether the hextuples' $\mathcal{G}_C$ eigenvalues sum to zero can be measured nondestructively:* $\tau_A + \tau_B = 0$.

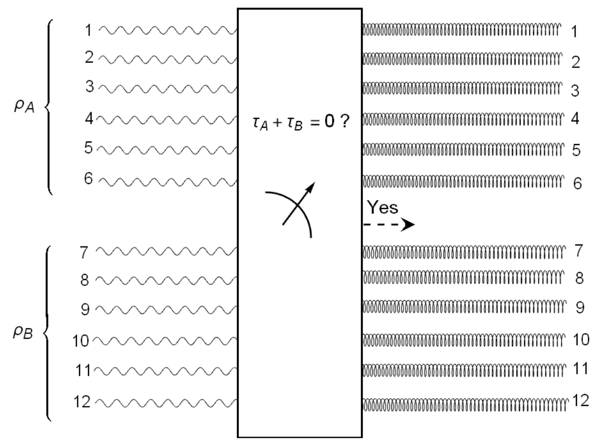

FIG. 7: Circuit-diagram element that represents a Posner-binding measurement (operation 5) that yields a positive outcome: Wavy lines represent qubits in hextuples that are not in a dodectuple (a pair of hextuples). Coils represent qubits in a dodectuple.

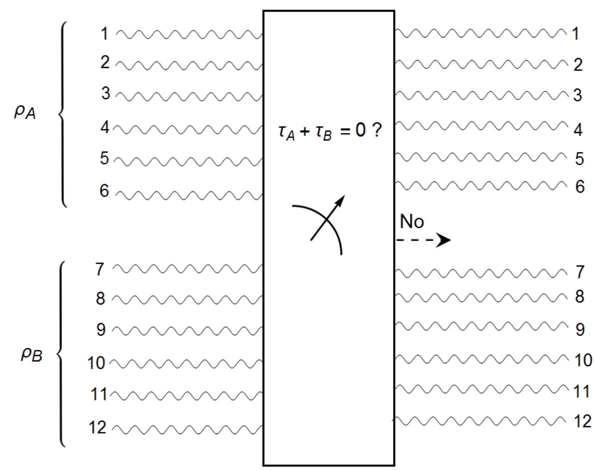

FIG. 8: Circuit-diagram element that represents a Posner-binding measurement (operation 5) that yields a negative outcome.

First, we discuss the measurement's physical manifestation. Then, we mathematize the operation with a PVM.

The measurement manifests in the binding, or failure to bind, of two Posners. Fisher conjectures as follows [1], supported by quantum-chemistry calculations [9]: Two Posners, A and B, can bind together. They bind upon approaching each other "head-on": Their directed symmetry axes (Fig. 1a) point oppositely each other.

Such Posners bind, Fisher conjectures [1], when and only when not rotating relative to each other. Relative rotation would hinder A in “grabbing onto” B. Hence if A and B approach head-on, whether they bind depends entirely on whether $\tau_A + \tau_B = 0$. The molecules' bound-together-or-not status serves as a classical measurement record. So does the environment, as in Posner creation (Sec. II): Posner binding releases about 1 eV of heat [1, 9].

Let us formalize the measurement, using the mathematics of QI. We define a projector on $\left(\mathcal{H}^{-}_{\text{no-coll.}}\right)^{\otimes 2}$:

$$\Pi_{AB} := (\Pi_{\tau_A=0} \otimes \Pi_{\tau_B=0}) + (\Pi_{\tau_A=\pm 1} \otimes \Pi_{\tau_B=\mp 1}) \ . \tag{30}$$

The PVM

$$\{\Pi_{AB}, \mathbb{1} - \Pi_{AB}\} \tag{31}$$

can be measured. Suppose that the first outcome obtains (that the Posners bind). The two-Posner state ρ updates as

$$\rho \mapsto \frac{\Pi_{AB}\, \rho\, \Pi_{AB}}{\mathrm{Tr}\,(\Pi_{AB}\, \rho\, \Pi_{AB})} \,. \tag{32}$$

The twelve qubits for a *dodectuple*. Suppose, instead, that the second outcome obtains (that the Posners fail to bind). The joint state updates as

$$\rho \mapsto \frac{\rho - \{\Pi_{AB}, \rho\} + \Pi_{AB}\, \rho\, \Pi_{AB}}{1 - \mathrm{Tr}\,(\Pi_{AB}\, \rho)} \,. \tag{33}$$

The anticommutator of operators O and O' is denoted by $\{O, O'\}$.

6. **Dodectuple operations:** *Suppose that hextuples A and B have been measured with the PVM* (31). *Suppose that outcome Π_{AB} has obtained. The twelve logical qubits can undergo operation 6a; or 6b; or 6a, followed by 6b.*

   (a) **Dodectuple-coordinated single-qubit unitaries** (Fig. 9): *The two hextuple's qubits can undergo identical arbitrary single-qubit rotations:* $[U_{\hat{n}}(\theta)]^{\otimes 12}$. The qubits rotate as the Posners tumble in the fluid.

   (b) **Dodectuple → 2 hextuples** (Fig. 10): *A dodectuple can separate into independent hextuples, the hextuples that joined together.* The Posners can drift apart. The hextuples can return to undergoing the operation 4 (and can, we posit, undergo operation 6).

   (c) **Dodectuple break-up** (Fig. 11): *The hextuples can break down into their constituents: The qubits can cease to correspond to meaningful geometries or to observables $\mathcal{G}_C$.* The qubits thereafter behave independently. They can, again, undergo operations 2-3.

   The hextuples break down as the Posners hydrolyze. Fisher conjectures that bound-together Posners hydrolyze more often than separated Posners [1], as discussed in the introduction.

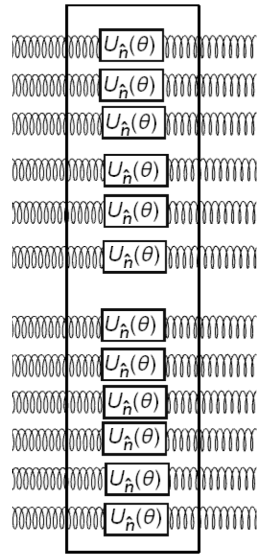

FIG. 9: Circuit-diagram element that represents dodectuple-coordinated single-qubit unitaries (operation 6a). $\hat{n}$ denotes the axis rotated about. θ denotes the angle rotated through.

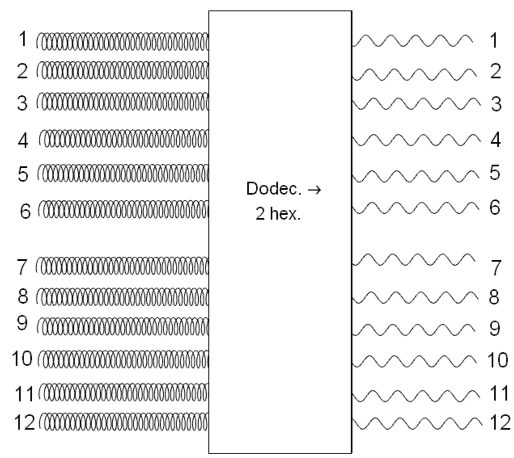

FIG. 10: Circuit-diagram element that represents the separation of a dodectuple into two hextuples (operation 6b): Each coil represents a qubit in a dodectuple. Each wavy line represents a qubit in a hextuple that is not in a dodectuple.

Fisher's narrative allows for, though does not require, another operation:

6. **Hextuple break-up** (Fig. 12): *One hextuple can break down into its constituents: The qubits can cease to correspond to geometries or to observables $\mathcal{G}_C$.*

   Different regions of the body have different pH's and different magnesium-ion (Mg^{2+}) concentrations. A Posner can migrate to a region packed with H^+ and/or with Mg^{2+}. These ions can bind to PO_4^{3-}, as Ca^{2+}

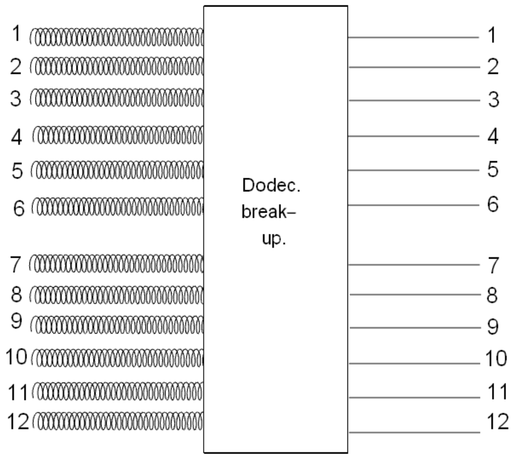

FIG. 11: Circuit-diagram element that represents dodectuple break-up (operation 6c): Each coil represents a qubit in a dodectuple. Each straight line represents a qubit not grouped with any other qubits.

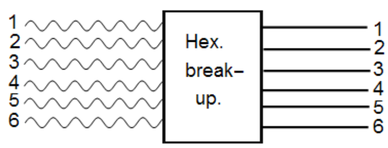

FIG. 12: Circuit-diagram element that represents hextuple break-up (operation 6): Each coil represents a qubit in a dodectuple. Each straight line represents a qubit not grouped with any other qubits.

can. The higher the H^+ and Mg^{2+} concentrations, the more H^+ and Mg^{2+} ions dislodge Posners' Ca^{2+} ions [6]. The dislodging hydrolyzes the molecules.

Operation 6 can be used to prepare Posners, efficiently, in resource states that can power universal measurement-based quantum computation (Sec. VII).

V B. Analysis of Posner quantum computation

We have dissected Fisher's narrative into physical processes, and we have abstracted out the computations that the processes effect. Fisher's narrative [1] can now be cast as a quantum circuit. The circuit appears in Fig. 13.

Four features of Posner operations merit analysis. Two operations entangle logical qubits. The entanglement generated is discussed in Sec. V B 1. Section V B 2 contains a criterion for realizing nonconstant-depth circuits: Posners must bind, hydrolyze, and rebind. Section V B 3 concerns control: To perform the QI-processing tasks introduced in Sections VI-VII, one might need fine control over Posners. Biofluids might not exert such control. But assuming control facilitates first-step QI analyses. One operation merits its own section: The measurement (31) is compared with a Bell measurement, and applied in QI-processing tasks, in Sec. VI.

V B 1. Entanglement generation

Entanglement enables quantum computers to solve certain problems quickly.[16] Two Posner operations create entanglement: Bell-pair creation (operation 1) and the Posner-binding measurement (operation 5).

Bell pairs serve as units of entanglement in QI [7]. We present two implications of Bell-pair creation for Posners. First, Bell-pair creation (operation 1), with the Posners' geometry, can efficiently prepare a state that fuels universal measurement-based quantum computation (Sec. VII). Second, distributing Bell pairs across Posners can affect their binding probabilities (Sec. VIII).

The role played by Bell pairs in QI processing is well-known. Less obvious is how much, and which kinds of, entanglement Π_{AB} creates and destroys. We characterize this entanglement in two ways (Sec. VI A). The PVM (31), we show, transforms a subspace as a coarse-grained Bell measurement. Bell measurements facilitate quantum teleportation [10]. The PVM (31) facilitates *incoherent teleportation*: A state's weights are teleported; the coherences are not. The dephasing comes from the PVM's simulation of a coarse-grained Bell measurement.

One might expect Posner binding to render Posner quantum computation universal: Conventional wisdom says, nearly any entangling gate, plus all single-qubit unitaries, form a universal gate set [44–48]. Posner operations include entangling gates and all single-qubit unitaries.

But the conventional wisdom appears inapplicable to Posner operations, for three reasons. First, conventional-wisdom gates evolve the system unitarily. The Posner-binding measurement (31) does not. (Hence our shift to measurement-based quantum computation in Sec. VII.) Second, many universality proofs decompose a desired entangling gate into implementable gates. The Posner-binding measurement seems unlikely to decompose.

Third, conventional-wisdom entangling gates are defined in terms of qubits' states. The Posner-binding measurement is defined in terms of τ. τ is an eigenvalue of an observable $\mathcal{G}_C$ of a hextuple of qubits. One must deduce how the measurement transforms any given qubit. Does this indirect entangler of qubit states, with all single-qubit rotations (operation 2), form a universal set? The answer merits further study.

---

[16] More precisely, contextuality underlies quantum speedups [42, 43].

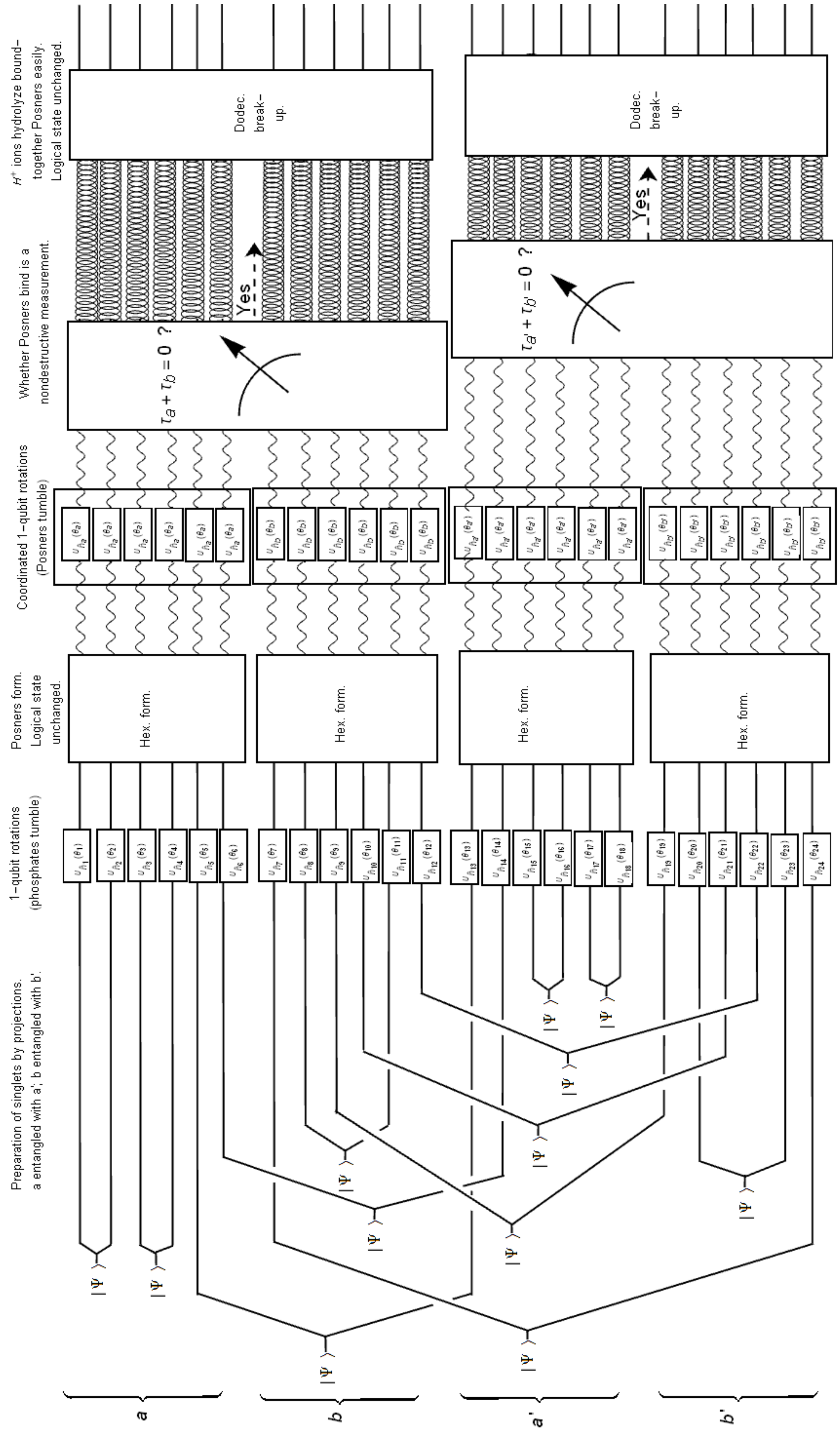

FIG. 13: Circuit representation of Fisher's quantum-cognition narrative: Fisher conjectures that certain chemical processes occur, in a certain sequence, in the body [1]. The sequence is reviewed in this paper's introduction. We abstracted out the computations effected by the chemical processes, in Sec. V A. The abstraction enables us to recast Fisher's narrative as a quantum circuit. Time progresses from left to right in the figure (from the bottom to the top of the page). The sets of six qubits are labeled a, b, a', and b', as in [1, p. 5, Fig. 3]. The circuit elements are defined in Sec. V A.

V B 2. Circuit depth

Consider attempting to implement universal quantum computation with Posner operations. One must be able to run finite-depth circuits, to perform many computations sequentially. One must be able to entangle qubits, and to rotate qubits independently, late in the computation.

Let us focus on the biological-circuit components that follow state preparation (on the operations beyond 1). Qubits can undergo entangling operations only when qubits are in Posners (via operation 5). Qubits can rotate independently only when phosphates are outside of Posners (via operation 2). Hence universal quantum computation would require (i) Posner binding and hydrolysis (operations 5 and 6c) and/or (ii) one-Posner hydrolysis (operation 6).

Suppose that all the Posners fail to hydrolyze. Posner operations can realize only depth-4 circuits. Realizing constant-depth circuits does not suffice for realizing universal quantum computation [49]. Hence Posner disintegration is necessary for realizing universal quantum computation. Whether Posner operations suffice remains an open question.

V B 3. Control required to perform quantum-information-processing tasks with Posner molecules

In Sec. VI–VIII, we concatenate Posner operations to form QI-processing protocols. Implementing the protocols may require fine control over the chemical processes that effect the computations. The body might seem unlikely to realize fine control. We illustrate with two examples. Then, we justify the assumption of fine control.

Consider, as a first example, running an arbitrary quantum circuit. Arbitrary qubits must rotate through arbitrary angles θ, about arbitrary axes $\hat{n}$, arbitrarily precisely. In the quantum-cognition setting, logical qubits rotate as phosphates tumble (via operation 2). Phosphates tumbles upon colliding with other particles. Fluid particles collide randomly, trading angular momentum randomly. Random collisions appear unlikely to generate the precise rotations required for a given circuit.

The $\tau_A + \tau_B = 0$ measurement (operation 5) provides a second example. Consider Posners A and B approaching each other with momenta $\mathbf{p}_A$ and $\mathbf{p}_B$. Consider observing whether the Posners bind. One might wish to infer, from the binding or lack thereof, whether $\tau_A + \tau_B = 0$. But the inference is justified only if $\mathbf{p}_A$ and $\mathbf{p}_B$ were such that whether the Posners would bind depended only on whether $\tau_A + \tau_B$ vanished.

Suppose that the Posners approached not head-on, but at a slight angle: $\hat{p}_A \neq -\hat{p}_B$. The Posners would fail to bind. But one could not infer that $\tau_A + \tau_B \neq 0$. Only finely tuned two-Posner encounters reflect whether $\tau_A + \tau_B = 0$. Only finely tuned encounters constitute measurements.[17]

But assuming perfect control can facilitate QI-theoretic analyses. Many QI protocols are phrased in the language of "agents." One imagines intelligent agents, Alice and Bob, who wish to process QI. One specifies and analyzes protocols in terms of the agents' intents and actions. Alice and Bob are often assumed to perform certain operations with perfect control. Examples of such "allowed operations" include local operations and classical communications [51].

Control partitions (i) what can be achieved in principle from (ii) what can be achieved easily with today's knowledge and techniques. Item (ii) shifts with our understanding and technology. Item (i) is permanent and is the focus of much QI theory.

A few decades ago, for example, experimentalists had trouble performing CNOT gates. Many groups have mastered the gate by now. These groups implement protocols devised before CNOTs appeared practical.

Similarly, precise phosphate rotations appear impractical. But some precise-rotation mechanism could be discovered. Also, by assuming perfect control, we derive a limit on what Posners can achieve without perfect control. We ascertain what QI processing is possible in principle.

VI. THE POSNER-BINDING MEASUREMENT AND APPLICATIONS THEREOF TO QUANTUM INFORMATION PROCESSING

The measurement (31) entangles two Posners' states. Yet the measurement projectors, Π_{AB} and $\mathbb{1} - \Pi_{AB}$, entangle states in different ways. How much either projector entangles is not obvious. Neither is the PVM's potential for processing QI.

This section sheds light on these unknowns. We compare the PVM to a *Bell measurement*, a standard QI operation (Sec. VI A). The next two sections detail applications of the PVM: The PVM facilitates incoherent teleportation (Sec. VI B). Also, the PVM can be used to project Posners onto their $\tau = 0$ eigenspaces (Sec. VI C).

---

[17] If two Posners bind, then $\tau_A + \tau_B = 0$; the inference is justified. But binding does not constitute merely a measurement. Binding constitutes a measurement followed by classical postprocessing. By *classical postprocessing*, we mean the following. Consider performing some protocol in each of several trials. Let the protocol involve a measurement. Consider the data collected throughout trials. Consider discarding some of the data, keeping only the data collected during the trials in which the measurement yielded some outcome x. One has classically postselected on x. If two Posners bind, then (i) whether $\tau_A + \tau_B = 0$ is measured and (ii) the "yes" outcome is classically postselected on. If two Posners bind, step (i) alone is not implemented; a measurement alone is not performed.

Classical postprocessing differs from the postselection in, e.g., [50]. The latter postselection affords computational power unlikely to grace quantum systems. In contrast, classical postprocessing happens in today's laboratories.

VI A. Comparison of the Posner-binding measurement with a Bell measurement

First, we review Bell states and measurements [7]. A Bell measurement prepares an entangled state of two qubits. Four maximally entangled states span the two-qubit Hilbert space, $\mathbb{C}^4$. The orthonormal *Bell basis* is

$$\{|\Phi^+\rangle := \frac{1}{\sqrt{2}}(|00\rangle + |11\rangle) \tag{34}$$

$$|\Phi^-\rangle := \frac{1}{\sqrt{2}}(|00\rangle - |11\rangle) \tag{35}$$

$$|\Psi^+\rangle := \frac{1}{\sqrt{2}}(|01\rangle + |10\rangle) \tag{36}$$

$$|\Psi^-\rangle := \frac{1}{\sqrt{2}}(|01\rangle - |10\rangle)\} . \tag{37}$$

A *Bell measurement* is represented by the PVM

$$\{|\Phi^+\rangle\langle\Phi^+|, |\Phi^-\rangle\langle\Phi^-|, |\Psi^+\rangle\langle\Psi^+|, |\Psi^-\rangle\langle\Psi^-|\} . \tag{38}$$

Many QI protocols involve Bell measurements. Examples include quantum teleportation [10], superdense coding (the effective transmission of two bits via the direct transmission of just one bit, with help from entanglement) [11], and teleportation-based quantum computation [52–55].

Posner binding simulates a coarse-grained Bell measurement. The Bell-state projectors (34) are defined on $\mathbb{C}^2$. In contrast, the Posner Hilbert space $\mathcal{H}^-_{\text{no-coll.}}$ is isomorphic to $\mathbb{C}^6$. We therefore define an effective qubit subspace. Let $|1_\tau\rangle$ denote an arbitrary $\tau = 1$ eigenstate of C; and $|2_\tau\rangle$, an arbitrary $\tau = 2$ eigenstate. $|1_\tau\rangle$ and $|2_\tau\rangle$ serve analogously to $|0\rangle$ and $|1\rangle$ in $\text{span}\{|1_\tau\rangle, |2_\tau\rangle\}$.

Proposition 1. *Let A and B denote two Posners. The measurement* (31) *transforms the effective two-qubit space*

$$\text{span}\{|1_\tau, 1_\tau\rangle, |1_\tau, 2_\tau\rangle, |2_\tau, 1_\tau\rangle, |2_\tau, 2_\tau\rangle\} \tag{39}$$

identically to the coarse-grained Bell measurement

$$\left\{|\Phi^+\rangle\langle\Phi^+| + |\Phi^-\rangle\langle\Phi^-|, |\Psi^+\rangle\langle\Psi^+| + |\Psi^-\rangle\langle\Psi^-|\right\} . \tag{40}$$

Proof. The projector (30) transforms the two-qubit space as

$$\Pi_{AB} = |1_\tau, 2_\tau\rangle\langle 1_\tau, 2_\tau| + |2_\tau, 1_\tau\rangle\langle 2_\tau, 1_\tau| . \tag{41}$$

Let us relabel 1_τ as 0 and 2_τ as 1. The projector becomes

$$\Pi_{AB} = |\Psi^+\rangle\langle\Psi^+| + |\Psi^-\rangle\langle\Psi^-| . \tag{42}$$

Direct substitution into the RHS yields the LHS.

Consider the complementary projector in the measurement (31). $\mathbb{1} - \Pi_{AB}$ transforms the effective two-qubit space as

$$\mathbb{1} - \Pi_{AB} = |1_\tau, 1_\tau\rangle\langle 1_\tau, 1_\tau| + |2_\tau, 2_\tau\rangle\langle 2_\tau, 2_\tau| . \tag{43}$$

Relabeling and direct substitution show that

$$\mathbb{1} - \Pi_{AB} = |\Phi^+\rangle\langle\Phi^+| + |\Phi^-\rangle\langle\Phi^-| . \tag{44}$$

□

Let us quantify the coarse-graining in Proposition 1. Let $|\chi\rangle$ denote an arbitrary two-qubit state. Consider measuring $|\chi\rangle$ in the Bell basis. One of four possible outcomes obtains. The outcome can be encoded in $\log_2(4) = 2$ bits. You could encode, in one bit, whether a Φ outcome or a Ψ outcome obtained. You could encode, in the second bit, whether a $+$ outcome or a $-$ outcome obtained.

Imagine knowing the first bit's value and forgetting the second bit's. The state most reasonably attributable to the system would be $(|\Phi^+\rangle\langle\Phi^+| + |\Phi^-\rangle\langle\Phi^-|)|\chi\rangle$ or $(|\Psi^+\rangle\langle\Psi^+| + |\Psi^-\rangle\langle\Psi^-|)|\chi\rangle$, depending on the first bit. This state would be the state most reasonably attributable to the system if, instead, (40) were measured and the outcome were known.

The information in the measurement outcome can be quantified differently. Appendix G contains details.

VI B. Application 1 of binding Posner molecules: Incoherent teleportation

Quantum teleportation transmits a state $|\psi\rangle$ from one system to another [10]. Consider agents Alice and Bob who live in the same town. Suppose that Bob moves away, across the world.

Let Alice hold a qubit A that occupies a state $|\psi\rangle = c_0|0\rangle + c_1|1\rangle$. Alice may wish to send Bob $|\psi\rangle$. Mailing A would damage the state. Alice should not measure A, call Bob on the telephone, and tell him the outcome. Bob would receive too little information to reconstruct $|\psi\rangle$ in his lab.

Suppose that, before Bob moved away, he and Alice created a Bell state, e.g., $|\Psi^-\rangle$. Let B and C denote the entangled qubits. Suppose that Bob takes C across the world. Alice should perform a Bell measurement (38) of AB. One of four possible outcomes will obtain. Alice should tell Bob which, via telephone. Her call communicates $\log_2(4) = 2$ bits. Bob should transform C with a unitary whose form depends on the news. C will come to occupy the state $|\psi\rangle$. A will occupy a different state. Alice will have teleported $|\psi\rangle$ to Bob.

We introduce a variation on quantum teleportation, *incoherent teleportation*. The protocol illustrates the power of Posner binding. The protocol relies on entanglement, classical information, and Posner binding.

Posner binding resembles a coarse-grained Bell measurement, as shown in Sec. VI A. Hence Posner binding fails to teleport all the information teleportable with a Bell measurement. The coherences in $|\psi\rangle$ are not sent. A classical random variable, which results from decohering $|\psi\rangle$, is.

The set-up is introduced in Sec. VI B 1. The protocol is introduced in Sec. VI B 2 and analyzed in Sec. VI B 3.

VI B 1. Set-up

Let $|j_\tau\rangle$ denote an arbitrary $\tau = j$ eigenstate of C, for $j = 0, 1, 2$. The $|j_\tau\rangle$'s form the computational basis for the qutrit space span$\{|0_\tau\rangle, |1_\tau\rangle, |2_\tau\rangle\}$. This basis serves, in incoherent teleportation, similarly to the σ_z eigenbasis in conventional teleportation.

Consider restricting the projector (30) to the space of two qutrits:

$$\Pi'_{AB} := |0_\tau, 0_\tau\rangle\langle 0_\tau, 0_\tau| + |1_\tau, 2_\tau\rangle\langle 1_\tau, 2_\tau| + |2_\tau, 1_\tau\rangle\langle 2_\tau, 1_\tau| \,. \tag{45}$$

Let $|+_\tau\rangle := \frac{1}{\sqrt{3}}(|0_\tau\rangle + |1_\tau\rangle + |2_\tau\rangle)$.

VI B 2. Incoherent-teleportation protocol

Let A, B, and C denote three Posners. Suppose that B and C begin in $|+_\tau, +_\tau\rangle$, then bind together.[18] The joint state becomes

$$\Pi_{BC}|+_\tau, +_\tau\rangle = \frac{1}{\sqrt{3}} \left(|0_\tau, 0_\tau\rangle + |1_\tau, 2_\tau\rangle + |2_\tau, 1_\tau\rangle \right) . \tag{46}$$

In the first term's absence, (46) would be a triplet. A triplet is a Bell pair, a maximally entangled state that can fuel quantum teleportation. (46), we will show, fuels incoherent teleportation.

Suppose that, after (46) is prepared, Posners B and C drift apart. (In quantum-computation language, Alice and Bob share a Bell pair.) Let B approach A. Let A occupy an arbitrary state

$$|\psi\rangle = c_0|0_\tau\rangle + c_1|1_\tau\rangle + c_2|2_\tau\rangle \,. \tag{47}$$

The complex coefficients satisfy the normalization condition $\sum_{j=0}^{2} |c_j|^2 = 1$. (In quantum-computation language, $|\psi\rangle$ is the unknown state that contains information that Alice will teleport to Bob.) The three Posners occupy the joint state

$$|\chi\rangle := |\psi\rangle \left(\Pi_{BC}|+_\tau, +_\tau\rangle \right) . \tag{48}$$

Suppose that Posners A and B bind together. (During the analogous quantum-teleportation step, Alice performs a Bell measurement of her qubits.) The three-Posner state becomes

$$\Pi_{AB}|\chi\rangle / \langle\chi|\Pi_{AB}|\chi\rangle \tag{49}$$
$$= c_0|0_\tau, 0_\tau, 0_\tau\rangle + c_1|1_\tau, 2_\tau, 1_\tau\rangle + c_2|2_\tau, 1_\tau, 2_\tau\rangle \tag{50}$$
$$=: |\chi'\rangle \,. \tag{51}$$

Posner C occupies (Bob holds) the reduced state

$$\rho_C := \mathrm{Tr}_{AB}(|\chi'\rangle\langle\chi'|) = |c_0|^2|0_\tau\rangle\langle 0_\tau| + |c_1|^2|1_\tau\rangle\langle 1_\tau| + |c_2|^2|2_\tau\rangle\langle 2_\tau| \,. \tag{52}$$

Posner C's state encodes information about $|\psi\rangle$, the square moduli of the coefficients in Eq. (47). Yet C has never interacted with A directly. Information has teleported from A to C, with help from $|+_\tau, +_\tau\rangle$ and from Posner binding.

Posners A and B had a probability

$$p_\Pi = \mathrm{Tr}(\Pi_{AB} \, \mathrm{Tr}_C(|\chi\rangle\langle\chi|)) \tag{53}$$

of binding together. (An analogous probability can be introduced into quantum teleportation: Let Alice have a nonzero probability of failing to perform her Bell measurement.)

Suppose, instead, that A and B fail to bind together. The projector

$$\begin{aligned} \mathbb{1} - \Pi_{AB} = &(\Pi_{\tau_A=0} \otimes \Pi_{\tau_B=1}) + (\Pi_{\tau_A=0} \otimes \Pi_{\tau_B=2}) \\ &+ (\Pi_{\tau_A=1} \otimes \Pi_{\tau_B=0}) + (\Pi_{\tau_A=1} \otimes \Pi_{\tau_B=1}) \\ &+ (\Pi_{\tau_A=2} \otimes \Pi_{\tau_B=0}) + (\Pi_{\tau_A=2} \otimes \Pi_{\tau_B=2}) \end{aligned} \tag{54}$$

projects the state of AB. The three-Posner state $|\chi\rangle$ [Eq. (48)] updates to

$$\begin{aligned} [(\mathbb{1} - \Pi_{AB}) \otimes \mathbb{1}] \, |\chi\rangle = &\frac{1}{2}[c_0(|0_\tau, 1_\tau, 2_\tau\rangle + |0_\tau, 2_\tau, 1_\tau\rangle) \\ &+ c_1(|1_\tau, 0_\tau, 0_\tau\rangle + |1_\tau, 1_\tau, 2_\tau\rangle) \\ &+ c_2(|2_\tau, 0_\tau, 0_\tau\rangle + |2_\tau, 2_\tau, 1_\tau\rangle)] \\ =: &|\chi''\rangle \,. \end{aligned} \tag{55}$$

Posner C occupies (Bob holds) the reduced state

$$\begin{aligned} \mathrm{Tr}_{AB}(|\chi''\rangle\langle\chi''|) = &\frac{1}{2}[(|c_1|^2 + |c_2|^2)|0_\tau\rangle\langle 0_\tau| \\ &+ (|c_2|^2 + |c_0|^2)|1_\tau\rangle\langle 1_\tau| + (|c_0|^2 + |c_1|^2)|2_\tau\rangle\langle 2_\tau|] \,. \end{aligned} \tag{56}$$

Again, C contains information about $|\psi\rangle$, despite never having interacted directly with A.

Suppose that Bob measures $\mathcal{G}_C$, the observable that generates the unitary C. Bob samples from a random variable whose values 0, 1, and 2 are distributed according to $(p'_0 = |c_1|^2 + |c_2|^2, p'_1 = |c_2|^2 + |c_0|^2, p'_2 = |c_0|^2 + |c_1|^2)$.

VI B 3. Analysis of incoherent teleportation

Five points merit analysis. First, we quantify the classical information teleported. Second, we characterize the QI not teleported. Third, we compare the resources required for incoherent teleportation to the resources required for quantum teleportation. Incoherent teleportation, we show fourth, implements superdense coding—the effective sending of much classical information via the direct sending of little classical information, with help from entanglement. Fifth, we explain how to prepare $|+_\tau, +_\tau\rangle$ and $|\psi\rangle$ with Posner operations.

[18] One might worry that the spin state would decohere before the Posners bound. But chemical binding consists of electronic dynamics. $|+_\tau, +_\tau\rangle$ is a state of nuclear spins. Nuclear dynamics tend to unfold much more slowly than electronic dynamics. The Born-Oppenheimer approximation reflects this separation of time scales. Hence the nuclear state appears unlikely to decohere before the Posners bind.

a. Quantification of the information teleported: Posners A and B teleport a trit to C. A *trit* is classical random variable that can assume one of three possible values. Imagine preparing a Posner in the state $|\psi\rangle$ [Eq. (47)] and measuring $\mathcal{G}_C$. The measurement has a probability $p_0 = |c_0|^2$ of yielding 0, a probability $p_1 = |c_1|^2$ of yielding 1, and a probability $p_2 = |c_2|^2$ of yielding 2. So does a $\mathcal{G}_C$ measurement of C, if A binds to B [Eq. (52)]. The distribution has been teleported from A to C.

Suppose that A fails to bind to B. Measuring Posner C has a probability $p'_0 = \frac{1}{2}(|c_1|^2 + |c_2|^2)$ of yielding 0, a probability $p'_1 = \frac{1}{2}(|c_2|^2 + |c_0|^2)$ of yielding 1, and a probability $p'_2 = \frac{1}{2}(|c_0|^2 + |c_1|^2)$ of yielding 2 [Eq. (56)]. The measurement of Posner C is equivalent to an encoded generalized measurement of $|\psi\rangle$.

A *positive-operator-valued measure* (POVM) $\{M_1, M_2, \ldots, M_\ell\}$ represents a generalized quantum measurement [7]. The measurement elements are positive operators $M_k > 0$. They satisfy the completeness condition $\sum_k M_k^\dagger M_k = \mathbb{1}$. The M_k's need not be projectors, unlike PVM elements.

Consider the POVM

$$\{|\overline{0_\tau}\rangle\langle\overline{0_\tau}| = \frac{1}{\sqrt{2}}(|1_\tau\rangle\langle 1_\tau| + |2_\tau\rangle\langle 2_\tau|), \tag{57}$$

$$|\overline{1_\tau}\rangle\langle\overline{1_\tau}| = \frac{1}{\sqrt{2}}(|2_\tau\rangle\langle 2_\tau| + |0_\tau\rangle\langle 0_\tau|), \tag{58}$$

$$|\overline{2_\tau}\rangle\langle\overline{2_\tau}| = \frac{1}{\sqrt{2}}(|0_\tau\rangle\langle 0_\tau| + |1_\tau\rangle\langle 1_\tau|)\}\,. \tag{59}$$

Measuring this POVM is equivalent to measuring the encoded observable $\overline{\mathcal{G}}_C := \sum_j j_\tau |\overline{j_\tau}\rangle\langle\overline{j_\tau}|$. Measuring the $\overline{\mathcal{G}}_C$ of $|\psi\rangle$ has a probability p'_j of yielding the encoded outcome $\overline{j_\tau}$.

Suppose that Posners A and B fail to bind. A measurement of the $\mathcal{G}_C$ of C simulates an encoded measurement of the $\mathcal{G}_C$ of $|\psi\rangle$.

b. Classicality of the teleported information: Only the square moduli $|c_j|^2$ are teleported. The coefficients' phases are not. Hence incoherent teleportation achieves less than quantum teleportation does.

Section VI A clarifies why: Quantum teleportation involves Bell measurements. Incoherent teleportation involves measurements of whether $\tau_A + \tau_B = 0$. The $\tau_A + \tau_B = 0$ measurement simulates a coarse-grained Bell measurement.

c. Comparison of resources required for incoherent teleportation with resources required for quantum teleportation: In quantum teleportation, qubit C undergoes a local unitary conditioned on the Bell measurement's outcome. Our Posner C needs no such conditional correcting.

Yet part of our story depends on the Posner-binding measurement's outcome: the interpretation of the outcome of a $\mathcal{G}_C$ measurement of Posner C. Suppose that A binds to B. A $\mathcal{G}_C$ measurement of Posner C simulates a measurement of the $\mathcal{G}_C$ of $|\psi\rangle$. Suppose, instead, that A fails to bind to B. A $\mathcal{G}_C$ measurement of Posner C simulates a measurement of the $\overline{\mathcal{G}}_C$ of $|\psi\rangle$.

d. Incoherent teleportation as superdense coding: Incoherent teleportation offers less power, we have seen, than quantum teleportation. Yet incoherent teleportation offers more power than classical communication. Suppose that Alice has incoherently teleported $|\psi\rangle$. Bob may wish to know which probability distribution he holds, $\{p_0, p_1, p_2\}$ or $\{p'_0, p'_1, p'_2\}$. Alice should send Bob a bit directly: a zero if A bound to B and a one otherwise.[19]

Alice would directly send Bob a bit, while effectively sending a trit, with help from entanglement and Posner binding. A trit is equivalent to $\log_2(3) > 1$ bits. Hence Alice packs much classical information (a trit) into a small classical system (a bit).

Much classical information packs into a small classical system, with help from a Bell pair and a Bell measurement, in *superdense coding* [11]. Conventional superdense coding packs two bits into one. Our protocol packs information less densely.

e. Preparing $|\psi\rangle$ and $|+_\tau, +_\tau\rangle$: Incoherent teleportation involves two coherent quantum states, $|\psi\rangle$ and $|+_\tau, +_\tau\rangle$. Instances of these states can be prepared with Posner operations. We illustrate with an example in App. H. To construct each state, one arranges singlets in each Posner. Then, one rotates spins about the y_{lab}-axis. Alternative preparation protocols might exist.

VI C. Application 2 of binding Posner molecules: Projecting Posner molecules onto their $\tau = 0$ subspaces

The AKLT state can be prepared via projections onto subspaces associated with the spin quantum number $s = \frac{3}{2}$. Posners can occupy a variation AKLT$'$ on the AKLT state. The Posners must be projected onto their $\tau = 0$ subspaces (Sec. VII). Posner-binding measurements can effect these projections.

Proposition 2. *Let $A, B, C, \ldots, M$ label m Posner molecules. The following sequence of events projects each Posner's state onto the $\tau = 0$ eigenspace:*

1. *A and B bind together, then drift apart.*
2. *B and C bind together, then drift apart.*
3. *C and A bind together, then drift apart. A, B, and C have been projected onto their $\tau = 0$ subspaces.*

---

[19] How could such classical communication manifest in biological systems? In ordinary QI protocols, classical communication manifests as telephone calls. Today's phones do not fit in human brains. But one can envision classical channels in a biofluid. For example, if A and B bind, they shove water molecules away together. If A and B fail to bind, water propagates away from them differently. The patterns in the fluid's motion may be distinguished. The fluid-motion pattern would encode the bit.

4. *Each remaining Posner $(D, \ldots, M)$ binds to a projected Posner, then drifts away.*

Proof. First, we prove that steps 1-3 project A, B, and C onto their $\tau = 0$ subspaces. Then, we address step 4.

A projector of the form (30) represents each binding. A product Π_{123} of projectors represents the sequence 1-3 of bindings:

$$\begin{aligned}
\Pi_{123} = \Big[& \left(\Pi_{\tau_A=0} \otimes \Pi_{\tau_B=0} \otimes \mathbb{1}^{\otimes(m-2)}\right) \qquad (60)\\
& + \left(\Pi_{\tau_A=\pm 1} \otimes \Pi_{\tau_B=\mp 1} \otimes \mathbb{1}^{\otimes(m-2)}\right) \Big] \\
& \times \Big[\left(\mathbb{1} \otimes \Pi_{\tau_B=0} \otimes \Pi_{\tau_C=0} \otimes \mathbb{1}^{\otimes(m-3)}\right) \\
& \quad + \left(\mathbb{1} \otimes \Pi_{\tau_B=\pm 1} \otimes \Pi_{\tau_C=\mp 1} \otimes \mathbb{1}^{\otimes(m-3)}\right) \Big] \\
& \times \Big[\left(\Pi_{\tau_A=0} \otimes \mathbb{1} \otimes \Pi_{\tau_C=0} \otimes \mathbb{1}^{\otimes(m-3)}\right) \\
& \quad + \left(\Pi_{\tau_A=\pm 1} \otimes \mathbb{1} \otimes \Pi_{\tau_C=\mp 1} \otimes \mathbb{1}^{\otimes(m-3)}\right) \Big] \\
& = \Pi_{\tau_A=0} \otimes \Pi_{\tau_B=0} \otimes \Pi_{\tau_C=0} \otimes \mathbb{1}^{\otimes(m-3)} \,. \qquad (61)
\end{aligned}$$

Equation (60) can be understood in terms of a frustrated lattice, as explained in App. I.

Step 4 of Proposition 2 is proved as follows. Suppose that Posners A and D bind together, then drift apart. The joint state of AD is acted on by

$$(\Pi_{\tau_A=0} \otimes \Pi_{\tau_D=0}) + (\Pi_{\tau_A=\pm 1} \otimes \Pi_{\tau_D=\mp 1}) \,. \qquad (62)$$

The state of A was projected onto the $\tau_A = 0$ subspace during steps 1-3. Hence the final term in Eq. (62) annihilates the AD state. Hence $\Pi_{\tau_D=0}$ projects the state of D. □

Proposition 2 will provide a subroutine in the following section's protocol.

VII. EFFICIENT PREPARATION OF POSNER MOLECULES IN UNIVERSAL QUANTUM-COMPUTATION RESOURCE STATES

How complicated an entangled state can Posner operations (Sec. V) prepare efficiently? Many measures quantify multipartite entanglement. We study computational resourcefulness. Posners operations, we show, can efficiently prepare a state that fuels universal MBQC: By operating on the state locally, one can efficiently simulate a universal quantum computer.

The Posner state is a variation on an *Affleck-Lieb-Kennedy-Tasaki (AKLT) state*. AKLT first studied a one-dimensional (1D) chain of spin-1 particles. They constructed a nearest-neighbor antiferromagnetic Hamiltonian [21–23]. The ground state, $|\mathrm{AKLT}_{\mathrm{1D}}\rangle$, has a known form. A constant gap, independent of the system size, separates the lowest two energies.

$|\mathrm{AKLT}_{\mathrm{1D}}\rangle$ has many applications in quantum computation [20, 24, 56–65]. For example, $|\mathrm{AKLT}_{\mathrm{1D}}\rangle$ was the first state recognized as a matrix product state (MPS) [59–61]. MPSs can efficiently be represented approximately by classical computers. Also, using $|\mathrm{AKLT}_{\mathrm{1D}}\rangle$, one can simulate arbitrary single-qubit rotations. One performs local operations, including adaptive single-qubit measurements,[20] on the state [56, 57, 63].

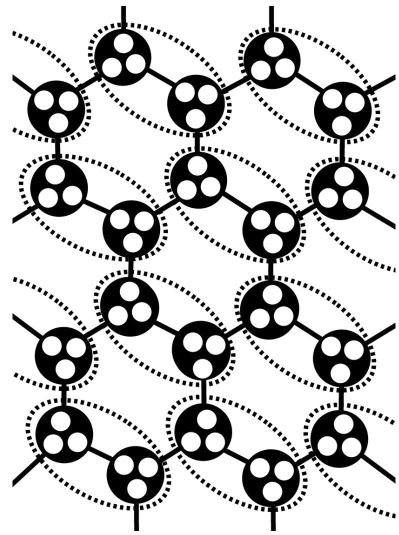

FIG. 14: AKLT′ state: Spins on a honeycomb lattice can occupy the Affleck-Lieb-Kennedy-Taski (AKLT) state $|\mathrm{AKLT}_{\mathrm{hon}}\rangle$ [21]. $|\mathrm{AKLT}_{\mathrm{hon}}\rangle$ serves as a universal resource in measurement-based quantum computation (MBQC) [20, 24]. So does the similar state $|\mathrm{AKLT}'_{\mathrm{hon}}\rangle$, which Posner operations can prepare efficiently. Each dashed oval encloses the spins in a Posner molecule. Each molecule consists of two trios of phosphorus nuclear spins. Each large black dot represents a trio. Each small white dot represents a spin. Each thin black line connects the two spins in a singlet. This figure resembles Fig. 3a of [24], as $|\mathrm{AKLT}'_{\mathrm{hon}}\rangle$ resembles $|\mathrm{AKLT}_{\mathrm{hon}}\rangle$. This figure does not illustrate the spatial arrangement of Posners in $|\mathrm{AKLT}'_{\mathrm{hon}}\rangle$. Rather, the figure illustrates the entanglement in $|\mathrm{AKLT}'_{\mathrm{hon}}\rangle$.

Two-dimensional (2D) analogs of $|\mathrm{AKLT}_{\mathrm{1D}}\rangle$ have been defined. Spin-$\frac{3}{2}$ particles on a honeycomb lattice can occupy the state $|\mathrm{AKLT}_{\mathrm{hon}}\rangle$ [21]. Local operations on $|\mathrm{AKLT}_{\mathrm{hon}}\rangle$ can efficiently simulate universal quantum computation [20, 24]. We will draw on the proof by Wei *et al.* [24]. Similar results appear in [20].

Wei *et al.* prove the universality of $|\mathrm{AKLT}_{\mathrm{hon}}\rangle$ as follows. Local POVMs, they show, reduce $|\mathrm{AKLT}_{\mathrm{hon}}\rangle$ to an encoded 2D graph state $|\overline{G(\mathcal{A})}\rangle$.[21] The graph G is random, depending on the set $\mathcal{A}$ of measurement outcomes. Also the encoding depends on $\mathcal{A}$. The overline in $|\overline{G(\mathcal{A})}\rangle$

[20] Measurements are *adaptive* if earlier measurements' outcomes dictate which measurements are performed later.

[21] A *graph state* is defined in terms of a graph G. Each vertex

represents the encoding. Wei *et al.* prescribe local measurements of a few qubits. The measurements convert $|G(\mathcal{A})\rangle$ into a cluster state on a 2D square lattice (if $\mathcal{A}$ is a typical set).[22] Such cluster states serve as resources in universal MBQC [12, 13, 19, 20]: By measuring single qubits adaptively, one can efficiently simulate a universal quantum computer.

We introduce a variation on $|\text{AKLT}_{\text{hon}}\rangle$. We call the variation the *AKLT′ state* and denote the state by $|\text{AKLT}'_{\text{hon}}\rangle$. Figure 14 illustrates the state. $|\text{AKLT}'_{\text{hon}}\rangle$ is prepared similarly to $|\text{AKLT}_{\text{hon}}\rangle$, resembles $|\text{AKLT}_{\text{hon}}\rangle$ locally, and fuels universal MBQC similarly.

This section is organized as follows. Section VII A reviews the set-up and the state construction of Wei *et al.* $|\text{AKLT}'_{\text{hon}}\rangle$ is defined in Sec. VII B. How to construct $|\text{AKLT}'_{\text{hon}}\rangle$ efficiently from phosphorus nuclear spins, using Posner operations, is detailed. Section VII C describes the reduction of $|\text{AKLT}'_{\text{hon}}\rangle$ to a 2D cluster state, known to fuel universal MBQC. The protocol is analyzed in Sec. VII D.

$|\text{AKLT}'_{\text{hon}}\rangle$ holds interest not only as a computational resource, but also in its own right. The state is analyzed in Sec. VII E. For instance, AKLT′ is shown to be a PEPS.

VII A. Set-up by Wei *et al.*

Wei *et al.* consider a 2D honeycomb lattice, illustrated in Fig. 3a of [24]. (Figure 14 has nearly the same form.) A black dot represents each site. At each site sit three spin-$\frac{1}{2}$ DOFs. White dots represent these DOFs, called *virtual spins*.

Let s_{123} and m_{123} denote a site's total spin quantum number and total magnetic spin quantum number. These numbers can assume the values $(s_{123}, m_{123}) = (\frac{1}{2}, \pm\frac{1}{2}), (\frac{3}{2}, \pm\frac{3}{2})$, and $(\frac{3}{2}, \pm\frac{1}{2})$. The qubit trio can behave as one *physical spin* of $s_{123} = \frac{1}{2}$ or $\frac{3}{2}$.

$|\text{AKLT}_{\text{hon}}\rangle$ may be prepared as follows [21]:

1. Consider two nearest-neighbor sites. Choose a virtual spin in each site. Form a singlet $|\Psi^-\rangle$ between these spins. Perform this process on every pair of nearest-neighbor sites.

2. Project each physical spin (each site) onto its $s_{123} = \frac{3}{2}$ subspace.

$|\text{AKLT}_{\text{hon}}\rangle$ is *trivalent*: Each site links, via singlets, to three other sites.

VII B. Preparing Posner molecules in $|\text{AKLT}'_{\text{hon}}\rangle$

Posner operations (Sec. V) can nearly prepare $|\text{AKLT}_{\text{hon}}\rangle$. Whether Posner operations can project trios onto their $s_{123} = \frac{3}{2}$ subspaces remains unknown. But Posner operations can project onto a molecule's $\tau = 0$ subspace.

The $\tau = 0$ subspace decomposes into a direct sum of tensor products of two three-qubit subspaces. The first three-qubit subspace is labeled by s_{123}, the total spin quantum number of the qubit triangle at $z_{\text{in}} = h_+$. The second three-qubit subspace is labeled by s_{456}. The $\tau = 0$ subspace has the form $\left(\frac{3}{2} \otimes \frac{3}{2}\right) \oplus \left(\frac{1}{2} \otimes \frac{1}{2}\right)^{\oplus 2}$. (See Appendices E and F for a derivation. See [66] for background and notation.) The first term represents the space $s_{123} \otimes s_{456} = \frac{3}{2} \otimes \frac{3}{2}$ of two spin-$\frac{3}{2}$ particles. Wei *et al.* project onto this space, in step 2.

Projecting onto the larger $\tau = 0$ space yields $|\text{AKLT}'_{\text{hon}}\rangle$. We now detail how Posners can come to occupy $|\text{AKLT}'_{\text{hon}}\rangle$. The steps are explained in physical terms (of molecules, binding, etc.). Figure 15 recasts the protocol in operational terms, as a quantum circuit:

1. Pyrophosphatase enzymes cleave some number N of diphosphates. N singlets $|\Psi^-\rangle$ are prepared (via operation 1).

2. The phosphates group together in trios. Singlets connect the trios as thin black lines connect the white dots in Fig. 14.

3. Each trio, with a nearest-neighbor trio, forms a Posner molecule (via operation 3).

4. Posners approach each other head-on, with opposite momenta, then drift apart, ideally as described in Proposition 2. For simplicity, we focus on the case in which each Posner P approaches only Posners P' that are nearest neighbors of P in the hexagonal lattice (Fig. 14). But this assumption is unnecessary.

   Suppose that each approach leads to binding. Proposition 2 is realized. Every Posner's state is projected onto the $\tau = 0$ subspace.

   But two approaching Posners might fail to bind. The success probability[23] $\approx \frac{7}{18}$. Suppose that Posners P and P' fail to bind. Suppose that P has already been

---

corresponds to a spin. Consider the Hamiltonian

$$H_G = \sum_{i \in G} \left(\sigma_i^x \bigotimes_{k \in \text{NB}(i)} \sigma_k^z \right) . \tag{63}$$

i indexes the vertices in G. The nearest neighbors of i are indexed by $k \in \text{NB}(i)$. H_G has a unique ground state. This ground state is called a *graph state* [12, 18].

[22] A *cluster state* is a graph state associated with a regular lattice G [12, 17, 18].

[23] This probability is calculated as follows. The N Posners occupy some pure state $|\psi\rangle$. Consider the two Posners' joint reduced state, $\rho_{PP'}$. The Posners share one singlet. The Posner pair contains ten other phosphorus nuclear spins. Let a denote an arbitrary one of these spins. a forms a singlet with a spin in some other Posner, P''. P'' is traced out from $|\psi\rangle$ in this calculation of $\rho_{PP'}$. Hence $\rho_{PP'}$ equals a tensor

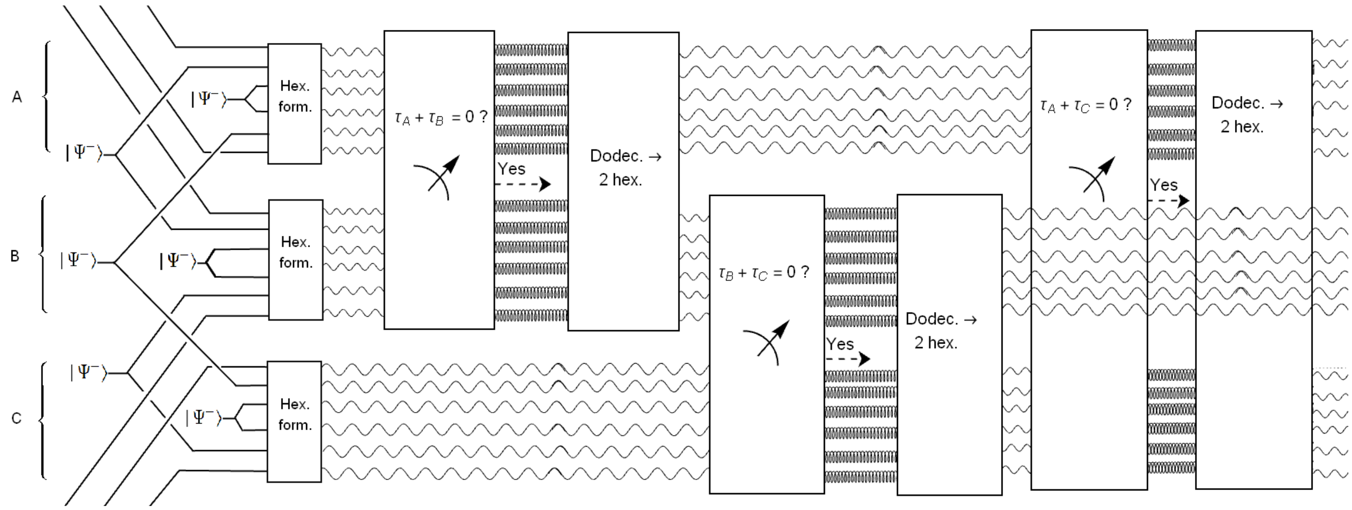

FIG. 15: Part of a circuit that efficiently prepares the AKLT$'$ state $|\mathrm{AKLT}'_{\mathrm{hon}}\rangle$: The circuit elements represent Posner operations, as explained in Sec. V A. Some thin black lines extend off the diagram. These lines represent singlets that terminate in Posners not drawn here.

projected onto its $\tau_P = 0$ subspace. P' can be "refreshed": Let P' drift into a region of high pH and/or high Mg^{2+} concentration. P' likely hydrolyzes (undergoes operation 6). Two of the phosphorus nuclear spins used to form a singlet. They form a singlet no longer, due to the binding failure. These two spins can drift away; a fresh singlet can replace them. Four other phosphorus nuclear spins remain. They continue to form singlets with spins in other Posners.[24] The two new, and four old, phosphates can form a Posner $\tilde{P}'$, via operation 3.

$\tilde{P}'$ occupies the state that P occupied before the binding failure. $\tilde{P}'$ can approach P head-on. If the binding fails, $\tilde{P}'$ can be refreshed again.

VII C. Reduction of $|\mathrm{AKLT}'_{\mathrm{hon}}\rangle$ to a cluster state known to fuel universal MBQC

Local operations can reduce $|\mathrm{AKLT}_{\mathrm{hon}}\rangle$ to a cluster state on a 2D square lattice [24]. Such cluster states serve as universal resources in MBQC [12, 13, 19]. Section VII C 1 reviews the reduction in [24]. Section VII C 2 explains the need to deviate from this reduction. Section VII C 3 details the deviation.

VII C 1. Model: Reduction of $|\mathrm{AKLT}_{\mathrm{hon}}\rangle$ to a cluster state

Wei *et al.* prescribe two steps. First, each site is measured with a POVM. The measurements yield a state equivalent to a random graph state. Second, a few qubits are measured with local POVMs.

Let us detail the initial measurements. Site v is measured with the POVM

$$\Bigg\{ F_{v,x} = \sqrt{\frac{2}{3}} \left(|\pm\pm\pm\rangle\langle\pm\pm\pm| \right), \tag{64}$$

$$F_{v,y} = \sqrt{\frac{2}{3}} \left(|i,i,i\rangle\langle i,i,i| + |-i,-i,-i\rangle\langle -i,-i,-i| \right),$$

$$F_{v,z} = \sqrt{\frac{2}{3}} \left(|000\rangle\langle 000| + |111\rangle\langle 111| \right) \Bigg\} .$$

The $F_{v,z}$ projects onto the subspace spanned by the $S_{123}^{z_{\mathrm{in}}}$ eigenstates associated with the magnetic spin quantum numbers $m_{123} = \pm\frac{3}{2}$. $F_{v,\alpha}$ projects onto the subspace spanned by the analogous $S_{123}^{\alpha_{\mathrm{in}}}$ eigenstates, for $\alpha = x, y$.

Each subspace has dimensionality two. Hence the POVM reduces each site's Hilbert space to a qubit space. The $\sqrt{\frac{2}{3}}$ leads to the the completeness relation $\sum_{\alpha=x,y,z} F_{v,\alpha}^\dagger F_{v,\alpha}$.

$\mathcal{A}$ denotes the set of POVM outcomes. The POVMs yield a state $|\overline{G(\mathcal{A})}\rangle$. $G(\mathcal{A})$ denotes a random graph whose form depends on $\mathcal{A}$. $|G(\mathcal{A})\rangle$ denotes the graph state associated with $G(\mathcal{A})$. The overline denotes an encoding dependent on $\mathcal{A}$. The system occupies a state equivalent, via the encoding, to $|G(\mathcal{A})\rangle$.

---

product of ten maximally mixed qubit states $\frac{\mathbb{1}_2}{2}$ and $|\Psi^-\rangle$: $\rho_{PP'} = \left(\frac{\mathbb{1}_2}{2}\right)^{\otimes 5} \otimes |\Psi^-\rangle\langle\Psi^-| \otimes \left(\frac{\mathbb{1}_2}{2}\right)^{\otimes 5}$. Posners P and P' have a probability $\approx \mathrm{Tr}\left(\Pi_{PP'}\rho_{PP'}\right) = \frac{7}{18}$ of binding. [$\Pi_{PP'}$ is defined as in Eq. (30).] This approximation does not account for many correlations amongst sites [24]. The exact calculations are left as an opportunity for future study.

[24] This claim can be checked via direct calculation. Computational resources limited our calculation to the reduced state of 13 spins. Whether longer-range correlations affect the results is left for future study. See footnote 23.

A random graph $G(\mathcal{A})$ defines $|G(\mathcal{A})\rangle$. In contrast, a regular graph defines a cluster state. The cluster state on a 2D square lattice serves as a universal resource in MBQC. This cluster state can be distilled from $|G(\mathcal{A})\rangle$, if $\mathcal{A}$ is typical. The distillation consists of a few single-qubit Pauli measurements [24].

VII C 2. Toward a reduction of $|\mathrm{AKLT}'_{\mathrm{hon}}\rangle$ to a cluster state

The Wei *et al.* system differs from the Posner system in two ways. First, Posner operations cannot necessarily simulate (i) the POVM (64) or (ii) the Pauli measurements in Sec. VII C 1. Whether Posner operations can remains an open question. Second, Wei *et al.* invoke $|\mathrm{AKLT}_{\mathrm{hon}}\rangle$. Posner operations can prepare $|\mathrm{AKLT}'_{\mathrm{hon}}\rangle$.

Posners therefore require a step absent from [24]. To facilitate the explanation, we invoke the agent framework of QI (Sec. V B 3). Different experimentalists can perform different operations easily. An agent Alice might run a biochemistry lab. She might be able to effect Posner operations. An agent Bob might be able to perform local POVMs but not to create and arrange singlets.

Together, Alice and Bob could produce cluster states. Alice would create $|\mathrm{AKLT}'_{\mathrm{hon}}\rangle$ and pass the state to Bob. Bob would perform local POVMs. (He might ask Alice to refresh a few Posners.) Together, the agents would form cluster states that fuel universal MBQC.

VII C 3. Reduction of $|\mathrm{AKLT}'_{\mathrm{hon}}\rangle$ to a cluster state

Bob will perform the protocol in Sec. VII C 1. But first, he measures each Posner's $\mathbf{S}^2_{123} \otimes \mathbf{S}^2_{456}$. Suppose that Posner P yields the outcome labeled by $\frac{3}{2}$ [yields the outcome $\hbar^2 \left(\frac{3}{2}\right)^2 \times 2 = \frac{9}{2}\,\hbar^2$]. The measurement has succeeded.

Now, suppose that Posner P yields the outcome labeled by $\frac{1}{2}$. The measurement has failed. Bob returns P to Alice. Alice hydrolyzes P via operation 6. She refreshes the internal singlet, as in step 4 in Sec. VII B. Let $\tilde{P}$ denote the refreshed Posner.[25] Bob measures the $\mathbf{S}^2_{123} \otimes \mathbf{S}^2_{456}$ of $\tilde{P}$. He and Alice "repeat until success" (until obtaining the $\frac{3}{2}$ outcome).

Bob holds an $|\mathrm{AKLT}_{\mathrm{hon}}\rangle$ state. He now follows the prescription of Wei *et al.* (Sec. VII C 1).

VII D. Analysis of $|\mathrm{AKLT}'_{\mathrm{hon}}\rangle$ preparation

Posner operations, we have shown, can prepare $|\mathrm{AKLT}'_{\mathrm{hon}}\rangle$ efficiently. A few local measurements reduce $|\mathrm{AKLT}'_{\mathrm{hon}}\rangle$ to a cluster state on a 2D square lattice. This cluster state can be used directly in universal MBQC. Posners' universality is remarkable. Most quantum states cannot power universal MBQC [16]. The Posners' singlets and their geometry (the decomposition of Posners into triangles, and the triangles' trivalence), underlie the state's universality.[26]

Opportunities for enhancing and simplifying our protocol exist:

1. A precise structure—a honeycomb lattice—underlies $|\mathrm{AKLT}'_{\mathrm{hon}}\rangle$. In contrast, biomolecules drift randomly. Biological singlets likely will not form honeycombs of

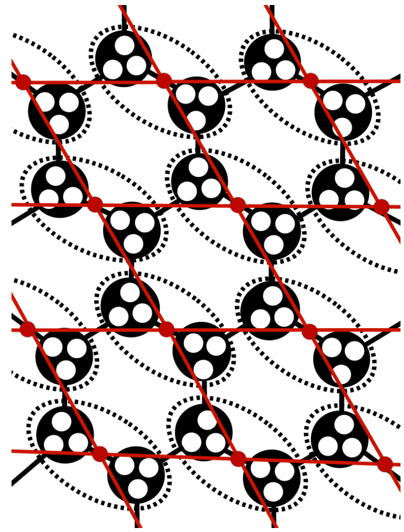

FIG. 16: Coarse-graining the hexagonal lattice into a square lattice: The black lines form a hexagonal lattice (see Fig. 14). Three qubits (small white dots) occupy each site (large black dot). Two neighboring sites form a Posner molecule (encircled with a dashed hoop). The lattice can be coarse-grained: Each Posner's two sites can be lumped together (into a red dot). The coarse-grained lattice is square (as shown by the long, red lines). This coarse-graining might facilitate a universality protocol simpler than the one in Sec. VII C 3.

[25] P contained four spins apart from the internal singlet. Each of these spins remains in a singlet with a spin in another Posner. See the calculational comments in footnote 24.

[26] $|\mathrm{AKLT}'_{\mathrm{hon}}\rangle$ is not the simplest universal Posner resource state. Singlets on a trivalent lattice would suffice. The $\tau = 0$ projections are unnecessary. The unnecessariness follows from the second equality in Eq. (31) of [24]. Yet $|\mathrm{AKLT}'_{\mathrm{hon}}\rangle$ merits defining, for three reasons. First, preparing $|\mathrm{AKLT}'_{\mathrm{hon}}\rangle$ is natural: In $|\mathrm{AKLT}_{\mathrm{hon}}\rangle$, pairs of sites are projected onto their $s_{123} \otimes s_{456} = \frac{3}{2} \otimes \frac{3}{2}$ subspaces. In $|\mathrm{AKLT}'_{\mathrm{hon}}\rangle$, pairs of sites are projected onto slightly larger subspaces. Hence $|\mathrm{AKLT}'_{\mathrm{hon}}\rangle$ resembles $|\mathrm{AKLT}_{\mathrm{hon}}\rangle$ locally. Second, suppose that Alice did not project the Posners onto their $\tau = 0$ subspaces. Bob would obtain more "error" outcomes, labeled by $\frac{1}{2}$'s, in Sec. VII C 3. Third, $|\mathrm{AKLT}'_{\mathrm{hon}}\rangle$ holds interest in its own right (Sec. VII E).

their own accord. Random graphs will more likely arise. Such graphs underlie states that might power MBQC.

Such graphs might have two or three dimensions. Three-dimensional (3D) graph states offer particular promise. First, they have substantial connectivity, needed for universality [24]. Second, 3D cluster states fuel fault-tolerant universal MBQC. The scheme relies on toplogical quantum error correction [67].

2. Bob might avoid returning Posners to Alice. The Posners' triangles (Fig. 1) form the sites in a hexagonal lattice (Fig. 14). Consider coarse-graining two sites into one. Triangle pairs are coarse-grained into Posners. Each Posner forms a site in a square lattice (Fig. 16).

   Imagine Bob measuring the $\mathbf{S}^2_{123} \otimes \mathbf{S}^2_{456}$ of a Posner P. Suppose that the "error" $\frac{1}{2}$ outcome obtains. Bob might discard P. Alternatively, he might measure the $S^{z_{\rm in}}_{1 \ldots 6}$ of P. The measurement would "terminate the lattice," forming a boundary.

   On average, ≈ 0.64 of the Posners yield the "good" $(\frac{3}{2})$ outcome.[27] The 2D square lattice has a site-percolation threshold of $p_* \approx 0.59$.[28] Hence Bob's site-deletion probability lies far above the threshold: $p \approx 0.64 > 0.59 \approx p_*$. A large, richly connected component spans Bob's graph. Such components underlie universality [24].

   Bob returns to regarding triangles, rather than Posners, as vertices. The lattice looks hexagonal but contains holes. A large connected component spans also this graph. Hence the Wei *et al.* prescription (Sec. VII C 1), or a related prescription, appears likely to turn the state into a universal cluster state.

   To check, one might refer to [68–70]. The authors consider faulty lattices: Sites might be deleted or measured.

3. Universal quantum computation is unnecessary for achieving quantum supremacy [71]. Suppose that $|\mathrm{AKLT}'_{\rm hon}\rangle$ has been converted into a cluster state on a 2D square lattice. Consider measuring single qubits nonadaptively. A random distribution $\mathcal{P}$ is sampled. Classical computers are expected not to be able to sample from $\mathcal{P}$ efficiently [72].

Aside from these opportunities, the calculational technique in footnote 23 may be rendered more precise.

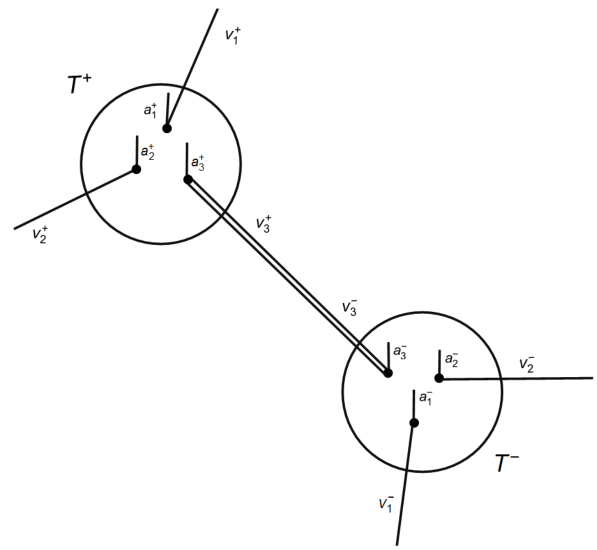

FIG. 17: The AKLT′ state $|\mathrm{AKLT}'_{\rm hon}\rangle$ as a projected entangled-pair state (PEPS): The two tensors, T^+ and T^-, are repeated to form the PEPS. T^+ represents the state of one triangle in a Posner (Fig. 1); T' represents the other triangle's state. Each tensor has three physical qubits, labeled a_j^+ or a_j^-, wherein $j = 1, 2, 3$. Each tensor has three virtual legs, labeled v_j^+ or v_j^-, wherein $j = 1, 2, 3$. Each of v_1^+ and v_2^+, and each of v_1^- and v_2^-, has bond dimension two. v_3^+ has bond dimension six, as does v_3^-. An implicit Kronecker delta $\delta_{v_3^+ \, v_3^-}$ constrains the virtual indices.

VII E. Analysis of the AKLT′ state

MBQC motivated the definition of $|\mathrm{AKLT}'_{\rm hon}\rangle$. Yet $|\mathrm{AKLT}'_{\rm hon}\rangle$ holds interest in its own right. $|\mathrm{AKLT}'_{\rm hon}\rangle$ resembles the AKLT state $|\mathrm{AKLT}_{\rm hon}\rangle$ on a honeycomb lattice. AKLT states have remarkable properties. We discuss analogous properties, and opportunities to seek more analogous properties, of $|\mathrm{AKLT}'_{\rm hon}\rangle$.

First, classical resources can represent AKLT states compactly. The 1D AKLT state $|\mathrm{AKLT}_{\rm 1D}\rangle$ is an MPS [59–61]. $|\mathrm{AKLT}_{\rm hon}\rangle$ is a PEPS [58, 62, 73]. $|\mathrm{AKLT}'_{\rm hon}\rangle$ is a PEPS, illustrated in Fig. 17 and detailed in App. J.

Hence $|\mathrm{AKLT}'_{\rm hon}\rangle$ is the ground state of some local, frustration-free Hamiltonian $H_{\mathrm{AKLT}'}$ [26]. The ground state is unique [27]. The relationship between $H_{\mathrm{AKLT}'}$ and the Posner Hamiltonian $H_{\rm Pos}$ merits study. So does whether $H_{\mathrm{AKLT}'}$ has a constant-size gap [21, 22]. If $H_{\mathrm{AKLT}'}$ has, $|\mathrm{AKLT}'_{\rm hon}\rangle$ can be prepared efficiently via cooling.

Third, $|\mathrm{AKLT}'_{\rm hon}\rangle$ results from deforming $|\mathrm{AKLT}_{\rm hon}\rangle$. AKLT states have been deformed via another strategy [70, 74–76]: Let $H_{\rm AKLT}$ denote the Hamiltonian whose ground state is the AKLT state of interest. $H_{\rm AKLT}$ is transformed with a deformation operator $\mathcal{D}(a)$ [70]. The parameter a is tuned, changing the ground state.

$|\mathrm{AKLT}'_{\rm hon}\rangle$ follows from a different deformation. We

---

[27] This probability is estimated via the technique in footnote 23.

[28] *Site percolation* is a topic in graph theory and statistical mechanics. Let G denote a graph of N sites. Consider deleting each site v with probability $1-p$. If v is deleted, so are the edges that terminate on v. Let G' denote the remaining graph. Does a path of edges traverse G' from top to bottom? If so, G' *percolates*. p_* denotes the *percolation threshold*. If $p \geq p_*$, in the limit as $N \to \infty$, G' percolates. G' does not if $p < p_*$. A phase transition occurs at $p = p_*$.

start not from a Hamiltonian, but from the Hilbert space $(\mathbb{C}^6)^{\otimes 2}$. Singlets are arranged; then the state is projected onto the $\tau = 0$ eigenspace $\mathcal{H}_{\tau=0}$. $\mathcal{H}_{\tau=0}$ contains the $\frac{3}{2} \otimes \frac{3}{2}$ subspace. Projecting onto the latter subspace would yield an AKLT state. Enlarging the projector deforms the state.

Wei *et al.* study an AKLT state's computational power as a function of a [70]. Our state's computational power might be studied as a function of the projected-onto space.

VIII. ENTANGLEMENT'S EFFECT ON MOLECULAR-BINDING RATES

Consider two Posners approaching each other head-on, as described below operation 5. The Posners might bind together. They could form subsystems in a many-body entangled system. Entanglement affects the binding probability, Fisher proposes [1].

Fisher supports his proposal with an example [1, p. 5, Fig. 3]. Let a, a', b, and b' denote Posners. Let a be entangled with a', and let b be entangled with b'. Suppose that a has bound to b. Suppose that a' approaches b' head-on. a' and b' have a higher probability of binding, Fisher argues, than in the absence of entanglement. We recast this narrative as a quantum circuit in Fig. 13.

Fisher supports his proposal by analyzing position-and-spin states. We use, instead, the Posner-binding PVM (31). Checking Fisher's example lies beyond our (classical) computational power. But we check the principle behind his example quantitatively: Entanglement, we show, can affect the probability that two Posners bind (Fig. 18 and Sec. VIII A). The effect is small, an $\approx 0.6\%$ increase. Yet this proof of principle paves a path toward large-scale QI-theoretic checking of Fisher's conjecture. Random tumbling, we find in Sec. VIII B, can eliminate entanglement's effect on binding rates.

VIII A. Illustration: Entanglement's effect on binding rates

Let A and B denote two Posners. Suppose that the AB system contains no singlets (Fig. 18a). Every phosphorus nuclear spin forms a singlet with an external molecule. The reduced state of AB equals a product of maximally mixed states: $\rho_{AB} = \frac{\mathbb{1}_{12}}{64} \otimes \frac{\mathbb{1}_{12}}{64}$. The identity operator defined on $\mathbb{C}^k$ is denoted by $\mathbb{1}_k$.

Suppose that the Posners approach each other head-on. The Posners have a probability

$$p_{AB} = \mathrm{Tr}\left(\Pi_{AB}\, \rho_{AB}\right) = \frac{43}{128} \approx 0.336 \qquad (65)$$

of binding, independently of any other event.

Suppose, instead, that AB contains the singlets shown in Fig. 18b. Each Posner contains one singlet. This singlet links the Posner's triangles. Another singlet links A

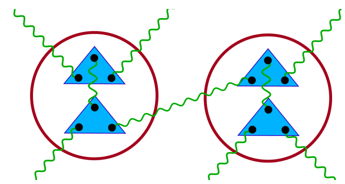

(a)

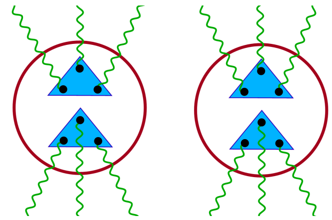

(b)

FIG. 18: Illustration of entanglement's effect on molecular-binding rates: Each maroon circle represents a Posner molecule. Each molecule contains six phosphorus nuclear spins, represented by black dots. The dots group together into trios (blue triangles) (see Fig. 1). Two dots connected by a green, wavy line form a singlet $|\Psi^-\rangle$ [Eq. (1)]. Some spins form singlets with spins in external molecules. Hence some green, wavy lines extend outside this Posner pair. Figure 18a shows a Posner pair that contains no singlets. These Posners have a probability $\frac{43}{128} = 0.336$ of binding together. Figure 18b shows a Posner pair that shares one singlet. Each Posner contains one singlet. These Posners have a probability $\frac{73}{216} \approx 0.338$ of binding. The entanglement pattern raises the binding probability by $\approx 0.6\%$.

to B. The Posners occupy the state

$$\rho'_{AB} = \left(\frac{\mathbb{1}_2}{2}\right)^{\otimes 3} \otimes \left(|\Psi^-\rangle\langle\Psi^-|\right)^{\otimes 3} \otimes \left(\frac{\mathbb{1}_2}{2}\right)^{\otimes 3} . \qquad (66)$$

Suppose that the Posners approach each other head-on. The Posners have a probability

$$p'_{AB} = \mathrm{Tr}\left(\Pi_{AB}\, \rho'_{AB}\right) = \frac{73}{216} \approx 0.338 \qquad (67)$$

of binding.

Entanglement raises the binding probability by a fraction

$$\frac{p'_{AB}}{p_{AB}} - 1 = \frac{1168}{1161} - 1 \approx 0.006 \,, \qquad (68)$$

or by $\approx 0.6\%$. This rise is small. But it illustrates quantitatively how, under Fisher's assumptions, entanglement influences binding rates.

The technique illustrated here can be scaled up. With more computational power, one can store larger quantum states. The conjecture associated with Fig. 13 can be checked.

VIII B. Random tumbling can eliminate entanglement's effect on molecular-binding rates.

Suppose that six phosphorus nuclear spins occupy the joint state ρ'_{AB} [Eq. (66)]. Suppose that each nucleus rotates randomly. Each qubit a evolves under some unitary $U_{\hat{n}_a}(\theta_a)$. The rotation axis $\hat{n}_a$ and the rotation angle θ_a may be distributed uniformly.

Suppose that six nuclei form Posner A, while the other nuclei form Posner B. The molecules occupy the joint state

$$\rho''_{AB}\left(\{\hat{n}_a\},\{\theta_a\}\right) = \left[\bigotimes_{a=1}^{12} U_{\hat{n}_a}(\theta_a)\right] \rho'_{AB} \left[\bigotimes_{a=1}^{12} U_{\hat{n}_a}(\theta_a)^\dagger\right]. \tag{69}$$

Suppose that A and B approach each other head-on. The Posners have a probability

$$p''_{AB}\left(\{\hat{n}_a\},\{\theta_a\}\right) = \mathrm{Tr}\big(\Pi_{AB}\, \rho''_{AB}\left(\{\hat{n}_a\},\{\theta_a\}\right)\big) \tag{70}$$

of binding.

On average over tumbles, the Posners have a probability

$$\overline{p''}_{AB} = \int_{\{\hat{n}_a\},\{\theta_a\}} \mathrm{Tr}\Big(\Pi_{AB}\, \rho''_{AB}\left(\{\hat{n}_a\},\{\theta_a\}\right)\Big) \tag{71}$$

$$= \mathrm{Tr}\Bigg(\Pi_{AB}\Bigg[\left(\frac{\mathbb{1}_2}{2}\right)^{\otimes 3} \otimes \int_{\{\hat{n}_a\}_{a=3}^{10},\{\theta_a\}_{a=3}^{10}} \tag{72}$$

$$\times \left[\bigotimes_{a=3}^{10} U_{\hat{n}_a}(\theta_a)\right] |\Psi^-\rangle\langle\Psi^-| \left[\bigotimes_{a=3}^{10} U^\dagger_{\hat{n}_a}(\theta_a)\right] \otimes \left(\frac{\mathbb{1}_2}{2}\right)^{\otimes 3}\Bigg]\Bigg)$$

$$= \mathrm{Tr}\left(\Pi_{AB}\left(\frac{\mathbb{1}_2}{2}\right)^{\otimes 12}\right) \tag{73}$$

$$= p_{AB} \tag{74}$$

of binding. Uniformly random rotations effectively decohere the internal singlets, on average. The binding probability reduces to its non-singlet-enhanced value.

IX. MEASURING QUANTUM COGNITION AGAINST DIVINCENZO'S CRITERIA FOR QUANTUM COMPUTATION AND COMMUNICATION

Consider attempting to realize universal quantum computation and quantum communication with any physical platform. Which requirements must the physical components and processes satisfy? DiVincenzo catalogued these requirements [28]. Five of *diVincenzo's criteria* underpin quantum computation. Quantum communication requires another two. Quantum cognition, we find, satisfies DiVincenzo's criteria, except perhaps universality.

We continue assuming that Posner operations can be performed with fine control. This assumption is discussed in Sec. V B 3. The assumption may appear questionable here: Practicalities partially concerned DiVincenzo. Attempting to realize arbitrary qubit rotations through biomolecular collisions appears impractical. Yet the fine-control assumption facilitates a first-step analysis of what the model can achieve in principle. Incorporating randomness forms an opportunity for future research.

1."A scalable physical system with well-characterized qubits": Different physical DOFs encode QI at different stages of a quantum-cognition computation (Sec. III). Initially, phosphorus-31 (^{31}P) atoms' nuclear spins serve as qubits. These atoms occupy free-floating phosphate ions.

Six phosphates can join together, forming a Posner molecule. Each state of six independent spins transforms into one antisymmetrized state (7). Hence antisymmetrized spin-and-position states store QI.

Third, each Posner has an observable $\mathcal{G}_C$ (Sec. IV A). The eigenvalue τ assumes one of three possible values: $\tau = 0, \pm 1$. The eigenspaces $\mathcal{H}_\tau$ have 24-, 20-, and 20-fold degeneracies. A state $|\tau{=}j\rangle$ can be chosen from each $\mathcal{H}_{\tau=j}$ eigenspace. span$\{|\tau{=}0\rangle, |\tau{=}1\rangle, |\tau{=}2\rangle\}$ forms an effective qutrit space (Sections IV D 1 and VI). But Posners are not associated uniquely with effective qutrits, to our knowledge (footnote 9).

QI-storing Posner systems can be scaled up spatially. ^{31}P nuclear spins can form singlets distributed across Posners. Entangled Posners can form lattices that can power universal MBQC (Sec. VII).

Just as Posner clusters can be scaled up across space, Posner computations can be scaled up across time. The ability to perform arbitrarily long computations hinges on the ability to form, dissolve, and reform Posners (Sec. V B 2). Only when qubits are in Posners can Posner binding create entanglement. Only outside of Posners can qubits rotate independently. Alternating entanglement generation with one-qubit rotations is necessary for performing arbitrary computations. Hence qubits must form Posners, then separate, repeatedly.

2. "The ability to initialize the state of the qubits to a simple fiducial state, such as $|000\ldots\rangle$": Phosphorus nuclear spins can be prepared in singlets $|\Psi^-\rangle$ (operation 1). A singlet forms as the enzyme pyrophosphatase cleaves a diphosphate ion. The resultant two phosphates are projected onto $|\Psi^-\rangle$.

3. "Long relevant decoherence times, much longer than the gate-operation time": Fisher has identified three sources of decoherence and has estimated coherence times [1, 6, 77]. Magnetic fields $\mathbf{B}$ threaten ^{31}P spins most: Nearby spins and electrons can generate $\mathbf{B}$'s. The fields can couple to the spins' magnetic dipole moments, $\boldsymbol{\mu}$: $H_{\mathrm{mag}} = -\boldsymbol{\mu}\cdot\mathbf{B}$.

Water molecules threaten ^{31}P the most. But phosphates and Posners tumble in solution. Tumbling changes the $\mathbf{B}$ experienced by a ^{31}P. On average over tumbles, $\mathbf{B}$ is expected to vanish.

^{31}P nuclear spins in free phosphates, Fisher estimates, remain coherent for about a second. ^{31}P nuclear spins in

Posners remain coherent for $\sim 10^5 - 10^6$ s.

Fisher writes also that τ labels a pseudospin "very isolated from the environment, with potentially extremely long (days, weeks, months, ...) decoherence times" [77]. As explained in Sec. IV A, to our knowledge, τ does not label any unique quantum three-level pseudospin. We translate Fisher's statement as follows: Consider preparing a $\mathcal{G}_C$ eigenstate associated with the eigenvalue $\tau = j$. Consider waiting, then measuring $\mathcal{G}_C$. How would long would you have to wait to have a high probability of obtaining an outcome $\tau = k \neq j$? At least days.

These coherence times, we expect, exceed entangling-gate times. Posner binding (operation 5) consists of electronic dynamics. Electrons have much shorter time scales than nuclei, in general. Posner binding releases about 1 eV of energy to the environment [1, 9]. A rough estimate for the binding's time scale is $t_{\rm bind} \sim \frac{\hbar}{1 \text{ eV}} \sim 10^{-15}$ s $\ll 10^5$ s. As many as 10^{20} entangling gates might be performed before the spins decohere.

Could many single-qubit rotations be performed? A qubit rotates as a phosphate tumbles in an aqueous fluid. Let us estimate a rotation's time scale. We classically approximate

$$\text{thermal energy} \sim \text{rotational energy}\,. \tag{75}$$

The thermal energy $\sim k_{\rm B}T$, wherein $k_{\rm B} \sim 10^{-23}$ J/K denotes Boltzmann's constant. The body has a temperature $T \sim 10^2$ K. The rotational energy $\sim I\omega^2$. The classical moment of inertia is denoted by I. The angular frequency is $\omega \sim \frac{2\pi}{t_{\rm rot}} \sim \frac{10}{t_{\rm rot}}$, wherein $t_{\rm rot}$ denotes the rotational time scale. We approximate a Posner molecule as a sphere and drop constants: $I \sim mr^2$, wherein m denotes the molecule's mass and r denotes the radius. The Posner has a mass $m \sim 10^{-24}$ kg [78, Supp. Mat., Table S1] and a radius $r \sim 10$ Å $= 10^{-9}$ m [4]. Substituting into (75) yields $k_{\rm B}T \sim mr^2\omega^2 \sim mr^2 \frac{10^2}{t_{\rm rot}^2}$. Solving for the rotational time scale yields

$$t_{\rm rot} \sim 10r\sqrt{\frac{m}{k_{\rm B}T}} \sim 10^{-10} \text{ s} \tag{76}$$

$$\ll 1 \text{ s}\,. \tag{77}$$

Hence the single-qubit-rotation time scale is much less than the out-of-Posner decoherence time.

4. "A 'universal' set of quantum gates": The biological qubits can undergo Posner operations, introduced in Sec. V A. The operations include arbitrary single-qubit unitaries and entangling operations. Analyses appear in Sections V B and VI.

These qubit operations induce gates on the effective qutrits. The induced gates depend on how the qutrits are defined.

Whether the gates form a universal set—in transforming the qubits or the qutrits—remains an open question. Posner operations can efficiently prepare a state $|\text{AKLT}'_{\rm hon}\rangle$ that can fuel universal MBQC (Sec. VII). Whether Posner operations can implement MBQC remains unknown.

5. "A qubit-specific measurement capability": Posner binding (operation 5) measures whether $\tau_A + \tau_B = 0$. Whether two molecules have bound together is a classical property. Each Posner's center of mass is a classical DOF: Water and other molecules bounce off the Posner frequently. The bounces measure the Posner's position, precluding coherence. Hence two Posners' closeness is a classical DOF. Closeness serves as a proxy for binding. Hence whether two Posners have bound is a classical DOF. This classical memory records whether $\tau_A + \tau_B = 0$.

Fisher proposed that the readout might be amplified further [1]. Posner binding could impact later Posner binding, then the hydrolyzation of Posners, then neurons' Ca^{2+} concentrations, and then neuron firing. This process is overviewed in this paper's introduction.

6. "The ability to interconvert stationary and flying qubits": Computing is often easiest with unmoving hardware. *Stationary qubits* remain approximately fixed. They undergo computation. Then, their state can be transferred to *flying qubits*. Flying qubits move easily. They can bring states together for joint processing.

Consider, for example, a quantum algorithm that contains subroutines. Different labs' quantum dots could implement different subroutines. The quantum dots' states could be converted into photonic states. The photons could travel down optical fibers to a central lab. There, the algorithm's final steps could be implemented.

Phosphorus nuclear spins could serve as stationary qubits and as flying qubits. Phosphorus atoms occupy lone phosphates and Posners. In each setting, the nuclear spins undergo computations (Sec. V A). But Posners protect the spins from decoherence better than lone phosphates do [1]. Hence Posners form better flying qubits.

The projector $\Pi^-_{\text{no-coll.}}$ [Eq. (8)] transforms phosphate states into a Posner state. The projection forms a one-to-one map. Hence "stationary" phosphates' states are converted into a "flying" Posner's state faithfully.

"The ability faithfully to transmit flying qubits between specified locations": Posners diffuse through intracellular and extracellular fluid. A protein could transport Posners into neurons [1, 6]. This protein has been called the *vesicular glutamate transporter* (VGLUT) [79–82] and the *brain-specific (B) sodium-dependent (*Na^+*) inorganic-phosphate (Pi) cotransporter* (BNPI) [83]. VGLUT sits in cell membranes, through which the protein could ferry Posners. Posners protect in-transit ^{31}P nuclear spins for $\sim 10^5 - 10^6$ s [1, 5], as discussed above.

For how long do Posners diffuse between neurons? We estimate by dimensional analysis. The diffusion constant D has dimensions of distance^2/time:

$$D \sim \frac{\ell^2}{t_{\rm diff}}\,. \tag{78}$$

The time scale over which a Posner diffuses between neurons is denoted by $t_{\rm diff}$. A typical synapse has an area of $\ell^2 \sim 10^{-2}$ μm^2 [84, Fig. 2].

We estimate D via the Einstein-Stokes relation,

$$D = \frac{k_{\rm B} T}{6\pi \eta r} \, . \tag{79}$$

Equation (79) describes a radius-r sphere in a viscosity-η fluid. Water has a viscosity $\eta \sim 10^{-3}$ N $\cdot$ s/m^2. A Posner molecule has a radius $r \sim 10$ Å [4].

We substitute these numbers, with $k_{\rm B} \sim 10^{-23}$ J/K, $T \sim 10^2$ K, and $6\pi \approx 10$, into Eq. (79): $D \sim 10^{-10}$ m^2/s. We substitute into Eq. (78), upon solving for $t_{\rm diff}$:

$$t_{\rm diff} \sim \frac{\ell^2}{D} \sim \frac{10^{-2}(10^{-6} \text{ m})^2}{10^{-10} \text{ m}^2/\text{s}} \tag{80}$$

$$= 0.1 \text{ ms} \ll 10^5 \text{ s} \, . \tag{81}$$

Hence Posners are expected to be able to traverse a synapse before their phosphorus nuclear spins decohere.

X. OUTLOOK

This paper establishes a framework for the QI-theoretic analysis of Posner chemistry. The paper also presents applications of Posners to QI processing: to QI storage and protection, to quantum communication, and to quantum computation. Many QI applications of Posners await discovery, we expect. In turn, QI motivates quantum-chemistry questions. Opportunities are discussed below.

Quantum error-correcting and -detecting codes: We presented one quantum error-detecting code and one error-correcting code accessible to Posners. Other accessible codes might protect more information against more errors.

Furthermore, one conserved charge "protects" each of our codes. In the error-detecting code, for example, the codewords $|j_\tau\rangle$ correspond to distinct eigenvalues of $\mathcal{G}_C$. The natural dynamics protect $\mathcal{G}_C$. Hence the dynamics should not map any codeword $|j_\tau\rangle$ into any other $|k_\mathcal{L}\rangle$. But the dynamics could map $|j_\tau\rangle$ to another state $|j'_\tau\rangle$ in the $\tau = j$ eigenspace.

Imagine a more robust code: A complete set of quantum numbers (e.g., $\{\tau, m_{1\ldots6}, \ldots\}$) would label each codeword. The dynamics could not map any codeword $|\tau, m_{1\ldots6}, \ldots\rangle$ into any other codeword $|\tau', m'_{1\ldots6}, \ldots\rangle$. Such a code would enjoy considerable protection by charge preservation.

Relatedly, quantum codes have been cast as the ground spaces of Hamiltonians. Every code's states, $|\bar{\psi}\rangle$, occupy a Hilbert space $\bar{\mathcal{H}}$. Suppose that $\bar{\mathcal{H}}$ is the ground space of a Hamiltonian H. Suppose that the system is in thermal equilibrium at a low temperature $T = \frac{1}{k_{\rm B} T}$. The system has a high probability of remaining in $\bar{\mathcal{H}}$. Entropy suppresses errors. Equivalently, the code detects errors. The Posner Hamiltonian $H_{\rm Pos}$ has yet to be characterized. The ground space might point to an entropically preserved a code.

Quantum algorithms: Posners might perform quantum algorithms of two types: (i) Known algorithms [85] might decompose into Posner operations. (ii) Posner operations could inspire hitherto-unknown quantum algorithms.

Reverse-engineering: QI processing could guide conjectures about quantum chemistry. Fisher reverse-engineered physical mechanisms by which entanglement could impact cognition [1]. Similarly, one might reverse-engineer physical mechanisms by which Posners could process QI. This paper motivates reverse-engineering opportunities:

1. Section VII B details how Posner operations can efficiently prepare states that can fuel universal MBQC. To use the states, one performs the operations in Sec. VII C. Example operations include measurements of the POVM $\{F_x, F_y, F_z, \}$ [Eq. (64)]. Then, one measures single qubits adaptively. Could biological systems implement these operations?

2. Reverse-engineer a measurement of the generator $\mathcal{G}_C$ of the permutation operator C. If $\mathcal{G}_C$ can be measured, incoherently teleported random variables can be used easily (Sec. VI B 2).

Quantum computational complexity and universality: Posner operations (Sec. V) constitute a model of quantum computation. Which set of problems can this model solve efficiently? Let PosQP denote the class of computational problems solvable efficiently with Posner quantum computation.

Whether Posner quantum computation is universal remains an open question. (See Sec. V B 1 for an elaboration.) Suppose that the model were universal. PosQP would equal BQP (the class of problems that a quantum computer can solve in polynomial time [7]). But perhaps PosQP $\subset$ BQP. PosQP merits characterization.

AKLT$'$ state and MBQC protocol: Posner operations can efficiently prepare a state $|\text{AKLT}'_{\text{hon}}\rangle$ that fuels universal MBQC (Sec. VII). The state preparation may be simplified. Opportunities are detailed in Sec. VII D. Also, $|\text{AKLT}'_{\text{hon}}\rangle$ holds interest outside of MBQC. Properties to explore are discussed in Sec. VII E.

Entanglement's effect on binding rates and biological Bell tests: Entanglement between Posners affects binding rates. So Fisher conjectured in [1]. The conjecture grew from analyses of spin-and-orbital states. We supported the conjecture with a small example, using a PVM (Sec. VIII). The example illustrates how to check Fisher's conjecture with the formalism of QI. Larger-scale calculations could test Fisher's conjecture more directly.

Moreover, the QI formalism could lead to a framework for *biological Bell tests.* Such tests might be cast as nonlocal games [86]. The Clauser-Holt-Shimony-Hauser (CHSH) game, which illustrates Bell's theorem [87, 88], can serve as a model.

Quantum chemistry: Physical conjectures populate Sections II C, II D, and III C. These conjectures merit testing and refinement. First, Posner creation was modeled with a Lennard-Jones potential. Second, pre-Posner spin states were assumed to transform deterministically into antisymmetric Posner states. The pre-Posner orbital state was assumed to determine the map. Third, Posner creation was assumed to preserve each spin's $S^{z_{\mathrm{lab}}}$ essentially. Fourth, Posner dynamics were assumed to preserve C and $S^{z_{\mathrm{in}}}_{1\ldots6}$.

Randomness: Our QI-processing protocols involve perfect executions of Posner operations. But Posners randomly collide with other molecules, tumble, and experience electric and magnetic fields. Randomness could hinder some, and improve some, QI processing.

For example, Sec. VII features a honeycomb lattice. Singlets would likely not form a honeycomb in solution. They would form a random graph. Randomness could improve the state's connectivity. Improved connectivity might lower the bar for fueling universal MBQC (Sec. VII D). What randomness helps, and what randomness hinders, merits investigation.

ACKNOWLEDGMENTS

The authors thank Ning Bao, Philippe Faist, Matthew Fisher, Steve Flammia, Leo Radzihovsky, and Tzu-Chieh Wei for discussions. We thank Fernando Pastawski for help with constructing the quantum error-detecting code. NYH thanks John Preskill for nudges toward this paper's topic and for feedback about drafts. We are grateful for funding from the Institute for Quantum Information and Matter, an NSF Physics Frontiers Center (NSF Grant PHY-1125565) with support from the Gordon and Betty Moore Foundation (GBMF-2644). This research was partially supported by the NSF also under Grant No. NSF PHY-1125915. NYH is grateful for partial support from the Walter Burke Institute for Theoretical Physics at Caltech, for a Graduate Fellowship from the Kavli Institute for Theoretical Physics, and for a Barbara Groce Women's Graduate Fellowship.

Appendix A BACKGROUND: QUANTUM INFORMATION THEORY

Quantum systems can process information more efficiently, transmit information more compactly, and secure information more reliably than classical systems can. Consider a system of N qubits, e.g., N phosphorus nuclear spins. The system corresponds to a Hilbert space $\mathcal{H}$ of dimensionality 2^N. Let $\{|\phi_j\rangle\}$ denote an orthonormal basis for $\mathcal{H}$. The system can occupy a quantum state $|\psi\rangle = \sum_j c_j |\phi_j\rangle \in \mathcal{H}$. The 2^N coefficients $c_j \in \mathbb{C}$ satisfy the normalization condition $\sum_j |c_j|^2 = 1$. Consider specifying one of the 2^N basis elements $|\phi_j\rangle$. One must use 2^N bits (two-level units of classical information). The specification requires only N qubits. One can leverage this discrepancy to process information quickly, using quantum systems. The state $|\psi\rangle$ constitutes QI.

QI can be processed with help from entanglement [7, 8]. *Entanglement* manifests in correlations stronger than any shareable by classical systems. Entanglement facilitates quantum computation, communication, and cryptography. We briefly review efficiency, quantum computational models and universality, and quantum error correction. Readers seeking more background are referred to [7, 8].

A 1 Efficiency

Quantum computers can efficiently solve certain problems that, according to widespread belief, classical computers cannot. *Efficiently* loosely means the following. Consider a family F of computational problems. For example, consider receiving a number $\mathcal{N}$ whose prime factors you must identify. An instance of F consists of, e.g., the number $\mathcal{N}$ to be factored. Let n quantify the resources required to specify an instance of F. For example, n might equal the number of bits needed to represent $\mathcal{N}$. Let t denote the time required to solve the instance. Suppose that the time grows, at most, polynomially in the amount of resources: $t \sim (\text{const.}) n^k$, for some $k \geq 0$. The problems in F can be solved efficiently.

Quantum computers can factor arbitrary numbers more quickly than classical computers can [89]. Imagine using a quantum computer to solve a problem more quickly than any classical computer. One would achieve *quantum speedup*, or *quantum supremacy* [71].[29]

[29] Preskill coined the term "quantum supremacy" in [71]. The paper concludes with quantum computing's potential: "How might quantum computers change the world? Predictions are never

A 2 Quantum-computation models and universality

A general quantum process consists of state preparations, evolutions, and measurements. Which operations can be implemented easily (which states $|\psi\rangle$ can be prepared easily, etc.) varies from platform to platform. Consider, for example, a nuclear-magnetic resonance (NMR) experiment. Let N denote the number of nuclear spins. Preparing the pure state $|0\rangle^{\otimes N}$ is difficult. Preparing a maximally mixed state $\mathbb{1}/2^{N-1}$ of $N-1$ spins, tensored with one pure $|0\rangle$, is easier [90]. A set of quantum resources—of performable quantum operations—forms a *model for quantum computation*. DiVincenzo catalogued the ingredients needed to realize a quantum-computation model physically [28].

Certain computational models are universal [91]. A universal quantum computer can perform every conceivable quantum computation. Every universal model can simulate every other universal model efficiently.

Many quantum-computation models exist. Two prove most pertinent to this paper: the circuit model [15] and measurement-based quantum computation (MBQC) [12–14]. Other models include the quantum Turing machine [91], the one-clean-qubit model [90], adiabatic quantum computation [92], anyonic quantum computation [93], teleportation-based quantum computation [52–55], quantum walks on graphs [94], and permutational quantum computation [95].

The *circuit model* is used most widely [15]. One solves a problem by running a quantum circuit, illustrated by a circuit diagram (e.g., Fig. 13). Wires represents the qubits, which are often prepared in pure states $|0\rangle$. Rectangles represent unitary operations U. The U's evolve the qubits, implementing gates. A rectangle inscribed with a dial represents a measurement. Single qubits can be measured with respect to some orthonormal basis, e.g., $\{|0\rangle, |1\rangle\}$, wherein $\langle 0|1\rangle = 0$.

Depth quantifies a circuit's length, or complexity. Consider grouping together the operations that can be performed simultaneously. For example, qubit 1 can interact with qubit 2 while qubit 3 interacts with qubit 4. Each group of gates occurs during one time slice. The number of time slices in a circuit equals the circuit's depth. Suppose that the depth does not depend on the number of qubits. Such a circuit has *constant depth*.

Primitive unitaries can be implemented directly. Composing primitives simulates more-complicated operations. One universal primitive set [7, 96] is natural to compare with ^{31}P dynamics: (i) Each qubit's state can rotate through a fixed angle θ about a fixed axis $\hat{n}$ of the Bloch sphere.[30] θ must be an irrational multiple of 2π. (ii) Each qubit can rotate through a fixed angle θ' about a fixed axis $\hat{n}' \neq \hat{n}$. (iii) Any two qubits can be entangled via some fixed unitary.

No unitary is known to entangle Posners' phosphorus nuclear spins. Hence we turn from the circuit model to MBQC [12–14]. To implement MBQC, one prepares a many-qubit entangled state $|\psi\rangle$. One measures single qubits adaptively. Measurements are *adaptive* if earlier measurements' outcomes dictate later measurements' forms.

Certain states $|\psi\rangle$ enable one to simulate efficiently, via MBQC, a universal quantum computer. Example states include the *Affleck-Kennedy-Lieb-Tasaki (AKLT) state* on a honeycomb lattice, $|\mathrm{AKLT_{hon}}\rangle$ [12, 13, 19, 20]. Posners can occupy a similar state, $|\mathrm{AKLT'_{hon}}\rangle$. $|\mathrm{AKLT'_{hon}}\rangle$ can fuel universal MBQC (Sec. VII).

A 3 Quantum error correction

Two sources of error threaten quantum computers. First, the operations performed might differ from the target operations. Consider, for example, trying to rotate a qubit through an angle $\frac{\pi}{2}$ about the z-axis. One might overshoot or undershoot. The qubit would rotate through an angle $\frac{\pi}{2} + \epsilon$, for some $\epsilon \neq 0$.

Second, a quantum computer might entangle with its environment. The environment decoheres the computer's state. QI leaks from the computer into the environment.

Quantum error correction preserves QI. Imagine wishing to process a state $|\psi\rangle$ of k qubits. One chooses an *error-correcting code*. The code maps $|\psi\rangle$ to a state $|\bar{\psi}\rangle$ of $n > k$ qubits. $|\bar{\psi}\rangle$ undergoes physical processes that effect *logical operations* on the encoded state. The logical operations constitute a computation.

Throughout the computation, certain observables O are measured. Which O's depends on the code. The measurements' outcomes imply whether an error has occurred and, if so, which sort of error. The code dictates how to counteract the error. The state is typically corrected with some unitary U. After the computation and correction terminate, the state is decoded. The computational problem's answer is read out.

---

easy, but it would be especially presumptuous to believe that our limited classical minds can divine the future course of quantum information science." Posners suggest that we have better chances than Preskill expected.

[30] The *Bloch sphere* represents pure qubit states geometrically [7]. A general pure qubit state has the form $|\psi\rangle = \cos\frac{\theta}{2}|0\rangle + e^{i\varphi}\sin\frac{\theta}{2}|1\rangle$, wherein $\theta, \varphi \in [0, 2\pi)$. The state is equivalent to the *Bloch vector* $(\sin\theta\,\cos\varphi, \sin\theta\,\sin\varphi, \cos\theta)$. The Bloch vector lies on the unit sphere, or Bloch sphere. Points inside the sphere represent mixed states $\rho \neq |\psi\rangle\langle\psi|$.

A code can *detect* more errors than it can correct. Suppose that, according to the O measurements, many errors have corrupted $|\psi\rangle$. Suppose that the code cannot correct all those errors. The state must be scrapped; and the computation, reinitiated. We present a quantum error-detecting code and an error-correcting code formed from states accessible to Posners (Sec. IV D).

Let us review the mathematics of quantum error correction and detection (QECD). Consider encoding $k < n$ logical qubits in n physical qubits. The physical Hilbert space $\mathbb{C}^{2n}$ has dimensionality 2^n. A QECD code is a subspace $\mathcal{H}_{\mathcal{L}} \subset \mathbb{C}^{2n}$ of dimensionality $2^k < 2^n$. Let $\mathcal{B}_{\mathcal{L}}^{\text{comp}} = \{|j_{\mathcal{L}}\rangle\}$ denote the code's computational basis. (See Sec. III B for an introduction to computational bases.)

Each quantum error-correcting/-detecting code corresponds to a set $\{E_\alpha\}$ of correctable/detectable errors. For example, a code of $n = 9$ physical qubits has been constructed [97]. This code corrects the set of single-qubit Pauli errors, $\{\sigma_1^x, \sigma_2^x, \ldots, \sigma_9^x, \sigma_1^z, \ldots, \sigma_9^z\}$. The shorthand $\sigma_j^\alpha \equiv \mathbb{1}^{\otimes(j-1)} \otimes \sigma_j^\alpha \otimes \mathbb{1}^{\otimes(n-j)}$. The ability to correct σ^y errors follows from the ability to correct σ^x and σ^z.

Under what conditions can a code $\mathcal{H}_{\mathcal{L}}$ detect a set $\{E_\alpha\}$ of errors? The code and set must satisfy the *quantum error-detection criteria*,

$$\langle j_{\mathcal{L}}|E_\alpha|k_{\mathcal{L}}\rangle = C_\alpha \, \delta_{jk} \qquad \forall j, k, \alpha \, . \tag{A1}$$

The Kronecker delta is denoted by δ_{jk}. C_α denotes a constant dependent only on the error E_α, not on the codeword labels j and k. Equation (A1) decomposes into two subcriteria: the off-diagonal criterion, in which $j \neq k$, and the diagonal criterion, in which $j = k$.

The *off-diagonal error-detecting criterion* has the form

$$\langle j_{\mathcal{L}}|E_\alpha|k_{\mathcal{L}}\rangle = 0 \qquad \forall j \neq k \, . \tag{A2}$$

No E_α maps any codeword $|k_{\mathcal{L}}\rangle$ into any other codeword $|j_{\mathcal{L}}\rangle$. The logical states retain their integrity under detectable errors.

The *diagonal criterion* has the form

$$\langle j_{\mathcal{L}}|E_\alpha|j_{\mathcal{L}}\rangle = C_\alpha \qquad \forall j, \alpha \, . \tag{A3}$$

Suppose that $|j_{\mathcal{L}}\rangle$ is prepared. The environment might effectively measure $\langle E_\alpha\rangle$. The environment gains no information about the state, according to Eq. (A3): Every codeword's expectation value equals every other codeword's. Typical detectable errors E_α operate nontrivially on just a few close-together qubits. The codewords are *locally indistinguishable* with respect to $\{E_\alpha\}$.

Local indistinguishability protects QI: Suppose that the environment had "learned" about $|j_{\mathcal{L}}\rangle$. Information would have leaked out of the system. Highly entangled states are locally indistinguishable: Entanglement distributes information throughout the system. Local operations cannot extract the distributed information.

We have reviewed the error-detection criteria. Under what conditions can a code $\mathcal{H}_{\mathcal{L}}$ correct $\{E_\alpha\}$? The code must satisfy the *quantum error-correction criteria* [8, 36–40],

$$\langle j_{\mathcal{L}}|E_\beta^\dagger E_\alpha|k_{\mathcal{L}}\rangle = C_{\alpha\beta} \, \delta_{jk} \quad \forall j, k, \alpha, \beta \, . \tag{A4}$$

Equation (A4) is interpreted similarly to Eq. (A1). A code that corrects $(d-1)/2$ errors detects $(d-1)$ errors. We refer readers to [8] for more background.

Appendix B MULTIPLICITY OF (NO-COLLIDING-NUCLEI ANTISYMMETRIC) SUBSPACES ACCESSIBLE TO A POSNER MOLECULE

A subtlety about $\mathcal{H}_{\text{no-coll.}}^-$ was glossed over in Sec. III C. Consider Eq. (7). In every term, the spin quantum number $m_{\pi_\alpha(j)}$ appears alongside the position $\mathbf{r}_{\pi_\alpha(j)}$. The tuple $(m_{\pi_\alpha(j)}, \mathbf{r}_{\pi_\alpha(j)})$ occupies different kets in different terms. But $m_{\pi_\alpha(j)}$ remains hitched to the same position $\mathbf{r}_{\pi_\alpha(j)}$ throughout the terms. How are the $m_{\pi_\alpha(j)}$'s assigned to positions?

This question has a two-part answer. The choice of coordinate system partially determines the assignments. So do initial conditions, the pre-Posner phosphates' positions and momenta.

The choice of coordinate system determines the φ-value associated with a given m-value. For example, suppose that $m_1 = 0$. Should this spin variable be assigned to $\mathbf{r}_1 = (\phi, h)$, to $\mathbf{r}_1 = (\phi + 2\pi/3, h)$, or to $\mathbf{r}_1 = (\phi + 4\pi/3, h)$? (Whether $h = h_+$ or $h = h_-$ is irrelevant.) This assignment is a convention, because the orientation of $\hat{x}_{\text{in}}$ is a convention.

We illustrate the answer's second part with an example. Suppose that three singlets,

$$|\Psi^-\rangle^{\otimes 3} = \frac{1}{\sqrt{2}}\left(|\uparrow\rangle|\downarrow\rangle - |\downarrow\rangle|\uparrow\rangle\right) \otimes \frac{1}{\sqrt{2}}\left(|\uparrow\rangle|\downarrow\rangle - |\downarrow\rangle|\uparrow\rangle\right) \otimes \frac{1}{\sqrt{2}}\left(|\uparrow\rangle|\downarrow\rangle - |\downarrow\rangle|\uparrow\rangle\right), \tag{B1}$$

join together to form a Posner. Molecule creation is assumed to preserve the entanglement within each pair of spins (Sec. II D). Posner creation maps each six-spin term in (B1) to a sum (7). Suppose we choose an intra-Posner coordinate system such that $\mathbf{r}_1 = (0, h)$, for $h = h_+$ or $h = h_-$. Given that coordinate system, which value should $\mathbf{r}_2$ assume? Should the spin at $(0, h_\pm)$ form a singlet with the spin at $(0, h_\mp)$, with the spin at $(2\pi/3, h_\pm)$, etc.? Different answers generate qualitatively different Posner states: The states transform differently under $S^{z_{\text{in}}}_{1\ldots6}$. Direct calculation supports this claim.

The correct answer, we posit, is determined by the positions and momenta that the phosphates had at the lip of the Lennard-Jones potential (Sec. II C). Different projections of the same initial state, we posit, would release different amounts of heat to the environment.

The PVM model in Sec. II D can now be refined: Posner creation projects the phosphates' state with the projector $\Pi^-_{\text{no-coll.}}$ onto *some* no-colliding-nuclei subspace $\mathcal{H}^-_{\text{no-coll.}}$ of the antisymmetric subspace. 6! such subspaces exist; 6! possible forms are available to $\Pi^-_{\text{no-coll.}}$. One subspace and projector correspond to entanglement between the $(0, h_\pm)$ spin and the $(0, h_\mp)$ spin; one subspace and projector correspond to entanglement between the $(0, h_\pm)$ spin and $(2\pi/3, h_\pm)$ spin; etc. Hence pre-Posner positions and momenta, with a choice of coordinate system, determine to which position each spin variable (e.g., m_1) is assigned during Posner creation.

Appendix C THE POSNER-MOLECULE HILBERT SPACE $\mathcal{H}^-_{\text{no-coll.}}$ HAS DIMENSIONALITY 64.

When a Posner forms, we posit, $\Pi^-_{\text{no-coll.}}$ projects the phosphorus nuclei's joint state [Eq. (8)]. $\Pi^-_{\text{no-coll.}}$ defines a map that preserves the dimensionality of the space available for storing QI, 64. A counting argument shows why.

Imagine that the phosphorus nuclei were classical and distinguishable. A tuple $(m_j, \mathbf{r}_j)$ would label the j^{th} nucleus's state. The spin variable m_j could assume one of two possible values. The position $\mathbf{r}_j$ could assume one of six possible values, $\uparrow$ or $\downarrow$. The tuple could therefore assume one of twelve possible values:

$$(\uparrow, (\phi, h_+)),\ (\uparrow, (\phi, h_-)),\ (\uparrow, (\phi + 2\pi/3, h_+)),\ (\uparrow, (\phi + 2\pi/3, h_-)),\ (\uparrow, (\phi + 4\pi/3, h_+)),\ (\uparrow, (\phi + 4\pi/3, h_-)),$$
$$(\downarrow, (\phi, h_+)),\ (\downarrow, (\phi, h_-)),\ (\downarrow, (\phi + 2\pi/3, h_+)),\ (\downarrow, (\phi + 2\pi/3, h_-)),\ (\downarrow, (\phi + 4\pi/3, h_+)),\ \text{or}\ (\downarrow, (\phi + 4\pi/3, h_-))\,. \tag{C1}$$

The nuclei would be "dodequits": $\dim(\mathcal{H}_{\text{nuc}})$ would equal $2 \times 6 = 12$.

Let us return to reality: The phosphorus nuclei are indistinguishable fermions. A hextuple of nuclei can occupy the antisymmetric basis state (7). This state is labeled by a set of six tuples. Each tuple must differ from each other tuple, for the state to be antisymmetric. To label a joint state, we choose six of the twelve possible tuples.

But we cannot choose six arbitrary tuples. No two tuples can contain the same position: No two nuclei can coincide. Hence we pair up the twelve possible tuples. Each pair's constituent tuples have the same positions and different spin states:

1. $(\uparrow, (\phi, h_+)), \quad (\downarrow, (\phi, h_+))$
2. $(\uparrow, (\phi, h_-)), \quad (\downarrow, (\phi, h_-))$
3. $(\uparrow, (\phi + 2\pi/3, h_+)), \quad (\downarrow, (\phi + 2\pi/3, h_+))$
4. $(\uparrow, (\phi + 2\pi/3, h_-)), \quad (\downarrow, (\phi + 2\pi/3, h_-))$
5. $(\uparrow, (\phi + 4\pi/3, h_+)), \quad (\downarrow, (\phi + 4\pi/3, h_+))$
6. $(\uparrow, (\phi + 4\pi/3, h_-)), (\downarrow, (\phi + 4\pi/3, h_-))$

We have formed six pairs of tuples. We choose one tuple from each pair, to label an antisymmetric joint basis state.

Let us count the ways in which we can choose the six tuples. We can choose one tuple from each pair in two ways. We choose from each of six pairs. Hence we have $2^6 = 64$ choices of labels for an antisymmetric joint state.

Appendix D WHY A POSNER MOLECULE'S $S^{z_{\text{in}}}_{1\ldots6}$ IS EXPECTED TO BE CONSERVED

A Posner's phosphorus nuclear spins resist decoherence for long times, according to Fisher [1]. We interpret this claim as meaning that the Posner's dynamics preserve $S^{z_{\text{in}}}_{1\ldots6}$ (the z-component, relative to the Posner's internal frame, of the six phosphorus nuclei's total spin) for long times. Fisher supports his claim by arguing that the spins (i) fail to couple to electric fields, (ii) couple to magnetic fields weakly, and (iii) cannot couple to the Posner's calcium and oxygen nuclear spins (as those atoms have spin quantum numbers $s = 0$) [1, 6].

We supplement Fisher's analysis to support our interpretation. Appendix D 1 concerns how phosphorus nuclear spins might interact. We identify candidate interactions that preserve the Posner's C_3 symmetry. These interactions preserve $S^{z_{\rm in}}_{1\ldots6}$. So might collisions with other molecules (Sec. D 2). Collisions are expected to decohere just irrelevant orbital DOFs. Throughout the rest of this section, components are implicitly defined with respect to the internal coordinate system.

D 1 Why interactions amongst phosphorus nuclear spins are expected to conserve $S^{z_{\rm in}}_{1\ldots6}$

The nuclei within a molecule can interact, in general. Intramolecule interactions include the Coulomb exchange, kinetic exchange, and superexchange [34].[31] These interactions have the Heisenberg form

$$\mathbf{S}_j \cdot \mathbf{S}_k = S^z_j S^z_k + S^+_j S^-_k + S^-_j S^+_k \,. \tag{D1}$$

The $j^{\rm th}$ single-nucleus spin operator is denoted by $\mathbf{S}_j$. Raising and lowering operators are denoted by $S^\pm_j := \frac{1}{2}(S^x_j \pm iS^y_j)$.

Suppose that arbitrary phosphorus nuclear spins in a Posner interact via Eq. (D1):

$$H_{\rm int} = \sum_{j=1}^{6} \sum_{k<j} J_{jk}\, \mathbf{S}_j \cdot \mathbf{S}_k \,. \tag{D2}$$

The pair-dependent interaction strength is denoted by J_{jk}. This $H_{\rm int}$ remains invariant under permutations of the spins via C. C represents the rotation that preserves the Posner's geometry. Hence the Posner's intrinsic Hamiltonian might contain $H_{\rm int}$.

The first term in Eq. (D1) conserves each spin's S^z_j. The second term does not. But suppose that any spin flips upward via S^+_j. Another spin flips downward via S^-_k. The compensation preserves the total spin's $z_{\rm in}$-component.

D 2 Why collisions with other molecules are expected to conserve a Posner molecule's $S^{z_{\rm in}}_{1\ldots6}$

The Posner Hilbert space $\mathcal{H}^-_{\text{no-coll.}}$ has the computational basis specified by Eq. (10). Each basis element depends on a collective coordinate ϕ. If one spin makes an angle ϕ with the $x_{\rm in}$-axis (Fig. 1b), the other spins make angles $\phi + 2\pi/3$ and $\phi + 4\pi/3$. But spins are quantum objects. The first spin need not localize at any particular ϕ-value. Rather, the spin can delocalize across multiple ϕ-values, via a superposition. Delocalizing the state (10) yields

$$\int d\phi \; \Psi(\phi) \; |(m_1, \mathbf{r}_1)(m_2, \mathbf{r}_2)(m_3, \mathbf{r}_3); (m_4, \mathbf{r}_4)(m_5, \mathbf{r}_5)(m_6, \mathbf{r}_6)\rangle \,. \tag{D3}$$

The kets depend on ϕ only through the $\mathbf{r}_j$'s. The coefficients $\Psi(\phi) \in \mathbb{C}$ satisfy the normalization condition $\int d\phi \; |\Psi(\phi)|^2 = 1$.[32] The state (D3) reduces to the basis element (10) when $\Psi(\phi)$ equals a Dirac delta function. A more general state of the Posner's phosphorus nuclei[33] has the form

$$|\Psi_{\rm Pos}\rangle = \int d\phi \; \Psi(\phi) \sum_{((m_1,\mathbf{r}_1)\ldots(m_6,\mathbf{r}_6))} |(m_1, \mathbf{r}_1)(m_2, \mathbf{r}_2)(m_3, \mathbf{r}_3); (m_4, \mathbf{r}_4)(m_5, \mathbf{r}_5)(m_6, \mathbf{r}_6)\rangle \,. \tag{D4}$$

The coefficients $\Psi(\phi)$ are wave functions, relative to the position basis, that represent an orbital DOF's quantum state. Molecular collisions are expected to alter the $\Psi(\phi)$'s: Jostling may change how tightly a spin is localized. Jostling is not expected to change the directions in which the spins point (since the spins are expected to have long coherence times). Hence molecular collisions are expected to preserve $S^{z_{\rm in}}_{1\ldots6}$.

---

[31] Superexchange within Posners is expected to be detailed in [9], according to [6].

[32] F&R introduce states of the form (D3) [1, 5]. They use second quantization and discuss transformation properties of the $\Psi(\phi)$'s. We cleave to the kets prevalent in QI theory.

[33] We continue to suppress the molecule's coordinates, and most components of the molecule's orientation, relative to the lab frame.

Appendix E DECOMPOSITION OF THE POSNER-MOLECULE HILBERT SPACE $\mathcal{H}^{-}_{\textbf{no-coll.}}$ IN TERMS OF COMPOSITE SPIN OPERATORS

A Posner encodes logical qubits (Sec. III). Three qubits correspond to the h_+ triangle in Fig. 1a, via Eq. (10).[34] We label these qubits 1, 2, and 3. The h_- triangle corresponds to logical qubits 4, 5, and 6. The 64-dimensional logical space decomposes into a direct sum of subspaces. Different subspaces transform in different ways under $\mathbf{S}^2_{123} + \mathbf{S}^2_{456}$, the composite spin-squared operator (13). Let us derive the decomposition. We refer readers to standard quantum-mechanics textbooks, such as [66], for background.

Let us focus on one triangle (one trio of qubits) first. Each trio corresponds to a Hilbert space $\mathbb{C}^2 \otimes \mathbb{C}^2 \otimes \mathbb{C}^2$. Each factor is replaced with the corresponding subsystem's spin quantum number, in useful conventional notation: $s_1 \otimes s_2 \otimes s_3 = \frac{1}{2} \otimes \frac{1}{2} \otimes \frac{1}{2}$. This tensor product can be rewritten as a direct sum.

To derive the direct sum, we follow rules for adding angular-momentum quantum numbers. Two spin quantum numbers, s_1 and s_2, sum as

$$s_{\text{tot}} = |s_1 - s_2|, |s_1 - s_2| + 1, \ldots s_1 + s_2 - 1, s_1 + s_2 \,. \tag{E1}$$

Two magnetic spin quantum numbers, m_1 and m_2, sum as

$$m_{\text{tot}} = m_1 + m_2 \,. \tag{E2}$$

We need not use Eq. (E2) here, however.

Since tensor products distribute across direct sums,

$$\frac{1}{2} \otimes \frac{1}{2} \otimes \frac{1}{2} = (0 \oplus 1) \otimes \frac{1}{2} \tag{E3}$$

$$= \frac{1}{2} \oplus \left(\frac{1}{2} \oplus \frac{3}{2} \right) . \tag{E4}$$

We can check Eq. (E4): A space that transforms with spin quantum number s has dimensionality $2s + 1$. That is, s corresponds to $2s + 1$ possible magnetic spin quantum numbers m. According to the LHS of Eq. (E3), therefore, each triangle corresponds to a space of dimensionality $\left(2 \times \frac{1}{2} + 1\right)^3 = 2^3 = 8$. Equation (E4) implies the same dimensionality: $2 + 2 + 4 = 8$.

Each Posner consists of two triangles. A triangle pair corresponds to the Hilbert space $\left(\frac{1}{2} \oplus \frac{1}{2} \oplus \frac{3}{2}\right)^{\otimes 2}$. Distributing the tensor product across the direct sums yields

$$\left(\frac{1}{2} \oplus \frac{1}{2} \oplus \frac{3}{2} \right)^{\otimes 2} = \left(\frac{1}{2} \otimes \frac{1}{2} \right)^{\oplus 4} \oplus \left(\frac{1}{2} \otimes \frac{3}{2} \right)^{\oplus 4} \oplus \left(\frac{3}{2} \otimes \frac{3}{2} \right) \tag{E5}$$

$$= (0 \oplus 1)^{\oplus 4} \oplus (1 \oplus 2)^{\oplus 4} \oplus (0 \oplus 1 \oplus 2 \oplus 3) \tag{E6}$$

$$= 0^{\oplus 5} \oplus 1^{\oplus 9} \oplus 2^{\oplus 5} \oplus 3 \,. \tag{E7}$$

Let us check Eq. (E7). According to the LHS of Eq. (E5), a Posner corresponds to a space of dimensionality $(2 + 2 + 4)^2 = 8^2 = 64$. Equation (E7) implies the same dimensionality: $5 + (3 \times 9) + (5 \times 5) + 7 = 64$.

Appendix F PREFERRED EIGENBASIS OF THE PERMUTATION OPERATOR C

The permutation operator C was introduced in Sec. IV A. The Posner dynamics is assumed to conserve C, as well as $S^{z_{\text{in}}}_{1\ldots6}$. An eigenbasis shared by C and $S^{z_{\text{in}}}_{1\ldots6}$ can facilitate the construction of natural quantum error-correcting codes (Sec. IV D).

Several eigenbases of C are eigenbases of $S^{z_{\text{in}}}_{1\ldots6}$. The operator $\mathbf{S}^2_{123} \otimes \mathbf{S}^2_{456}$ breaks the degeneracy satisfactorily, as discussed in Sections IV C and VII. C, $S^{z_{\text{in}}}_{1\ldots6}$, and $\mathbf{S}^2_{123} \otimes \mathbf{S}^2_{456}$ share the eigenbasis in Tables II, III, and IV. Each table corresponds to one value of $\tau = 0, \pm 1$ (equivalently, $\tau = 0, 1, 2$).

---

[34] No particular nucleus can be associated with any particular pure spin-and-position state, by Pauli's principle. But a spin can be associated with a position. Loosely speaking, some nucleus A occupies the spin state $|m_j\rangle$ if and only if A occupies the position state $|\mathbf{r}_j\rangle$.

State	$s_{123} \otimes s_{456}$	m_{123}	m_{456}	$m_{1\ldots6}$	$\tau_{123} \otimes \tau_{456}$	Decomposition
$\lvert c^1_{\tau=0}\rangle$	$\frac{3}{2} \otimes \frac{3}{2}$	$\frac{3}{2}$	$\frac{3}{2}$	3	$1 \otimes 1$	$\lvert 000\rangle\lvert 000\rangle$
$\lvert c^2_{\tau=0}\rangle$	$\frac{3}{2} \otimes \frac{3}{2}$	$\frac{3}{2}$	$\frac{1}{2}$	2	$1 \otimes 1$	$\lvert 000\rangle\lvert W\rangle$
$\lvert c^3_{\tau=0}\rangle$	$\frac{3}{2} \otimes \frac{3}{2}$	$\frac{3}{2}$	$-\frac{1}{2}$	1	$1 \otimes 1$	$\lvert 000\rangle\lvert \bar{W}\rangle$
$\lvert c^4_{\tau=0}\rangle$	$\frac{3}{2} \otimes \frac{3}{2}$	$\frac{3}{2}$	$-\frac{3}{2}$	0	$1 \otimes 1$	$\lvert 000\rangle\lvert 111\rangle$
$\lvert c^5_{\tau=0}\rangle$	$\frac{3}{2} \otimes \frac{3}{2}$	$\frac{1}{2}$	$\frac{3}{2}$	2	$1 \otimes 1$	$\lvert W\rangle\lvert 000\rangle$
$\lvert c^6_{\tau=0}\rangle$	$\frac{3}{2} \otimes \frac{3}{2}$	$\frac{1}{2}$	$\frac{1}{2}$	1	$1 \otimes 1$	$\lvert W\rangle\lvert W\rangle$
$\lvert c^7_{\tau=0}\rangle$	$\frac{3}{2} \otimes \frac{3}{2}$	$\frac{1}{2}$	$-\frac{1}{2}$	0	$1 \otimes 1$	$\lvert W\rangle\lvert \bar{W}\rangle$
$\lvert c^8_{\tau=0}\rangle$	$\frac{3}{2} \otimes \frac{3}{2}$	$\frac{1}{2}$	$-\frac{3}{2}$	-1	$1 \otimes 1$	$\lvert W\rangle\lvert 111\rangle$
$\lvert c^9_{\tau=0}\rangle$	$\frac{3}{2} \otimes \frac{3}{2}$	$-\frac{1}{2}$	$\frac{3}{2}$	1	$1 \otimes 1$	$\lvert \bar{W}\rangle\lvert 000\rangle$
$\lvert c^{10}_{\tau=0}\rangle$	$\frac{3}{2} \otimes \frac{3}{2}$	$-\frac{1}{2}$	$\frac{1}{2}$	0	$1 \otimes 1$	$\lvert \bar{W}\rangle\lvert W\rangle$
$\lvert c^{11}_{\tau=0}\rangle$	$\frac{3}{2} \otimes \frac{3}{2}$	$-\frac{1}{2}$	$-\frac{1}{2}$	-1	$1 \otimes 1$	$\lvert \bar{W}\rangle\lvert \bar{W}\rangle$
$\lvert c^{12}_{\tau=0}\rangle$	$\frac{3}{2} \otimes \frac{3}{2}$	$-\frac{1}{2}$	$-\frac{3}{2}$	-2	$1 \otimes 1$	$\lvert \bar{W}\rangle\lvert 111\rangle$
$\lvert c^{13}_{\tau=0}\rangle$	$\frac{3}{2} \otimes \frac{3}{2}$	$-\frac{3}{2}$	$\frac{3}{2}$	0	$1 \otimes 1$	$\lvert 111\rangle\lvert 000\rangle$
$\lvert c^{14}_{\tau=0}\rangle$	$\frac{3}{2} \otimes \frac{3}{2}$	$-\frac{3}{2}$	$\frac{1}{2}$	-1	$1 \otimes 1$	$\lvert 111\rangle\lvert W\rangle$
$\lvert c^{15}_{\tau=0}\rangle$	$\frac{3}{2} \otimes \frac{3}{2}$	$-\frac{3}{2}$	$-\frac{1}{2}$	-2	$1 \otimes 1$	$\lvert 111\rangle\lvert \bar{W}\rangle$
$\lvert c^{16}_{\tau=0}\rangle$	$\frac{3}{2} \otimes \frac{3}{2}$	$-\frac{3}{2}$	$-\frac{3}{2}$	-3	$1 \otimes 1$	$\lvert 111\rangle\lvert 111\rangle$
$\lvert c^{17}_{\tau=0}\rangle$	$\frac{1}{2} \otimes \frac{1}{2}$	$\frac{1}{2}$	$\frac{1}{2}$	1	$\omega \otimes \omega^2$	$\lvert \omega\rangle\lvert \omega^2\rangle$
$\lvert c^{18}_{\tau=0}\rangle$	$\frac{1}{2} \otimes \frac{1}{2}$	$\frac{1}{2}$	$-\frac{1}{2}$	0	$\omega \otimes \omega^2$	$\lvert \omega\rangle\lvert \overline{\omega^2}\rangle$
$\lvert c^{19}_{\tau=0}\rangle$	$\frac{1}{2} \otimes \frac{1}{2}$	$\frac{1}{2}$	$\frac{1}{2}$	1	$\omega^2 \otimes \omega$	$\lvert \omega^2\rangle\lvert \omega\rangle$
$\lvert c^{20}_{\tau=0}\rangle$	$\frac{1}{2} \otimes \frac{1}{2}$	$\frac{1}{2}$	$-\frac{1}{2}$	0	$\omega^2 \otimes \omega$	$\lvert \omega^2\rangle\lvert \bar{\omega}\rangle$
$\lvert c^{21}_{\tau=0}\rangle$	$\frac{1}{2} \otimes \frac{1}{2}$	$-\frac{1}{2}$	$\frac{1}{2}$	0	$\omega \otimes \omega^2$	$\lvert \bar{\omega}\rangle\lvert \omega^2\rangle$
$\lvert c^{22}_{\tau=0}\rangle$	$\frac{1}{2} \otimes \frac{1}{2}$	$-\frac{1}{2}$	$-\frac{1}{2}$	-1	$\omega \otimes \omega^2$	$\lvert \bar{\omega}\rangle\lvert \overline{\omega^2}\rangle$
$\lvert c^{23}_{\tau=0}\rangle$	$\frac{1}{2} \otimes \frac{1}{2}$	$-\frac{1}{2}$	$\frac{1}{2}$	0	$\omega^2 \otimes \omega$	$\lvert \overline{\omega^2}\rangle\lvert \omega\rangle$
$\lvert c^{24}_{\tau=0}\rangle$	$\frac{1}{2} \otimes \frac{1}{2}$	$-\frac{1}{2}$	$-\frac{1}{2}$	-1	$\omega^2 \otimes \omega$	$\lvert \overline{\omega^2}\rangle\lvert \bar{\omega}\rangle$

TABLE II: Preferred eigenbasis for the $\tau = 0$ eigenspace of the permutation operator C: Twenty-four states span the eigenspace. Each basis element equals a product of two three-qubit states. The final column displays the product, explained in Sec. IV C. The state's first factor represents a state of the qubits (labeled $j = 1, 2, 3$) in the top triangle in Fig. 1a. The second factor represents a state of the qubits (labeled $j = 4, 5, 6$) in the bottom triangle. Each factor is an eigenstate shared by the total-spin operators $\mathbf{S}^2_{123}$ and $S^{z_{\text{in}}}_{123}$ or by $\mathbf{S}^2_{456}$ and $S^{z_{\text{in}}}_{456}$. The operators are defined in Sec. IV C. Table I displays the three-qubit eigenstates. The spin quantum number s_{123} denotes the eigenvalue of $\mathbf{S}^2_{123}$. The magnetic spin quantum number m_{123} denotes the eigenvalue of $S^{z_{\text{in}}}_{123}$. s_{456} and m_{456} are defined analogously. The total magnetic spin quantum number $m_{1\ldots6} = m_{123} + m_{456}$. The notation in column two follows from [66]: Eigenspaces of $\mathbf{S}^2_{123} \otimes \mathbf{S}^2_{456}$ bear the label $s_{123} \otimes s_{456}$. Column six is notated similarly. τ_{123} denotes the eigenvalue of the permutation operator that cyclically permutes qubits 1, 2, and 3. τ_{456} is defined analogously. The permutation eigenvalues multiply to $\tau_{123} \times \tau_{456} = \tau$.

Appendix G QUANTIFICATION OF THE INFORMATION ENCODED IN THE OUTCOME OF A POSNER-BINDING MEASUREMENT: ANALYSIS 2

The Posner-binding measurement is analyzed in Sec. VI. The measurement yields an outcome that encodes classical information. This information is quantified in Sec. VI A. The quantification is explained alternatively here.

Imagine wishing to measure the τ_A and τ_B of Posners A and B. Each measurement would yield one of three possible outcomes (0, 1, or 2). The pair of measurements would yield one of nine possible outcomes. The pair of outcomes could be recorded in $\lceil \log_2(9) \rceil = 4$ bits.

Whether two Posners bind implements a measurement of whether $\tau_A + \tau_B = 0$. The yes-or-no answer constitutes one bit. You forfeit three of the bits you wanted, measuring just whether the Posners bind. Three is the number of bits you would need to specify the value of (τ_A, τ_B), given that $\tau_A + \tau_B \neq 0$. Why? Suppose that $\tau_A + \tau_B \neq 0$.

State	$s_{123} \otimes s_{456}$	m_{123}	m_{456}	$m_{1\ldots6}$	$\tau_{123} \otimes \tau_{456}$	Decomposition
$\lvert c^1_{\tau=1}\rangle$	$\frac{3}{2} \otimes \frac{1}{2}$	$\frac{3}{2}$	$\frac{1}{2}$	2	$1 \otimes \omega$	$\lvert 000\rangle\lvert\omega\rangle$
$\lvert c^2_{\tau=1}\rangle$	$\frac{3}{2} \otimes \frac{1}{2}$	$\frac{3}{2}$	$-\frac{1}{2}$	1	$1 \otimes \omega$	$\lvert 000\rangle\lvert\bar{\omega}\rangle$
$\lvert c^3_{\tau=1}\rangle$	$\frac{3}{2} \otimes \frac{1}{2}$	$\frac{1}{2}$	$\frac{1}{2}$	1	$1 \otimes \omega$	$\lvert W\rangle\lvert\omega\rangle$
$\lvert c^4_{\tau=1}\rangle$	$\frac{3}{2} \otimes \frac{1}{2}$	$\frac{1}{2}$	$-\frac{1}{2}$	0	$1 \otimes \omega$	$\lvert W\rangle\lvert\bar{\omega}\rangle$
$\lvert c^5_{\tau=1}\rangle$	$\frac{3}{2} \otimes \frac{1}{2}$	$-\frac{1}{2}$	$\frac{1}{2}$	0	$1 \otimes \omega$	$\lvert \bar{W}\rangle\lvert\omega\rangle$
$\lvert c^6_{\tau=1}\rangle$	$\frac{3}{2} \otimes \frac{1}{2}$	$-\frac{1}{2}$	$-\frac{1}{2}$	-1	$1 \otimes \omega$	$\lvert \bar{W}\rangle\lvert\bar{\omega}\rangle$
$\lvert c^7_{\tau=1}\rangle$	$\frac{3}{2} \otimes \frac{1}{2}$	$-\frac{3}{2}$	$\frac{1}{2}$	-1	$1 \otimes \omega$	$\lvert 111\rangle\lvert\omega\rangle$
$\lvert c^8_{\tau=1}\rangle$	$\frac{3}{2} \otimes \frac{1}{2}$	$-\frac{3}{2}$	$-\frac{1}{2}$	-2	$1 \otimes \omega$	$\lvert 111\rangle\lvert\bar{\omega}\rangle$
$\lvert c^9_{\tau=1}\rangle$	$\frac{1}{2} \otimes \frac{3}{2}$	$\frac{1}{2}$	$\frac{3}{2}$	2	$\omega \otimes 1$	$\lvert\omega\rangle\lvert 000\rangle$
$\lvert c^{10}_{\tau=1}\rangle$	$\frac{1}{2} \otimes \frac{3}{2}$	$\frac{1}{2}$	$\frac{1}{2}$	1	$\omega \otimes 1$	$\lvert\omega\rangle\lvert W\rangle$
$\lvert c^{11}_{\tau=1}\rangle$	$\frac{1}{2} \otimes \frac{3}{2}$	$\frac{1}{2}$	$-\frac{1}{2}$	0	$\omega \otimes 1$	$\lvert\omega\rangle\lvert \bar{W}\rangle$
$\lvert c^{12}_{\tau=1}\rangle$	$\frac{1}{2} \otimes \frac{3}{2}$	$\frac{1}{2}$	$-\frac{3}{2}$	-1	$\omega \otimes 1$	$\lvert\omega\rangle\lvert 111\rangle$
$\lvert c^{13}_{\tau=1}\rangle$	$\frac{1}{2} \otimes \frac{1}{2}$	$\frac{1}{2}$	$\frac{1}{2}$	1	$\omega^2 \otimes \omega^2$	$\lvert\omega^2\rangle\lvert\omega^2\rangle$
$\lvert c^{14}_{\tau=1}\rangle$	$\frac{1}{2} \otimes \frac{1}{2}$	$\frac{1}{2}$	$-\frac{1}{2}$	0	$\omega^2 \otimes \omega^2$	$\lvert\omega^2\rangle\lvert\overline{\omega^2}\rangle$
$\lvert c^{15}_{\tau=1}\rangle$	$\frac{1}{2} \otimes \frac{3}{2}$	$-\frac{1}{2}$	$\frac{3}{2}$	1	$\omega \otimes 1$	$\lvert\bar{\omega}\rangle\lvert 000\rangle$
$\lvert c^{16}_{\tau=1}\rangle$	$\frac{1}{2} \otimes \frac{3}{2}$	$-\frac{1}{2}$	$\frac{1}{2}$	0	$\omega \otimes 1$	$\lvert\bar{\omega}\rangle\lvert W\rangle$
$\lvert c^{17}_{\tau=1}\rangle$	$\frac{1}{2} \otimes \frac{3}{2}$	$-\frac{1}{2}$	$-\frac{1}{2}$	-1	$\omega \otimes 1$	$\lvert\bar{\omega}\rangle\lvert \bar{W}\rangle$
$\lvert c^{18}_{\tau=1}\rangle$	$\frac{1}{2} \otimes \frac{3}{2}$	$-\frac{1}{2}$	$-\frac{3}{2}$	-2	$\omega \otimes 1$	$\lvert\bar{\omega}\rangle\lvert 111\rangle$
$\lvert c^{19}_{\tau=1}\rangle$	$\frac{1}{2} \otimes \frac{1}{2}$	$-\frac{1}{2}$	$\frac{1}{2}$	0	$\omega^2 \otimes \omega^2$	$\lvert\overline{\omega^2}\rangle\lvert\omega^2\rangle$
$\lvert c^{20}_{\tau=1}\rangle$	$\frac{1}{2} \otimes \frac{1}{2}$	$-\frac{1}{2}$	$-\frac{1}{2}$	-1	$\omega^2 \otimes \omega^2$	$\lvert\overline{\omega^2}\rangle\lvert\overline{\omega^2}\rangle$

TABLE III: Preferred eigenbasis for the $\tau = 1$ eigenspace of the rotation symmetry operator C: The notation is defined below Table II.

(τ_A, τ_B) can equal one of six possible values, $(0,1)$, $(0,2)$, $(1,0)$, $(1,1)$, $(2,0)$, or $(2,2)$. Specifying one of six possible values requires $\lceil \log_2(6) \rceil = 3$ bits.[35] Hence measuring Posner binding is equivalent to each of two QI processes:

1. Measuring (τ_A, τ_B) and coarse-graining away three bits (all information except whether $\tau_A + \tau_B = 0$).

2. Measuring the Bell basis and coarse-graining away one bit (whether a + outcome or a − outcome occurred).

Appendix H HOW TO PREPARE, WITH POSNER OPERATIONS, STATES USED IN INCOHERENT TELEPORTATION

Section VI B details how Posners can teleport QI incoherently. The protocol involves states $|+_\tau\rangle = \frac{1}{\sqrt{3}}(|0_\tau\rangle + |1_\tau\rangle + |2_\tau\rangle)$ and $|\psi\rangle = c_0|0_\tau\rangle + c_1|1_\tau\rangle + c_2|2_\tau\rangle$. Each $|j_\tau\rangle$ denotes an arbitrary state in the $\tau = j$ subspace. How can Posner operations (Sec. V A) prepare a $|+_\tau\rangle$ and a $|\psi\rangle$? One protocol is described below. Other protocols may await discovery.

Each state is of one Posner and is pure. Hence the Posner contains three singlets. Consider preparing three singlets via operation 1. Consider rotating one spin via operation 2. Let the rotation be about the y_{lab}-axis, through an angle θ.

[35] Imagine learning, instead, that $\tau_A + \tau_B = 0$. Given this information, would you need three bits to specify the value of (τ_A, τ_B)? No: (τ_A, τ_B) can assume one of three possible values. Hence you would need $\lceil \log_2(3) \rceil = 2$ bits. But you could encode the tuple's value in three bits.

State	$s_{123} \otimes s_{456}$	m_{123}	m_{456}	$m_{1\ldots6}$	$\tau_{123} \otimes \tau_{456}$	Decomposition
$\|c^1_{\tau=-1}\rangle$	$\frac{3}{2} \otimes \frac{1}{2}$	$\frac{3}{2}$	$\frac{1}{2}$	2	$1 \otimes \omega^2$	$\|000\rangle\|\omega^2\rangle$
$\|c^2_{\tau=-1}\rangle$	$\frac{3}{2} \otimes \frac{1}{2}$	$\frac{3}{2}$	$-\frac{1}{2}$	1	$1 \otimes \omega^2$	$\|000\rangle\|\overline{\omega^2}\rangle$
$\|c^3_{\tau=-1}\rangle$	$\frac{3}{2} \otimes \frac{1}{2}$	$\frac{1}{2}$	$\frac{1}{2}$	1	$1 \otimes \omega^2$	$\|W\rangle\|\omega^2\rangle$
$\|c^4_{\tau=-1}\rangle$	$\frac{3}{2} \otimes \frac{1}{2}$	$\frac{1}{2}$	$-\frac{1}{2}$	0	$1 \otimes \omega^2$	$\|W\rangle\|\overline{\omega^2}\rangle$
$\|c^5_{\tau=-1}\rangle$	$\frac{3}{2} \otimes \frac{1}{2}$	$-\frac{1}{2}$	$\frac{1}{2}$	0	$1 \otimes \omega^2$	$\|\bar{W}\rangle\|\omega^2\rangle$
$\|c^6_{\tau=-1}\rangle$	$\frac{3}{2} \otimes \frac{1}{2}$	$-\frac{1}{2}$	$-\frac{1}{2}$	-1	$1 \otimes \omega^2$	$\|\bar{W}\rangle\|\overline{\omega^2}\rangle$
$\|c^7_{\tau=-1}\rangle$	$\frac{3}{2} \otimes \frac{1}{2}$	$-\frac{3}{2}$	$\frac{1}{2}$	-1	$1 \otimes \omega^2$	$\|111\rangle\|\omega^2\rangle$
$\|c^8_{\tau=-1}\rangle$	$\frac{3}{2} \otimes \frac{1}{2}$	$-\frac{3}{2}$	$-\frac{1}{2}$	-2	$1 \otimes \omega^2$	$\|111\rangle\|\overline{\omega^2}\rangle$
$\|c^9_{\tau=-1}\rangle$	$\frac{1}{2} \otimes \frac{1}{2}$	$\frac{1}{2}$	$\frac{1}{2}$	1	$\omega \otimes \omega$	$\|\omega\rangle\|\omega\rangle$
$\|c^{10}_{\tau=-1}\rangle$	$\frac{1}{2} \otimes \frac{1}{2}$	$\frac{1}{2}$	$-\frac{1}{2}$	0	$\omega \otimes \omega$	$\|\omega\rangle\|\bar{\omega}\rangle$
$\|c^{11}_{\tau=-1}\rangle$	$\frac{1}{2} \otimes \frac{3}{2}$	$\frac{1}{2}$	$\frac{3}{2}$	2	$\omega^2 \otimes 1$	$\|\omega^2\rangle\|000\rangle$
$\|c^{12}_{\tau=-1}\rangle$	$\frac{1}{2} \otimes \frac{3}{2}$	$\frac{1}{2}$	$\frac{1}{2}$	1	$\omega^2 \otimes 1$	$\|\omega^2\rangle\|W\rangle$
$\|c^{13}_{\tau=-1}\rangle$	$\frac{1}{2} \otimes \frac{3}{2}$	$\frac{1}{2}$	$-\frac{1}{2}$	0	$\omega^2 \otimes 1$	$\|\omega^2\rangle\|\bar{W}\rangle$
$\|c^{14}_{\tau=-1}\rangle$	$\frac{1}{2} \otimes \frac{3}{2}$	$\frac{1}{2}$	$-\frac{3}{2}$	-1	$\omega^2 \otimes 1$	$\|\omega^2\rangle\|111\rangle$
$\|c^{15}_{\tau=-1}\rangle$	$\frac{1}{2} \otimes \frac{1}{2}$	$-\frac{1}{2}$	$\frac{1}{2}$	0	$\omega \otimes \omega$	$\|\bar{\omega}\rangle\|\omega\rangle$
$\|c^{16}_{\tau=-1}\rangle$	$\frac{1}{2} \otimes \frac{1}{2}$	$-\frac{1}{2}$	$-\frac{1}{2}$	-1	$\omega \otimes \omega$	$\|\bar{\omega}\rangle\|\bar{\omega}\rangle$
$\|c^{17}_{\tau=-1}\rangle$	$\frac{1}{2} \otimes \frac{3}{2}$	$-\frac{1}{2}$	$\frac{3}{2}$	1	$\omega^2 \otimes 1$	$\|\overline{\omega^2}\rangle\|000\rangle$
$\|c^{18}_{\tau=-1}\rangle$	$\frac{1}{2} \otimes \frac{3}{2}$	$-\frac{1}{2}$	$\frac{1}{2}$	0	$\omega^2 \otimes 1$	$\|\overline{\omega^2}\rangle\|W\rangle$
$\|c^{19}_{\tau=-1}\rangle$	$\frac{1}{2} \otimes \frac{3}{2}$	$-\frac{1}{2}$	$-\frac{1}{2}$	-1	$\omega^2 \otimes 1$	$\|\overline{\omega^2}\rangle\|\bar{W}\rangle$
$\|c^{20}_{\tau=-1}\rangle$	$\frac{1}{2} \otimes \frac{3}{2}$	$-\frac{1}{2}$	$-\frac{3}{2}$	-2	$\omega^2 \otimes 1$	$\|\overline{\omega^2}\rangle\|111\rangle$

TABLE IV: Preferred eigenbasis for the $\tau = -1$ eigenspace (equivalently, the $\tau = 2$ eigenspace) of the rotation symmetry operator C: The notation is defined below Table II.

Consider forming a Posner from the spins, via operation 3. Let the singlets be arranged as in Fig. 19. Recall that a Posner contains two triangles of phosphorus nuclear spins (Sec. II B). One triangle sits at $z_{\text{in}} = h_+$; and the other triangle, at $z_{\text{in}} = h_-$. Each triangle contains one singlet (illustrated with a green, wavy line). One singlet extends from the h_+ triangle to the h_- triangle. (How a singlet corresponds to positions in a Posner is discussed in Sec. III C and App. B.) The red hoop encircles the rotated spin. The rotated spin is entangled with a spin in the same triangle.

Let $|\phi(\theta)\rangle$ denote the Posner's state. $|\phi(\theta)\rangle$ can have weight on each $\tau = j$ eigenspace:

$$|\phi(\theta)\rangle = \sum_{j=0}^{2} \sum_{\lambda_j=1}^{d_j} C_{j,\lambda_j}(\theta) |c^{\lambda_j}_{\tau=j}\rangle \, . \tag{H1}$$

The $\tau = j$ eigenspace has degeneracy d_j. The degeneracy parameter is denoted by λ_j. The coefficients $C_{j,\lambda_j}(\theta)$ satisfy the normalization condition $\sum_j \sum_{\lambda_j} \left| C_{j,\lambda_j}(\theta) \right|^2 = 1$.

The dependence on θ can be calculated analytically: The state has an amount

$$\sum_{\lambda_0=1}^{24} |C_{0,\lambda_0}(\theta)|^2 = \cos^2\theta \tag{H2}$$

of weight on the $\tau = 0$ eigenspace, an amount

$$\sum_{\lambda_1=1}^{20} |C_{1,\lambda_1}(\theta)|^2 = \frac{1}{2}\sin^2\theta \tag{H3}$$

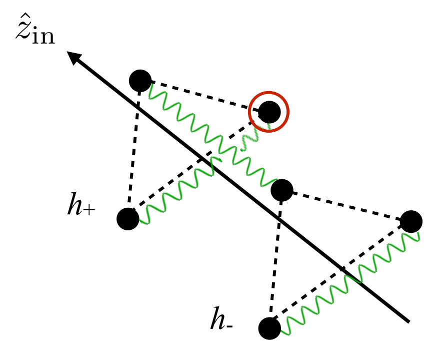

FIG. 19: Posner-molecule state usable in incoherent teleportation: Each black dot represents a phosphorus nuclear spin. The internal z-axis $\hat{z}_{\rm in}$ remains fixed with respect to the atoms' positions. Three spins sit at $z_{\rm in} = h_+$; and three spins, at $z_{\rm in} = h_-$. The spins occupy a pure state of three singlets. Each green, wavy line represents one singlet. The red hoop encircles a spin that has been rotated through an angle θ. The rotation is about the $y_{\rm lab}$-axis, which remains fixed relative to the lab that contains the Posner. The angle labels the Posner's state, $|\phi(\theta)\rangle$. Instances of $|\phi(\theta)\rangle$ can serve as the $|+_\tau\rangle$ and the $|\psi\rangle$ in incoherent teleportation (Sec. VI B 2).

on the $\tau = 1$ eigenspace, and an amount

$$\sum_{\lambda_2=1}^{20} |C_{2,\lambda_2}(\theta)|^2 = \frac{1}{2}\sin^2\theta \tag{H4}$$

on the $\tau = 2$ eigenspace.

At which θ-value does the weight on each eigenspace equal the weight on every other? Let us equate (H2), (H3), and (H4). Solving for the angle yields $\theta = \tan^{-1}(\sqrt{2})$. The corresponding state can serve as the equal-weight superposition $|+_\tau\rangle$:

$$|+_\tau\rangle = |\phi(\tan^{-1}(\sqrt{2}))\rangle\,. \tag{H5}$$

The basis vectors $|j_\tau\rangle$ inherit the definition

$$|j_\tau\rangle = \sum_{\lambda_j=1}^{d_j} C_{j,\lambda_j}(\tan^{-1}(\sqrt{2}))|c_j^{\lambda_j}\rangle\,. \tag{H6}$$

Now, let θ assume an arbitrary value. Information about $|\phi(\theta)\rangle$ can be teleported incoherently:

$$|\psi\rangle = |\phi(\theta)\rangle\,. \tag{H7}$$

Granted, $|\phi(\theta)\rangle$ might not decompose as $\sum_{j=0}^{2} c_j |j_\tau\rangle$, in terms of the $|j_\tau\rangle$'s defined in Eq. (H6). Yet the incoherent-teleportation protocol continues to work: Equation (H7) defines new basis elements $|j_\tau(\theta)\rangle$:

$$|j_\tau(\theta)\rangle = \sum_{\lambda_j=1}^{d_j} C_{j,\lambda_j}(\theta)|c_j^{\lambda_j}\rangle\,. \tag{H8}$$

States $|j_\tau\rangle$ of Posner A appear in Eqs. (47) and (50). Each such $|j_\tau\rangle$ must be replaced with a $|j_\tau(\theta)\rangle$. The projector Π_{AB} transforms the $|j_\tau(\theta)\rangle$'s as it would transform the $|j_\tau\rangle$'s.

Appendix I FRUSTRATED-LATTICE INTUITION ABOUT PROJECTING ONTO THE $\tau = 0$ SUBSPACE

We can understand Eq. (61) in terms of a frustrated lattice. Consider a triangular lattice of three sites, A, B, and C. Let a spin-1 DOF occupy each site. The site-K magnetic spin quantum number $m_K = 0, \pm 1$ stands in place of τ_K.

Let us regress to Eq. (60). We ignore the final $m-3$ identity operators in each term. How does Π_{123} transform the lattice's state? Consider multiplying out the terms in the RHS. We label as a *cross-term* each term that contains at least one $\Pi_{\tau_K=0}$ and one $\Pi_{\tau_K=\pm 1}$, for some $K = A, B, C$. These projectors annihilate each other; the cross-terms vanish. Each surviving term in Π_{123} contains only $\tau_K = 0$ projectors or only $\tau_K = \pm 1$ projectors.

Each $\tau_K = \pm 1$ projector represents an antiferromagnetic interaction between two lattice sites. The $\tau_K = \pm 1$ projectors form a term that represents a frustrated lattice. No set (τ_A, τ_B, τ_C) satisfies all the constraints encoded in the frustration term. Hence the lattice must occupy its $\tau_A = \tau_B = \tau_C = 0$ subspace.

Appendix J PEPS REPRESENTATION OF $|\mathrm{AKLT}'_{\mathrm{hon}}\rangle$

The AKLT′ PEPS is a repeating pattern of two tensors, T^+ and T^- (Fig. 17). We will focus primarily on T^+. The tensor has six indices. Three (v_1^+, v_2^+, and v_3^+) are virtual. Three more indices (a_1^+, a_2^+, and a_3^+) are physical.

Each small, black dot represents a virtual spin. Each short leg, extending upward from the plane occupied by the large circle, represents a physical qubit. We denote the physical qubits' computational-basis states by $|a_1^+ \, a_2^+ \, a_3^+\rangle$. For each $j = 1, 2, 3$, the physical index $a_j^+ = 0, 1$.

Each long leg, extended across the plane occupied by the large circle, represents a virtual index. The v_1^+ and v_2^+ lines represents singlets. Consider, as an illustration, the physical qubit associated with a_1^+. This qubit forms a singlet with some physical qubit in another tensor. Suppose that $a_1^+ = 0$. The T^+ physical qubit points upward. Hence the partner physical qubit must point downward: The partner qubit's a must equal one. This necessity is conveyed to the second tensor by the virtual index v_1^+: If $a_1^+ = 0$, $T^+_{a_1^+, a_2^+, a_3^+, v_1^+, v_2^+, v_3^+} \neq 0$ only if $v_1^+ = 0$.

The virtual index v_3^+ differs from v_1^+ and v_2^+: The tensor lacks isotropy. v_3^+ connects two tensors associated with the same Posner, T^+ and T^-. The two tensors, together, determine which C eigenspace the Posner occupies. Hence v_3^+ carries not only "singlet" information about one physical qubit. v_3^+ conveys also how the T^+ qubit trio transforms under C_3 (the final column in Table I). This C information dictates how the T^- physical qubits must transform, such that the Posner occupies the $\tau = 0$ eigenspace.

We ascribe to v_3^+ a tuple $(\tilde{v}_3^+, \tau^+)$. The first entry conveys information about the a_3^+ physical qubit. Only if $\tilde{v}_3^+ = a_3^+$ can the tensor have a nonzero value. The second entry, τ^+, equals 0, 1, or 2. Hence v_3^+ assumes one of six possible values:

$$v_3^+ = (\tilde{v}_3^+, \tau^+) = \{(0,0), (0,1), (0,2), (1,0), (1,1), (1,2)\} \tag{J1}$$
$$= \{0, 1, 2, 3, 4, 5\} \, . \tag{J2}$$

Hence v_3^+ has a bond dimension of six.

Having overviewed the tensor's six indices, we consider the whole tensor, $T^+_{a_1^+, a_2^+, a_3^+, v_1^+, v_2^+, v_3^+}$. This tensor equals the coefficient that multiplies the computational-basis state $|a_1^+, a_2^+, a_3^+\rangle$ when the virtual indices have the values v_1^+, v_2^+, and v_3^+. Suppose, for simplicity, that the T^+ triangle lacked connections to any other triangles. The triangle would occupy the physical state

$$(\text{const.}) \sum_{a_1^+, a_2^+, a_3^+, v_1^+, v_2^+, v_3^+} T^+_{a_1^+, a_2^+, a_3^+, v_1^+, v_2^+, v_3^+} |a_1^+, a_2^+, a_3^+\rangle \, . \tag{J3}$$

The v's do not label the ket, because they are virtual.

The tensor can be evaluated, with help from Table I, after a normalization convention is chosen. We illustrate with three examples.

First, let us evaluate T^+_{000000}. Since $v_3^+ = 0$, Eq. (J2) implies that T^+_{000000} can $\neq 0$ only if $a_3^+ = 0$. Indeed, $a_3^+ = 0$. In fact, every a vanishes. This tensor equals the coefficient of the one-triangle state $|a_1^+ \, a_2^+ \, a_3^+\rangle = |000\rangle$. This state occupies the $\tau = 0$ eigenspace, according to Table I. We choose the following normalization condition: $|000\rangle$ appears once, with a unit coefficient, in the table's second column. Hence we choose for T^+_{000000} to equal one.

The second example consists of $T^+_{a_1^+ \, a_2^+ \, a_3^+ \, 001}$, wherein the a's have arbitrary values. According to the final three indices [and Eq. (J2)], the tensor can be nonzero only if $a_j^+ = 0$ for all $j = 1, 2, 3$. That is, $T^+_{a_1^+ \, a_2^+ \, a_3^+ \, 001} = 0$ except, perhaps, if the coefficient of $|a_1^+ \, a_2^+ \, a_3^+\rangle = |000\rangle$.

The tensor's final index implies that $v_3^+ = 1$. Hence, by Eq. (J2), the qubit trio transforms under C with $\tau^+ = 1$. No qubit-trio state (i) transforms with τ^+ and (ii) equals a linear combination of computational-basis states including $|000\rangle$, by Table (I). Hence $T^+_{000001} = 0$.

The final example consists of T^+_{100100}. The physical indices "agree with" the virtue indices: $a_1^+ = v_1^+$, $a_2^+ = v_2^+$, and [by Eq. (J2)] $a_3^+ = \tilde{v}_3^+$. Hence the tensor does not necessarily vanish. This tensor multiplies the physical one-triangle ket $|a_1^+\, a_2^+\, a_3^+\rangle = |100\rangle$. This ket appears three times in the second column of Table I. Only one of those appearances is relevant: Since $v_3^+ = 0$, Eq. (J2) implies that $\tau_+ = 0$. Hence the physical qubit trio occupies the first ket in the $|W\rangle$ decomposition (in the third row of Table I). This ket multiples a $\frac{1}{\sqrt{3}}$ in the table's second column. We might wish to ascribe the value $\frac{1}{\sqrt{3}}$ to T^+_{100100}.

But the physical qubits' state is constructed from singlets. Singlets carry minus signs. We must incorporate these minus signs into our convention. We choose for the tensor to carry a factor of $(-1)^{a_j^+}$ for each $j = 1, 2, 3$. Hence $T^+_{100100} = -\frac{1}{\sqrt{3}}$.

REFERENCES

[1] M. P. A. Fisher, Annals of Physics **362**, 593 (2015).
[2] G. Treboux, P. Layrolle, N. Kanzaki, K. Onuma, and A. Ito, The Journal of Physical Chemistry A **104**, 5111 (2000), http://dx.doi.org/10.1021/jp994399t.
[3] N. Kanzaki, G. Treboux, K. Onuma, S. Tsutsumi, and A. Ito, Biomaterials **22**, 2921 (2001).
[4] X. Yin and M. Stott, J. Chem. Phys. **118**, 3717 (2003).
[5] M. P. A. Fisher and L. Radzihovsky, ArXiv e-prints (2017), 1707.05320.
[6] M. P. A. Fisher, private communication.
[7] M. A. Nielsen and I. L. Chuang, *Quantum Computation and Quantum Information* (Cambridge University Press, 2010).
[8] J. Preskill, Ch. 7: Quantum error correction, in *Phys. 219: Quantum Computation and Information*, Lecture Notes, 1999.
[9] M. Swift, C. Van de Walle, and M. Fisher, (in prep).
[10] C. H. Bennett *et al.*, Phys. Rev. Lett. **70**, 1895 (1993).
[11] C. H. Bennett and S. J. Wiesner, Phys. Rev. Lett. **69**, 2881 (1992).
[12] H. J. Briegel and R. Raussendorf, Phys. Rev. Lett. **86**, 910 (2001).
[13] R. Raussendorf, D. E. Browne, and H. J. Briegel, Phys. Rev. A **68**, 022312 (2003).
[14] H. J. Briegel, D. E. Browne, W. Dur, R. Raussendorf, and M. Van den Nest, Nat Phys , 19 (2009).
[15] D. Deutsch, Proceedings of the Royal Society of London A: Mathematical, Physical and Engineering Sciences **425**, 73 (1989), http://rspa.royalsocietypublishing.org/content/425/1868/73.full.pdf.
[16] D. Gross, S. T. Flammia, and J. Eisert, Phys. Rev. Lett. **102**, 190501 (2009).
[17] R. Raussendorf and H. J. Briegel, Phys. Rev. Lett. **86**, 5188 (2001).
[18] M. Hein *et al.*, Entanglement in Graph States and its Applications, in *Proceedings of the International School of Physics "Enrico Fermi" on "Quantum Computers, Algorithms and Chaos"*, 2006.
[19] M. Van den Nest, A. Miyake, W. Dür, and H. J. Briegel, Phys. Rev. Lett. **97**, 150504 (2006).
[20] A. Miyake, Annals of Physics **326**, 1656 (2011), July 2011 Special Issue.
[21] I. Affleck, T. Kennedy, E. H. Lieb, and H. Tasaki, Phys. Rev. Lett. **59**, 799 (1987).
[22] I. Affleck, T. Kennedy, E. H. Lieb, and H. Tasaki, Communications in Mathematical Physics **115**, 477 (1988).
[23] T. Kennedy, E. H. Lieb, and B. S. Shastry, Journal of Statistical Physics **53**, 1019 (1988).
[24] T.-C. Wei, I. Affleck, and R. Raussendorf, Phys. Rev. A **86**, 032328 (2012).
[25] F. Verstraete, V. Murg, and J. Cirac, Advances in Physics **57**, 143 (2008), http://dx.doi.org/10.1080/14789940801912366.
[26] D. Perez-Garcia, F. Verstraete, J. I. Cirac, and M. M. Wolf, ArXiv e-prints (2007), 0707.2260.
[27] A. Molnar, Y. Ge, N. Schuch, and J. I. Cirac, ArXiv e-prints (2017), 1706.07329.
[28] D. P. Divincenzo, Fortschritte der Physik **48**, 771 (2000), quant-ph/0002077.
[29] K. Onuma and A. Ito, Chemistry of Materials **10**, 3346 (1998), http://dx.doi.org/10.1021/cm980062c.
[30] A. Oyane, K. Onuma, T. Kokubo, and I. Atsuo, The Journal of Physical Chemistry B **103**, 8230 (1999), http://dx.doi.org/10.1021/jp9910340.
[31] A. Dey *et al.*, Nat. Mat. **9**, 1010 (2010).
[32] D. C. Rapaport, *The Art of Molecular Dynamics Simulation*, 2 ed. (Cambridge University Press, 2004).
[33] B. Misra and E. C. G. Sudarshan, Journal of Mathematical Physics **18**, 756 (1977), http://dx.doi.org/10.1063/1.523304.
[34] N. W. Ashcroft and N. D. Mermin, *Solid State Physics* (Brooks/Cole, Belmont, CA, 1976).
[35] C. Cohen-Tannoudji, B. Diu, and F. Laloë, *Quantum Mechanics* (Wiley, 1991).
[36] E. Knill and R. Laflamme, Phys. Rev. A **55**, 900 (1997).
[37] C. H. Bennett, D. P. DiVincenzo, J. A. Smolin, and W. K. Wootters, Phys. Rev. A **54**, 3824 (1996).
[38] D. Kribs, R. Laflamme, and D. Poulin, Phys. Rev. Lett. **94**, 180501 (2005).
[39] D. W. Kribs, R. Laflamme, D. Poulin, and M. Lesosky, eprint arXiv:quant-ph/0504189 (2005), quant-ph/0504189.
[40] M. A. Nielsen and D. Poulin, Phys. Rev. A **75**, 064304 (2007).
[41] J. Watrous, Ch. 16: Quantum error correction, in *CPSC 519/619: Quantum Computation*, Lecture Notes, 2006.
[42] R. W. Spekkens, Phys. Rev. Lett. **101**, 020401 (2008).
[43] M. Howard, J. Wallman, V. Veitch, and J. Emerson, Nature **510**, 351 (2014).
[44] and and, Proceedings of the Royal Society of London A: Mathematical, Physical and Engineering Sciences **449**, 669 (1995), http://rspa.royalsocietypublishing.org/content/449/1937/669.full.pdf.
[45] S. Lloyd, Phys. Rev. Lett. **75**, 346 (1995).
[46] J.-L. Brylinski and R. Brylinski, eprint arXiv:quant-ph/0108062 (2001), quant-ph/0108062.

[47] M. Freedman, A. Kitaev, and J. Lurie, eprint arXiv:quant-ph/0209113 (2002), quant-ph/0209113.
[48] A. W. Harrow, ArXiv e-prints (2008), 0806.0631.
[49] L. Eldar and A. W. Harrow, ArXiv e-prints (2015), 1510.02082.
[50] S. Aaronson, Proceedings of the Royal Society of London A: Mathematical, Physical and Engineering Sciences **461**, 3473 (2005), http://rspa.royalsocietypublishing.org/content/461/2063/3473.full.pdf.
[51] R. Horodecki, P. Horodecki, M. Horodecki, and K. Horodecki, Rev. Mod. Phys. **81**, 865 (2009).
[52] D. Gottesman and I. L. Chuang, Nature **402**, 390 (1999).
[53] E. Knill, R. Laflamme, and G. J. Milburn, Nature **409**, 46 (2001).
[54] M. A. Nielsen, Physics Letters A **308**, 96 (2003).
[55] X. Zhou, D. W. Leung, and I. L. Chuang, Phys. Rev. A **62**, 052316 (2000).
[56] D. Gross and J. Eisert, Phys. Rev. Lett. **98**, 220503 (2007).
[57] D. Gross, J. Eisert, N. Schuch, and D. Perez-Garcia, Phys. Rev. A **76**, 052315 (2007).
[58] F. Verstraete and J. I. Cirac, Phys. Rev. A **70**, 060302 (2004).
[59] S. Östlund and S. Rommer, Phys. Rev. Lett. **75**, 3537 (1995).
[60] M. Fannes, B. Nachtergaele, and R. F. Werner, Comm. Math. Phys. **144**, 443 (1992).
[61] A. Klümper, A. Schadschneider, and J. Zittartz, Journal of Physics A: Mathematical and General **24**, L955 (1991).
[62] F. Verstraete and J. I. Cirac, eprint arXiv:cond-mat/0407066 (2004), cond-mat/0407066.
[63] G. K. Brennen and A. Miyake, Phys. Rev. Lett. **101**, 010502 (2008).
[64] A. Miyake, Phys. Rev. Lett. **105**, 040501 (2010).
[65] S. D. Bartlett, G. K. Brennen, A. Miyake, and J. M. Renes, Phys. Rev. Lett. **105**, 110502 (2010).
[66] R. Shankar, *Principles of Quantum Mechanics* (Plenum Press, New York, 1994).
[67] R. Raussendorf, J. Harrington, and K. Goyal, Annals of Physics **321**, 2242 (2006).
[68] D. E. Browne *et al.*, New Journal of Physics **10**, 023010 (2008).
[69] T.-C. Wei, P. Haghnegahdar, and R. Raussendorf, Phys. Rev. A **90**, 042333 (2014).
[70] T.-C. Wei and R. Raussendorf, Phys. Rev. A **92**, 012310 (2015).
[71] J. Preskill, Quantum computing and the entanglement frontier, in *The Theory of the Quantum World: Proceedings of the 25th Solvay Conference on Physics*, edited by D. Gross, M. Henneaux, and A. Sevrin, World Scientific Publishing, 2013.
[72] E. Farhi and A. W. Harrow, ArXiv e-prints (2016), 1602.07674.
[73] T. Nishino *et al.*, Progress of Theoretical Physics **105**, 409 (2001).
[74] H. Niggemann, A. Klümper, and J. Zittartz, Zeitschrift für Physik B Condensed Matter **104**, 103 (1997).
[75] F. Verstraete, M. A. Martín-Delgado, and J. I. Cirac, Phys. Rev. Lett. **92**, 087201 (2004).
[76] A. S. Darmawan, G. K. Brennen, and S. D. Bartlett, New Journal of Physics **14**, 013023 (2012).
[77] M. P. A. Fisher, International Journal of Modern Physics B **31**, 1743001 (2017), http://www.worldscientific.com/doi/pdf/10.1142/S0217979217430019.
[78] A. Heiss, V. Pipich, W. Jahnen-Dechent, and D. Schwahn, Biophysical Journal **99**, 3986 (2010).
[79] E. Bellocchio, R. J. Reimer, R. T. Fremeau, and R. H. Edwards, Science **289**, 957 (2000).
[80] M. Liguz-Lecznar and J. Skangiel-Kramska, Acta Neurobiol Exp **67**, 207 (2007).
[81] S. Sreedharan *et al.*, BMC Genomics **11**, 17 (2010).
[82] R. Reimer, Molecular Aspects of Medecine **34**, 350 (2013).
[83] B. Ni, P. R. Rosteck, N. S. Nadi, and S. M. Paul, Proc. Nod. Acad. Sci. **91**, 5607 (1994).
[84] R. Milo and R. Phillips, How big is a synapse?, in *Cell Biology by the Numbers*, Garland Science, 2015.
[85] S. Jordan, Quantum algorithm zoo, Online resource.
[86] C. Palazuelos and T. Vidick, Journal of Mathematical Physics **57**, 015220 (2016).
[87] J. F. Clauser, M. A. Horne, A. Shimony, and R. A. Holt, Phys. Rev. Lett. **23**, 880 (1969).
[88] J. Preskill, Ch. 4: Quantum entanglement, in *Phys. 219: Quantum Computation and Information*, Lecture Notes, 2001.
[89] P. W. Shor, SIAM Journal on Computing **26**, 1484 (1997), https://doi.org/10.1137/S0097539795293172.
[90] E. Knill and R. Laflamme, Phys. Rev. Lett. **81**, 5672 (1998).
[91] D. Deutsch, Proceedings of the Royal Society of London A: Mathematical, Physical and Engineering Sciences **400**, 97 (1985), http://rspa.royalsocietypublishing.org/content/400/1818/97.full.pdf.
[92] E. Farhi *et al.*, Science **292**, 472 (2001), http://science.sciencemag.org/content/292/5516/472.full.pdf.
[93] A. Kitaev, Annals of Physics **303**, 2 (2003).
[94] A. M. Childs, Phys. Rev. Lett. **102**, 180501 (2009).
[95] S. P. Jordan, Quantum Information and Computation **10**, 470 (2010).
[96] A. Y. Kitaev, Russian Math. Surveys **52**, 1191 (1997).
[97] P. W. Shor, Phys. Rev. A **52**, R2493 (1995).